DOE/ID/12079-1

TOPICAL REPORT

GRAVITY SURVEY OF THE ESCALANTE DESERT AND VICINITY, IN IRON AND WASHINGTON COUNTIES, UTAH

By

Win Pe and Kenneth L. Cook

Work performed under Contract No.

DE-AC07-80ID12079

Department of Geology and Geophysics
University of Utah
Salt Lake City, Utah (USA)

AUGUST, 1980

Prepared for
DEPARTMENT OF ENERGY
Division of Geothermal Energy

DISCLAIMER

NOTICE

This report was prepared to document work sponsored by the United States Government. Neither the United States nor its agent, the United States Department of Energy, nor any Federal employees, nor any of their contractors, subcontractors or their employees, makes any warranty, express or implied, or assumes any legal liability or responsibility for the accuracy, completeness, or usefulness of any information, apparatus, product or process disclosed, or represents that its use would not infringe privately owned rights.

NOTICE

Reference to a company or product name does not imply approval or recommendation of the product by the University of Utah or the U.S. Department of Energy to the exclusion of others that may be suitable.

DOE/ID/12079-14

GRAVITY SURVEY OF THE ESCALANTE DESERT AND VICINITY IN IRON AND WASHINGTON COUNTIES, UTAH

by

Win Pe and Kenneth L. Cook

August, 1980

PREFACE

The attached report was submitted by Win Pe in partial fulfillment of the requirements for the degree of Master of Science in Geophysics, Department of Geology and Geophysics at the University of Utah. The work was performed under the direction of Dr. Kenneth L. Cook.

ABSTRACT

During the summers of 1978 and 1979, a total of 436 new gravity stations were taken in the southern part of the Escalante Desert and vicinity in Iron and Washington counties, Utah. The new stations were combined with 917 other stations taken in previous surveys, and a total of 1,353 stations were used in this study, covering an area of about 2,700 mi^2 (7,000 km^2). The purpose of the study was to help evaluate the potential of geothermal resources within the survey area, which includes the Newcastle and Lund KGRA's. All the gravity data were terrain corrected out to a radial distance of 166.7 km from each station, using a computer terrain-correction program. The data were compiled and presented as a complete Bouguer gravity anomaly map with a 2-mgal contour interval. A geologic interpretation of the gravity data was made qualitatively from the gravity map and also quantitatively from four easterly trending gravity profiles taken across the area.

The complete Bouguer gravity anomaly map shows gravity anomaly values ranging from about -182 mgal over the mountainous region, west of Enterprise, to -230 mgal over the flat surface of Hamblin Valley in the northwest corner of the study area. Because the entire study area lies over a broad regional gravity saddle, the variation of the regional gravity is generally assumed to be negligible. Over most of the study area are dominant northeastward-trending gravity highs and

lows, which reflect the Basin and Range features, generally along the flexures associated with the Laramide orogeny. In the western portion of the area are several eastward-trending gravity patterns that are interpreted as caused by subsurface geologic features that have been shaped mostly by the easterly trending pre-Basin and Range igneous activity.

The gravity lows indicate grabens in the area, including the (1) Cedar Valley graben, (2) Parowan Valley graben, (3) Avon graben, (4) Lund graben, (5) Newcastle graben, (6) South Beryl graben, and (7) East Modena graben. The maximum depth to basement beneath the grabens, as indicated from gravity modeling, is about 3 km, beneath the Newcastle graben. The gravity highs indicate horsts, including the (1) Red Hills horst, (2) Black Ridge horst, (3) Table Butte horst, (4) Beryl horst, and (5) Enterprise Reservoir horst. The gravity high over the Iron Springs district indicates an extensive and continuous quartz monzonite body at shallow depth between the individual outcropping quartz monzonite bodies comprising Stoddard Mountain, Iron Mountain, Granite Mountain, and The Three Peaks. The gravity high over the Antelope Range is interpreted provisionally as an igneous mass at shallow depth which possibly has the same origin as the quartz monzonite bodies nearby. The easterly trending gravity highs over the Mount Escalante area and the western part of the Black Mountains are interpreted as caused by basement structural blocks at shallow depth, which have been intruded by eastward-trending deeply rooted igneous vein-like bodies.

The northeastward extent of the Basin and Range-type grabens and

horsts, and the offsets, bending, and bulging of the intrusive igneous bodies are believed to be confined within an area of structural control, possibly associated with a proposed southeastward-trending minor intrusive belt, which probably forms as a bridge joining the two major easterly trending igneous belts, Pioche-Marysvale on the north and Delamar-Iron Springs on the south. The existence of the minor intrusive belt is partially supported by the belt of southeastward-trending aeromagnetic anomalies across the Escalante Desert.

Even though no gravity anomaly that indicates a geologic feature directly related to the geothermal process or heat source (such as a magma chamber), is observed in the study area, the gravity survey delineates well the steeply dipping faults or fault zones which bound the deep grabens and associated structures that may partly control the geothermal systems in this area. In particular, in the Newcastle and Lund KGRA's, the gravity data indicate that steeply dipping fault zones along the east (with a downthrow of about 3 km) and west (with a downthrow of about 1 km) margins of the Newcastle and Lund grabens, respectively, probably form conduits for the upward circulation of hot water observed at shallow depth near Newcastle (220°F) and Lund. According to Clement (1980), the water in the Newcastle KGRA is probably heated by the geothermal gradient in this region and probably originates at a depth of about 3 km.

CONTENTS

LIST OF FIGURES

LIST OF TABLES

ACKNOWLEDGMENTS

I would like to thank my Committee Chairman, Dr. K. L. Cook, and the other members of my Supervisory Committee, Dr. M. P. Nackowski, and Dr. W. R. Sill, for their consultations and critical reviews of the manuscript.

Eckhard Kuennemann assisted during the field work, and Laura F. Serpa and Stephen C. Gabbert assisted in using the terrain correction program. I also wish to express my thanks to many other students of the University of Utah for helping me in various aspects of this research.

My special thanks are given to Mrs. Kay Nackowski for her encouragement throughout the period of my study in the United States.

This study was initially arranged by the Higher Educational Department, Ministry of Education, Rangoon, Burma, and was performed under the United Nations Fellowships Program during the period 1977-1979 and under the Fulbright Scholarships Program sponsored by the Institute of International Education during the period 1979-1980.

This work was supported by the Department of Energy, Division of Geothermal Energy (DOE/DGE) contract numbers DE-AC07-78ET28392 and DE-AC07-80ID12079.

Financial support for the taking of certain gravity stations (see Table 2 and Appendix A) and the preliminary compilation of the gravity data used in this report was given as follows: (1) "EH" stations (taken by Elwood Hardman during 1963-64) and "WU" stations (taken by J. R. Montgomery during 1971) by the National Science Foundation under Research Grants NSF-G13649, GA-30182, and/or DES71-00422-A02; and (2) "LU" stations (taken by D. K. Selk during 1974) by the University Research Fund of the University of Utah.

INTRODUCTION

Location of Survey

During the summers of 1978 and 1979, a regional gravity survey was made in the southern part of the Escalante Desert and adjoining areas in Iron and Washington counties, Utah. The survey area (Fig. 1) is located between latitudes 37°30' N and 38°07.5' N and is bounded on the west by longitude 114°00' W and on the east by the Hurricane fault zone (approximately between longitudes 112°45' W and 113°00' W), which forms the western margin of the Colorado Plateau. The survey area also includes Parowan Valley. The important cities and towns in the area include: Cedar City, Parowan, Paragonah, Newcastle, Enterprise, Lund, and Modena. The purpose of the study was to help evaluate the geothermal potential of the region. The study was made as part of a larger study of the geothermal resource evaluation in southwestern Utah being performed by the Geothermal Team of the Department of Geology and Geophysics, University of Utah.

Topography

About 75 percent of the study area is covered by the flat valley surface of the Escalante Desert, Cedar Valley, and Parowan Valley (Fig. 2). The lowest elevation in the survey area is about 5,080 ft (1,548 m) on the Escalante Desert floor, near Lund, and the highest elevation is about 10,000 ft (3,048 m), in the Hurricane Cliffs area near Cedar City.

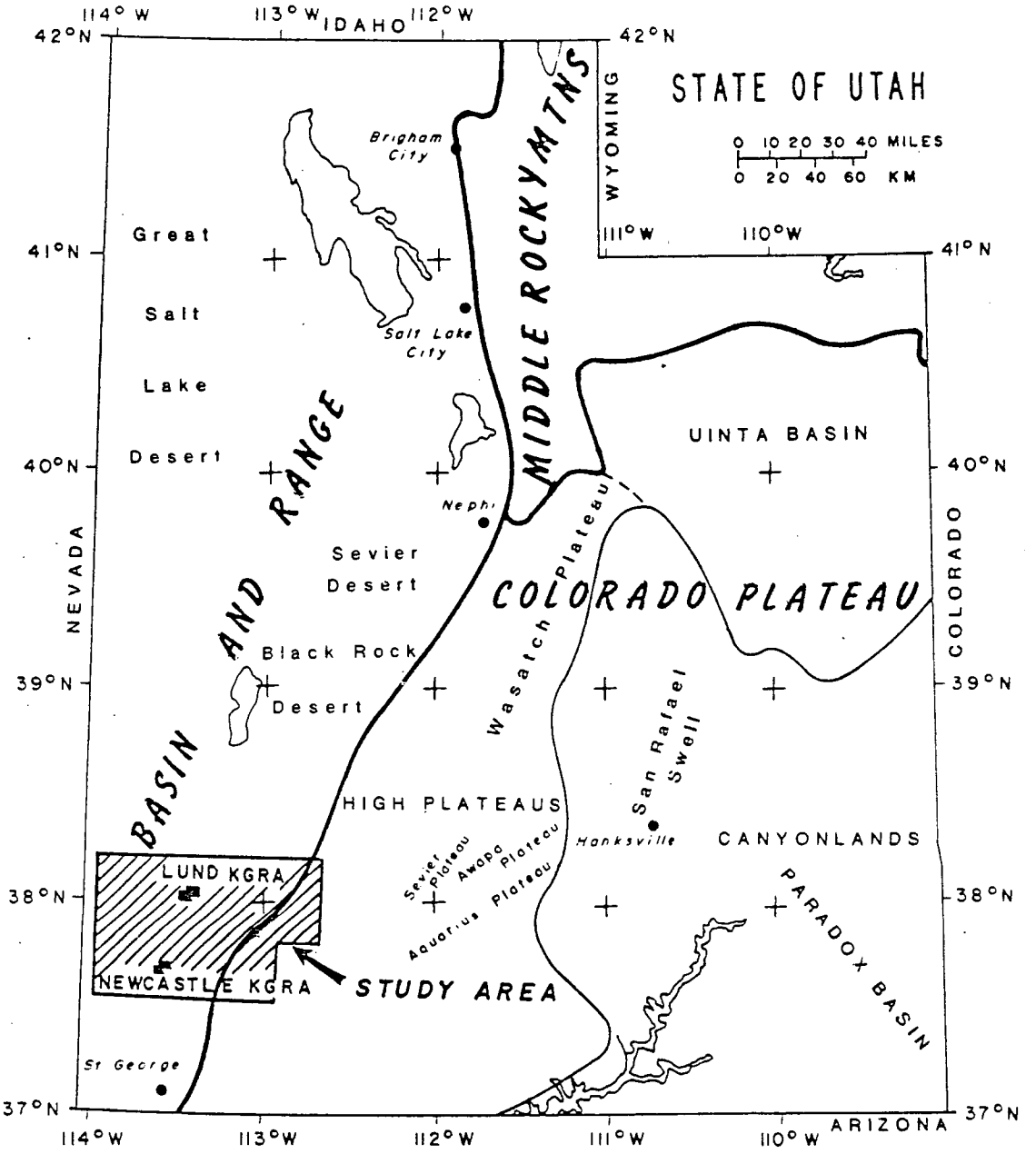

Figure 1. Map of Utah showing location of the study area.

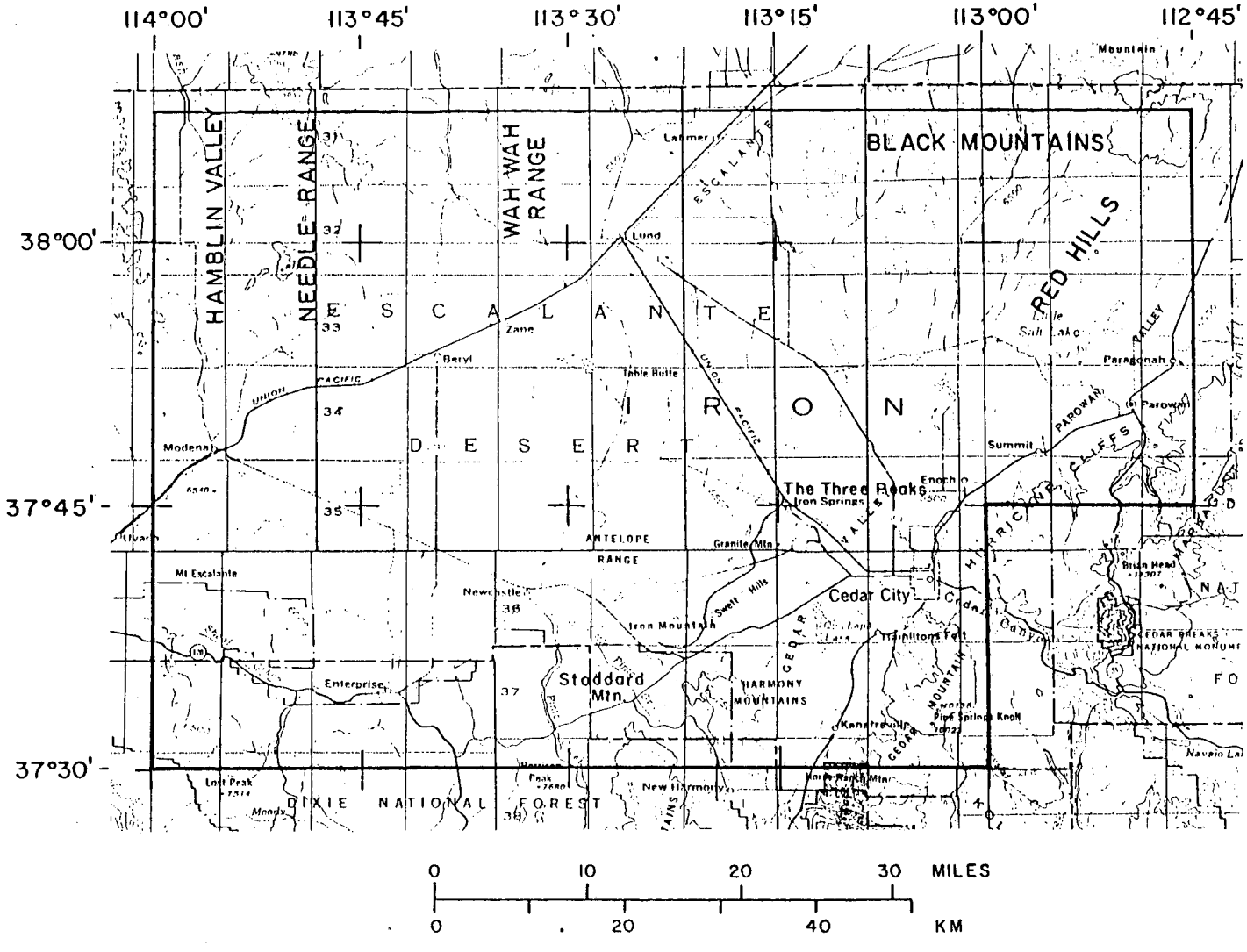

Figure 2. Topographic map showing outline of the study area.

The central topographic feature of the survey area is a northeastward-trending belt of low mountains, 20 miles (32 km) long and 3 to 5 miles (4.8 to 8 km) wide, located 10 to 20 miles (16 to 32 km) west of Cedar City. The belt includes, from southwest to northeast: Stoddard Mountain, Iron Mountain, Granite Mountain, and The Three Peaks. In the Iron Springs district, the elevation ranges from 5,300 ft (1,616 m) on the valley floor to 7,800 ft (2,378 m) at the summit of Iron Mountain. Cedar Valley lies between this belt of mountains on the west and the Hurricane Cliffs in the Cedar City region, on the east. Cedar Valley is terminated on the south by the Harmony Mountains, which rise more than 3,000 ft (915 m) above the valley floor. Cedar Valley extends northward to join the Escalante Desert in the area west of the Red Hills. The westward-facing Hurricane Cliffs, the most prominent feature in the area with generally up to 3,000 ft (915 m) of relief, bound the survey area on the east. The Escalante Desert extends westward from the belt of mountains and Antelope Range to the southern extension of the Needle Range near Modena, and extends northward to the edge of the survey area and beyond.

In the area north of Cedar City, Parowan Valley is separated from Cedar Valley by the Red Hills, which have a maximum relief of more than 1,000 ft (305 m) from the valley floor. To the north of the Red Hills, the Black Mountains, which lie on the eastern margin of the Escalante Desert in the northern part of the survey area, are composed of low hills with a relief of about 1,000 ft (305 m) above the desert floor. The elevation of the highest peak in the Black Mountains is about 8,600 ft (2,622 m).

Near the northwestern corner of the survey area, Hamblin Valley is bounded on the east and south by the southern arm of the Needle Range, with peaks more than 8,000 ft (2,439 m) in elevation; and the valley extends northwestward beyond the survey area. In the southwestern part of the study area near Enterprise, the area is covered with nearly east-west-trending low hills, including Mt. Escalante, with a relief of about 1,000 ft (305 m) above the desert floor.

In the eastern portion of the survey area, several closed topographic basins, ranging in area from a few hundred square meters to 1 km^2, are found in Cedar Valley and Parowan Valley along the west margin of the Colorado Plateau. The average elevation of Cedar Valley is lower than that of Parowan Valley; and the average elevation of the Escalante Desert is the lowest of all. The elevation of the floor of the Escalante Desert decreases slightly to the north. These three valleys are major important ground-water reservoirs in southwestern Utah.

Newcastle and Lund KGRA's

The Newcastle Known Geothermal Resource Area (KGRA) is on the eastern margin of the Escalante Desert, and includes the town of Newcastle. Hot water, with a temperature of about 220° F (104° C), occurs at a depth of about 230 ft (70 m) in the shallow water wells drilled by local farmers. The hot water found in this area is so pure (with relatively little mineral content) that the farmers use the water for irrigation after cooling it down through a series of ponds. The hot water has been used by the local people for many years. No hot

springs occur in this area. Because the hot water is fresh, no alteration of alluvium or rocks is found at the surface. According to Clement (1980), the hot water apparently rises from a deep source and leaks into the cold water near the surface; and the water is probably heated by the geothermal gradient in this region and probably originates at a depth of about 3 km to reach the present temperature at the surface.

The Lund KGRA is near the western margin of the Escalante Desert, and includes the hamlet of Lund. In this area, warm water occurs in shallow water wells west of Lund (M. Clement, 1980, personal communication). No hot springs occur in this area; and the area is designated a "KGRA" because the land has been leased for its geothermal potential.

Prior Investigations

A pioneering study by Leith and Harder (1908) in the Iron Springs district appears to be the first detailed geologic study in the area. More recently, Mackin (1947, 1954, 1960) studied the intrusions in detail as well as the structural relationships in the surrounding area of southwestern Utah. The ground-water resources of the Escalante Desert were investigated by White (1932), whose study was probably the first of its kind in this area. The geology of the Bull Valley district, south of Enterprise, was studied in detail by Blank (1959). A reconnaissance geologic map of the Red Hills area north of Cedar City was made by Harold Thomas (Thomas and Taylor, 1946), in connection with a study of ground-water resources of Cedar Valley and Parowan Valley.

A detailed study of the geology of the Cedar City area and vicinity was made by Threet (1952).

The Hurricane fault zone, near the eastern margin of the study area, was studied in detail by Huntington and Goldthwait (1903, 1904), Dobbin (1959), Gardner (1941), Gregory and Williams (1947), Cook (1957, 1960a), and many others.

Previous published geophysical data in the Iron Springs district include a ground magnetometer survey by the U.S. Bureau of Mines (Cook, K. L., 1950) and an aeromagnetic survey by the U.S. Geological Survey (Blank and Mackin, 1967). Several mining companies that are exploring for and developing iron ores in this area have conducted additional detail magnetometer surveys; but the results have not been published. A regional aeromagnetic survey which included the whole study area was made by Scintrex Mineral Surveys, Inc. over southwestern Utah along east-west flight lines with 2-mile spacing (U.S. Geological Survey, 1972a, b). The part of the aeromagnetic map that overlies the present study area is shown in Figure 5.

A regional gravity survey over the eastern portion of the present study area (east of longitude 113°30' W) was made by Hardman (1964). The regional gravity survey of western Utah by Montgomery (1973) covers the whole study area with relatively sparse data.

Currently, heat flow measurements, geochemical, and additional geophysical surveys are being made in the Escalante Desert area by the Geothermal Team of faculty and students of the University of Utah and other teams from private industry to determine the geothermal potential of the region.

Purpose and Scope

The present detailed gravity survey augments the regional gravity survey of Hardman (1964) and gives a more complete regional picture of the gravity variations surrounding the southern Escalante Desert and Cedar City region. The purpose of this study is to aid in the evaluation of potential geothermal resources within the survey area. The study area includes the Newcastle and Lund KGRA's (Map of Geothermal Resources of the Western United States, 1977). One particular objective is to provide information that will assist in the development of the Newcastle KGRA at the east margin of the Escalante Desert. In this area, hot water with a temperature of about 220°F (104° C) is found at shallow depth (Mr. Christensen, 1980, personal communication); and this area will probably be a target of further geothermal exploration and development activity in the near future.

The gravity method has been extensively used in the investigation of geothermal prospects. In some areas, the relationship between gravity observation and the geothermal prospect is direct. However, anomalies which have been observed over known geothermal areas are variable in character and must be carefully interpreted in relationship to the geological data.

At the Imperial Valley KGRA, in southern California, small positive gravity anomalies observed over areas of high heat flow have been attributed to either an emplacement of higher density rhyolite domes or a densification process in which the loosely consolidated sediments are cemented and/or thermally metamorphosed by circulating hot fluids (Biehler and Combs, 1972). At the Geysers geothermal field,

located 120 km north of San Francisco, a gravity low (about 20-km wide and with about 30-mgal closure) northeast of the steam field has been interpreted as a magma chamber (Isherwood, 1975), which is thought to be the heat source for the geothermal system. At the Lake City KGRA, in Modoc County, California, a pronounced gravity gradient of 25 mgal in 2 miles (3.2 km) is centered over a mud volcano and hot spring (Anderson and Axtel, 1972). The gradient is attributed to a fault with over 5,000 ft (1,524 m) of vertical displacement which may serve as a conduit for the circulation of thermal fluids.

Since the present survey area may contain one or more collapse caldera features within a volcanic field (Crosby, 1973), previous investigations of the gravity pattern over major volcanic fields and volcanic subsidence structures elsewhere should be mentioned here. Investigations by Yokoyama (1958) show gravity results over selected calderas in the Japanese island arc. Gravity lows with more than 20-mgal closure were observed over the Kuttyaro and Aso calderas, whereas a gravity high with about 15-mgal closure was observed over the Mihara volcano. Pakiser (1964) noted a gravity low with about 70-mgal amplitude in the southern Cascade Range near Lassen Peak in California. Kane and others (1976) discuss a gravity low with about 50-mgal closure over the Long Valley caldera, California, which is interpreted to be the result of about 3 km of low-density volcanic material in the caldera assuming a density contrast of 0.45 g/cc. Studies by Eaton and others (1975) show a large gravity low with about 50 mgal closure in Yellowstone National Park. Here the gravity low was interpreted as due not to low-density volcanic fill but rather to a crystalline or molten

batholith.

The investigation of the present gravity survey was done in an attempt to (1) decipher the structural features in the survey area such as north-northeastward trending typical Basin and Range fault zones, local Larimide thrusts and folds in front of the main thrust sheet in an east-southeast direction, the possible east-west trending fault system controlled by the pre-Basin and Range eastward-trending structural lineament, and the size and extent of the subsurface intrusive igneous masses which prevail throughout southwestern Utah, and (2) discover any gravity expression of a possible geothermal system such as steam reservoir or the heat source.

A complete Bouguer gravity anomaly map and aeromagnetic map of the study area are presented. The gravity and aeromagnetic data are correlated with the geologic data. Four gravity profiles in an approximately east-west direction are modeled to provide geologic interpretation of the subsurface.

GENERAL GEOLOGY

Regional Structure

The survey area is located within the transition zone between the undeformed strata of the Colorado Plateau and severely deformed rocks of the Basin and Range province (Fig. 1). Along the western margin of the transition zone, which extends in a northeastward direction across the study area, Tertiary volcanic rocks are exposed on the west side of the Escalante Desert near the western margin of the survey area. The study area is bounded on the east by the Hurricane fault zone and on the west by the southern extension of the Needle Range. The survey area includes the southern extension of the Needle Range and Wah Wah Range, the southern part of the Escalante Desert, the northern part of the Bull Valley area (lying south of Enterprise), the Iron Springs district, the southern part of the Black Mountains, the Red Hills area (north of Cedar City), Parowan Valley, and Cedar Valley (Fig. 3). The area is dominated by northeastward-trending Basin and Range features, and the northeastward-trending belt of intrusions that were partly controlled by the earlier Laramide thrusts and folds (Mackin, 1960). The eastward-trending lineaments, which reflect the pre-Basin and Range igneous activities, are also found on the western part of the survey area (Stewart and others, 1977).

Tectonically, the study area is located between the eastward-trending Pioche-Marysvale igneous belt on the north and

Figure 3. Generalized geologic map of the Escalante Desert and vicinity, Utah (Adapted from Hintze, 1963).

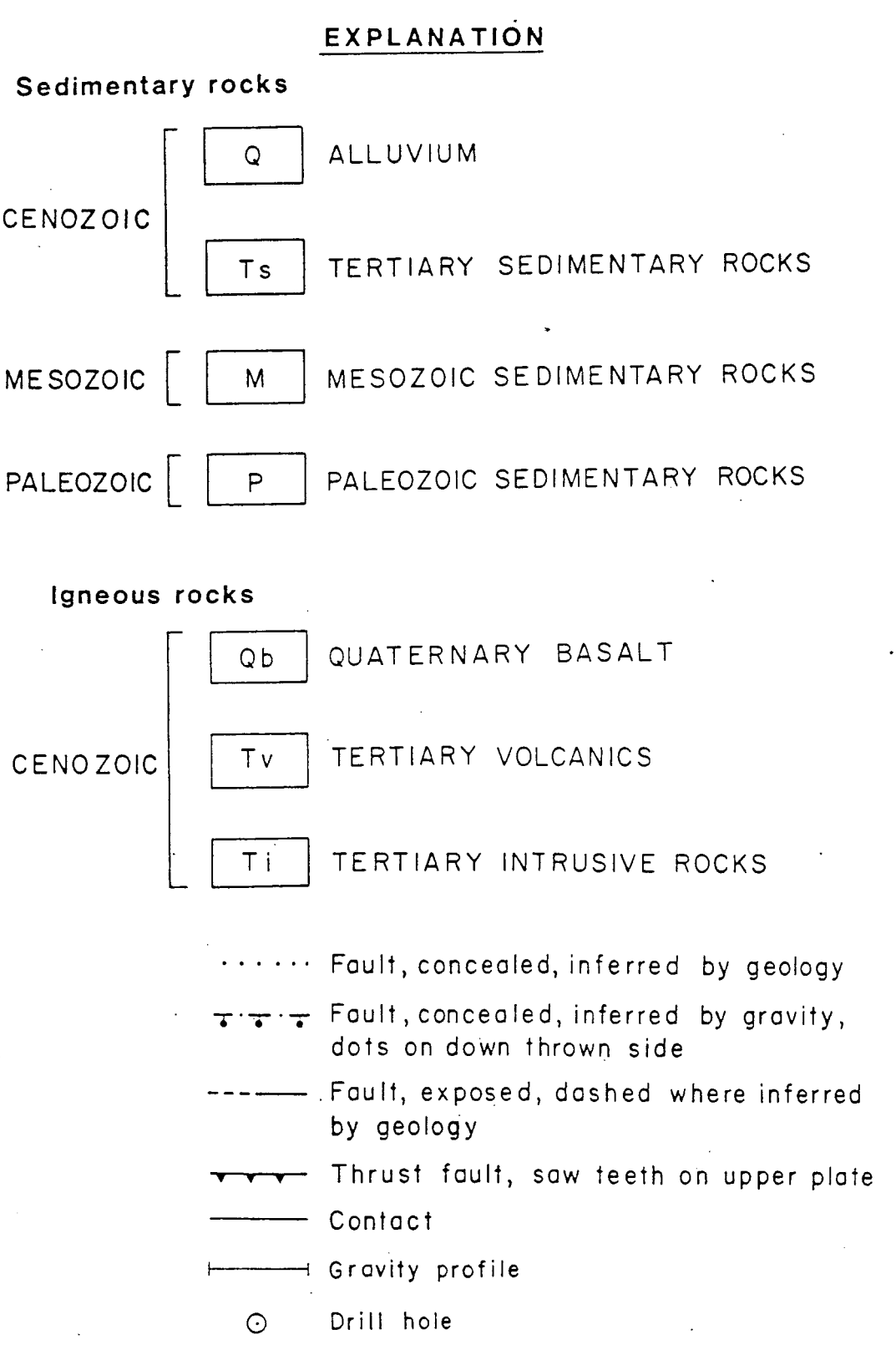

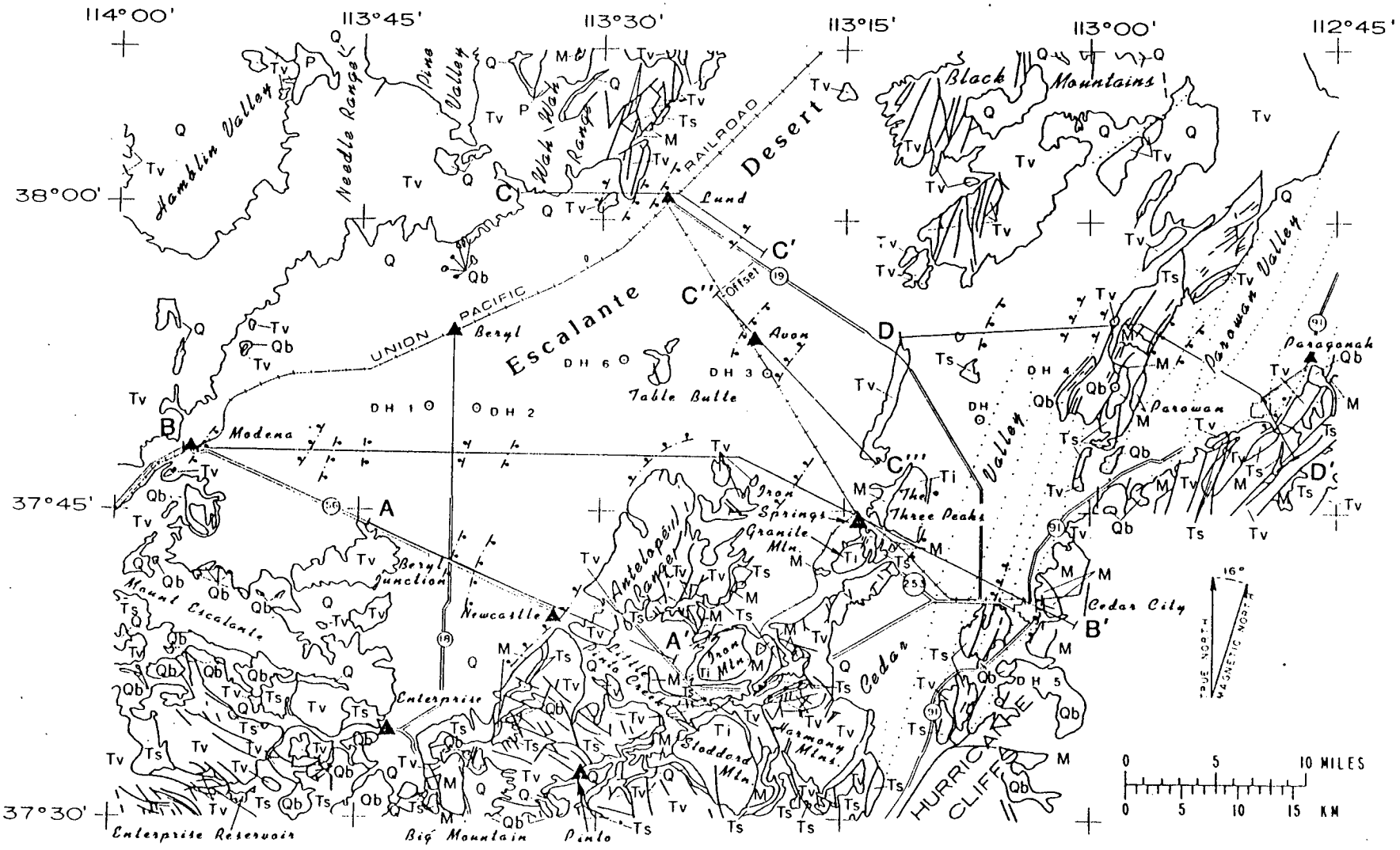
114°00'
113°45'
113°30'
113°15'
113°00'
112°45'
38°00'
37°45'
37°30'
Hamblin Valley
Needle Range
Pine Valley
Wah Wah Range
RAILROAD
Desert
Lund
Black Mountains
Escalante
Offset
UNION PACIFIC
Beryl
Avon
Table Butte
DH 6
DH 3
DH 1
DH 2
DH 4
DH 5
Modena
Beryl Junction
Newcastle
Enterprise
Enterprise Reservoir
Mount Escalante
Antelope Range
Iron Springs
Granite Mtn.
Three Peaks
Iron Mtn.
Cedar
Cedar City
Harmony Mts.
Sloddard Mtn.
Big Mountain
Pinto
HURRICANE CLIFFS
Parowan Valley
Paragonah
Parowan
A
A'
B
B'
C
C'
C''
C'''
D
D'
TRUE NORTH
MAGNETIC NORTH
16°
0 5 10 MILES
0 5 10 15 KM

Delamar-Iron Springs igneous belt on the south, which are characterized by known volcanic centers, plutons, hot springs, igneous-related mineralized rocks, hydrothermally altered rocks, and aeromagnetic anomalies in southern Nevada and southwestern Utah (Rowley and others, 1979). Both igneous belts are included in the Wah Wah-Tushar volcanic belt based on outcrops of calc-alkaline rocks (Stewart and others, 1977).

Stewart and others (1977) postulated that the east-west patterns are the result of a southward migrating front of igneous activity which, in Nevada and Utah, started about 43 to 34 m.y. ago near latitude 40°00' N and ended about 17 to 6 m.y. ago near latitude 37°00' N. During any one time interval, igneous activity was concentrated near the leading edge of the east-trending front. The volcanic front may be related to igneous activity localized along a southward-propagating transverse break or structural warp in a subducting plate.

Rowley and others (1979) also suggested that east-west extension started about 20 m.y. ago to imprint a northerly striking pattern of basin-range faults onto the older east-trending igneous belts and underlying sedimentary rocks. Uplifted blocks were eroded and sediments were deposited in the adjacent developing basins. Concurrently a bimodal assemblage of mostly small volumes of basaltic and rhyolitic rocks was erupted. Basalt flows were widely distributed, but the rhyolitic rocks were erupted from local centers, many of which are located along the east-trending lineaments within the older igneous belts.

Within the study area, the surface rocks range in age from Paleozoic to Recent. The sedimentary section is mostly of Mesozoic age. With the exception of the Quaternary basalt flows, all igneous rocks, both intrusive and extrusive, are Tertiary in age (Hintze, 1963). In nearly all valley areas, both the pre-Tertiary and Tertiary rocks are overlain unconformably by alluvium of Quaternary age.

Escalante Desert Area

The southern part of the Escalante Desert was the southermost arm of ancient Lake Bonneville, possibly as recently as 13,000 years ago. According to Anderson and Bucknam (1979), the shore line of Lake Bonneville was found near Lund and Table Butte, whereas the shore line at the southermost area near Enterprise and Modena is obscure. Nevertheless, they discovered from observations that a 800-km^2 area in the southern Escalante Desert has experienced uplift of at least 30 m, probably in Holocene time, after the Lake Bonneville abandoned this area, possibly as a result of isostatic rebound.

Structurally, the Escalante Valley in the study area is apparently bounded on the north by the eastward-trending Pioche-Marysvale igneous belt (about 26 m.y. old), and on the south and west by the Delamar-Iron Springs igneous belt (about 20 m.y. old), both of which extend from southern Nevada into southwestern Utah. The lack of volcanism in the desert area may be due to the fact that the southward migration of igneous activity appears to have taken place in "shifts or jumps" in Utah (Stewart and others, 1977). The valley area was probably modified later by the Basin and Range tectonic activity.

Iron Springs Area

In the Iron Springs area, the dominant geologic feature is the northeast-trending belt of outcropping intrusions of quartz monzonite from which sediments dip outward asymmetrically (Fig. 3). The intrusions are, from southwest to northeast; Stoddard Mountain, Iron Mountain, Granite Mountain, and The Three Peaks. The quartz monzonite stocks are associated with replacement iron ore bodies, except for Stoddard Mountain. Pre-volcanic sedimentary rocks are exposed for the most part only where they have been arched up by the intrusions, and therefore the early geologic history of the area around the Escalante Desert is relatively obscure. Although the intrusive bodies in the Iron Springs district were originally described by Leith and Harder (1908) as laccoliths, the monzonite bodies are now generally considered to be stocks (Granger, 1963). That the monzonite may be deeper and more widespread than originally believed is evidenced by the monzonite that was penetrated at a depth of about 3,490 ft (1,064 m) in an oil test hole near Parowan Gap, which lies in the Red Hills area a few miles northeast of the iron belt. In the Iron Springs area, minor thrusts and overfolds lying in front of the main Laramide thrust belt have been mapped by Mackin (1947).

In the Iron Springs area, the lowest stratigraphic unit exposed is the Homestake Formation, a massive to thick-bedded limestone, generally 300 ft (92 m) thick. The Entrada Formation, which overlies the Homestake Formation, consists of shale, siltstone, and arkosic sandstone with a total thickness of about 200 ft (61 m). Both formations are of Upper Jurassic age. Overlying the Entrada Formation

disconformably is the Iron Springs Formation, of possible Upper Cretaceous age, which consists of series of conglomerate limestones and limy sandstones up to 3,000 ft (915 m) in total thickness. Overlying the Iron Springs Formation, with a marked angular unconformity, is the Claron Formation, of Late Cretaceous or Early Eocene age, composed of about 1,000 ft (305 m) of conglomerate, sandstone, shale, and limestone. The Claron Formation is covered by up to 2,000 ft (610 m) of Tertiary lavas and pyroclastics. Sometime during the post-Claron period, the quartz monzonite stocks were emplaced; and subsequently block faulting occurred.

Enterprise Area

The area lying south of the Escalante Desert and in the vicinity of Enterprise is the northern edge of the Bull Valley district (Fig. 3), which is at the western margin of the transition zone betwen the Colorado Plateau and Basin-Range type of tectonic environments (Dobbin, 1939, p. 125; Cook, 1957, p. 87). The Bull Valley district was the site of intermittent volcanism from early Tertiary time until Recent. Most of the structural features are associated directly or indirectly with eruptive igneous activities. Some features, such as an intrusive arch, a trough, and deformed blocks, are caused by the emplacement of the intrusions. The overall igneous activity was accompanied by intensive deformation characterized by closely spaced high-angle faulting (Blank, 1959). Several east-trending transcurrent faults that show both left- and right-lateral displacements were traced in this area by Walton (Smith and Sbar, 1974). The area is mostly covered by

Tertiary volcanics and Quaternary basalt. The small exposures of Tertiary intrusive rock are found just beyond the southern margin of the study area about 7 miles (11 km) southeast of Enterprise. Mesozoic rocks are exposed along the boundary of the Escalante Desert east of Enterprise. The post-volcanic, late Tertiary sediments and Quaternary alluvium cover the low regions of the area south and southwest of Enterprise.

Needle Range Area

In the northwestern part of the survey area lie the southern extensions of the Needle and Wah Wah ranges (Fig. 3). The area is mostly covered by Tertiary volcanic rocks. A few small outcrops of Quaternary basalt are found at the northwest boundary of Escalante Valley. Paleozoic rocks are exposed in the Needle and Wah Wah ranges near the northern margin of the survey area. Paleozoic rock that is thrust over Mesozoic rock is exposed in the Wah Wah Mountains. A few small exposures of Paleozoic rock thrusting over Mesozoic rock and Tertiary sedimentary rocks are found at a place about 5 miles (8 km) northwest of Lund (see geologic map of southwestern Utah by Miller, 1963). Hamblin Valley and Pine Valley (which lies between the Wah Wah Range and the Needle Range) are covered with Recent alluvium.

The Mesozoic sequence overridden by the Paleozoic sequence is well exposed at Blue Mountain, which lies beyond the survey area about 12 miles (19 km) north of Lund (see geologic map of southwestern Utah by Miller, 1963). This thrust is the first major overthrust on the west side of the Escalante Desert. The direction of the movement is to the

east-southeast. At its easternmost exposure at Blue Mountain, the thrust dips below the alluvium of the Escalante Desert, and therefore its eastward limit is not known (Miller, 1963). Beyond the survey area and about 15 miles (24 km) northwest of Blue Mountain, the Paleozoic sequence is overridden by the Precambrian quartzite along the Wah Wah thrust. All these thrusts may be related to the Snake Range "decollement" in eastern Nevada (Miller, 1963).

Red Hills and Black Mountains Area

The Black Mountains, which lie in the northeastern part of the survey area (Fig. 3), are comprised mostly of late Tertiary volcanics, although limited exposures of Paleozoic and Mesozoic sedimentary rocks occur beyond the survey area to the north. These sedimentary rocks are postulated to underlie the extrusions at a depth of only about 300 m (Erickson, 1968).

In the Red Hills area, the Mesozoic strata are exposed in the vicinity of Parowan Gap (Fig. 3). The early Tertiary sedimentary rocks are exposed over the Red Hills, and the overlying volcanics cover the area in the northern part. Post-volcanic late Tertiary sedimentary rocks, with associated basaltic cinder cones and lava flows, cover the south end of the Red Hills.

The Red Hills area is a composite range block, separating Parowan Valley and Cedar Valley (Threet, 1963). The area was involved in block faulting associated with the initiation of the Colorado Plateau margin along the Hurricane fault zone in the late Tertiary period (Threet, 1952). Laramide folding, accompanied by minor thrust faulting, is

exposed in the vicinity of Parowan Gap; and the late Tertiary block faulting accompanied by minor tilting, occurred throughout the Red Hills area. The Laramide flexure in Parowan Gap may be a northward extension of the toe of the Kanarra fold near Cedar City (Gregory and Williams, 1947). Geologic mapping in this area indicates that Cedar Valley and Parowan Valley are located over a north-trending structural graben in which rocks of Cretaceous, Tertiary, and Quaternary age are complexly deformed. Anderson and Bucknam (1979) noted Holocene deformation at the margins of Cedar and Parowan Valleys.

Hurricane Fault Zone

The survey area is bounded on the east by the Hurricane fault zone, which is a pronounced Basin and Range structure that extends through southwestern Utah. The fault zone has been studied extensively by many authors. In the area immediately east of the Hurricane fault near Cedar City, the Mesozoic strata are well exposed, with a few areas covered with Quaternary basalt flows. The Mesozoic strata are also exposed in the Hurricane fault zone near Parowan, where they are associated with Tertiary volcanics and sedimentary rocks.

In the segment near Cedar City, the Hurricane fault is a normal slip fault, downthrown to the west about 8,000 ft (2,439 m) (Threet, 1963). The plateau margin between Cedar City and Paragonah is transected by a series of en echelon faults, rather than paralleled by a master "Hurricane fault" (Thomas and Taylor, 1946). However, it was suggested by Threet (1963a) that the complex scarp between Cedar City and Paragonah is related essentially to a Neogene monocline that was

developed as a structural bridge between the Hurricane fault and the Paragonah fault.

REGIONAL GEOPHYSICS

Seismic Studies

The study area is located at the junction of the north-south trending Intermountain Seismic Belt (ISB) and an easterly trending secondary seismic zone, which extends westward from southwestern Utah through southern Nevada to join the north-trending Nevada seismic zone. The activity of ISB extends along the well-defined northward- trending East Cache and Wasatch fault zones in Utah from the north-trending Grand Valley fault zone of southeastern Idaho and continues southward along the Sevier, Tushar, and Hurricane fault zones of central Utah (Smith and Sbar, 1974). The easterly trending secondary zone of seismicity, which extends 200 km from southwestern Utah into southeastern Nevada, is not aligned with the regional tectonic grain, which is primarily north-south normal faulting; rather, it corresponds with an east-trending zone of Tertiary volcanic rocks that extends through the Enterprise area within this study area.

During 1966, an earthquake of magnitude 6.1 occurred near the southwest corner of the study area in southeastern Nevada near the Utah border. The fault plane solution indicated strike-slip motion, which is different from the normal faulting that characterizes the regional Basin and Range structure. Despite insufficient seismic data, the movement was interpreted in an east-west direction and with left-lateral displacement (Smith and Sbar, 1974).

The most recent earthquake swarm along the ISB within the study area occurred during 1971 along the Hurricane fault zone, 7 km north of Cedar City. A composite fault-plane solution indicated normal faulting along a north-northwest-trending fault plane with a most likely dip of 62° NE. The activity was located along the zone that bounds Tertiary and Quaternary basalt flows and outlines a prominent line of springs. Field investigations revealed north-trending fractures with east-west horizontal extension (Smith and Sbar, 1974).

Smith and Sbar (1974) postulated that the southern section of the ISB forms the eastern boundary of the Great Basin subplate. The limits of this subplate are defined on the south by the east-trending secondary seismic zone that lies across the study area and on the west by the north-trending Nevada seismic zone. On the north, the subplate is separated from the northern Rocky Mountain subplate by the Idaho seismic zone.

A teleseismic P-wave anomaly with a +2-sec residual was observed in southwestern Utah approximately centered over the present survey area (Jacob, 1972).

Gravity Features

The smoothed Bouguer gravity anomaly map of western Utah by Montgomery (1973) shows interesting features of the regional gravity in southwestern Utah that occur in the study area and vicinity. This smoothed gravity map can be considered as a low-pass filtered gravity map. Throughout the smoothed Bouguer gravity map, the regional gravity high on the west is separated from the regional low on the east by the

Wasatch gravity gradient, which is attributed to the combined effect of the Paleozoic thrusting and the crustal thickening of the Colorado Plateau (Montgomery, 1973).

To the south, from the gravity offset over the Black Rock area near the northern edge of the Mineral Mountains, the steep gravity gradient continues along the eastern flank of the Mineral Range to the southern end of the range. However, the steep gradient becomes less prominent where it extends over the Black Mountains near the northern margin of the present survey area. Only a slight gravity gradient can be traced southward along the western boundary of the Colorado Plateau over the Hurricane fault zone. Thus it is possible that the easternmost boundary of the thrust sheet may no longer be associated with the plateau margin near the eastern boundary of the study area. Moreover, Montgomery (1973) suggested that the trend of the Wasatch Line, which extends southwestward across the northwestern part of the present survey area and which leaves the western boundary at about latitude 37°40' N, after its direction changes from southward to southwestward over the Black Mountains, is indicated by the gravity features on both smoothed Bouguer gravity anomaly map and smoothed free-air gravity anomaly map.

On the smoothed Bouguer gravity anomaly map of Montgomery (1973), the present survey area is actually located over the broad regional gravity saddle between the Sevier gravity high on the north and the St. George-Kanab gravity high on the southwest. The gravity saddle is located between the gravity low over the Colorado Plateau to the east and the slight regional gravity low over Hamblin Valley on the

northwest. According to Montgomery (1973), the Sevier gravity high on the north is interpreted as related to the Sevier uplift, and the St. George-Kanab gravity high on the south may be partly related to the crustal thinning associated with the isostatic adjustment after the removal of large amounts of earth by the Colorado River. This easterly trending gravity saddle, which occupies approximately the present study area, can be attributed to a crustal downwarping between the two structural highs on the north and south, within the transition zone that is characterized by a thin crust with a thickness of about 25 km associated with a 9-km mantle upwarp (Smith, et al., 1975). The existence of crustal thickening in this region may be related to (1) the +2-sec teleseismic P-wave residual delay anomaly which centers over the survey area in southwestern Utah: or (2) a southward-propagating transverse break or structural warp associated with igneous activity proposed by Stewart and others (1977).

In the survey area the gravity patterns are mostly characterized by northeast-trending Basin and Range features. The gravity highs are generally attributed to the horsts, the igneous intrusive belt associated with the Laramide anticlinal structure, and the existence of the Paleozoic rocks at shallow depth. The gravity lows are generally related to the grabens covered with the lower-density valley fill. Hardman (1964) observed (1) a gravity high with about 6-mgal closure over the Iron Springs intrusive belt, and (2) gravity lows, with closures of about -8 mgal and -10 mgal, over the Lund graben and Avon graben, respectively. The greatest depth to bedrock beneath these grabens was interpreted to be about 6,000 ft (1,829 m), below the

surface, assuming a density contrast of 0.4 g/cc between the bedrock and valley fill. A series of gravity lows were observed over Cedar Valley and the Harmony Mountains. The relatively large gravity low over the Rush Lake area (in Cedar Valley), with a closure of about -10 mgal, was modeled by Hardman (1964) as a graben with the maximum valley-fill thickness of about 4,000 ft (1,220 m), assuming a density contrast 0.4 g/cc between the bedrock and valley fill.

A high gravity ridge, with a steep gradient on the west side, was observed by Hardman (1964) over the upthrown side of the Hurricane fault zone along Cedar Mountain. He interpreted the gravity gradient as due partly to the Basin and Range normal type Hurricane fault, with downthrow on the west, and partly due to the Kanarra fold. The detail of each gravity feature will be discussed in the interpretation of the gravity map.

Magnetic Features

The general aeromagnetic features over southwestern Utah reveal a broad band of prominent gravity highs in the east-west alignment which corresponds with the eastward-trending Pioche-Marysvale igneous belt, approximately between lat 38°00' N and 38°30' N (see the aeromagnetic map of Utah, Zietz et al., 1976). The magnetic highs typically overlie the intrusive igneous rock exposures, and the magnetic lows are generally caused by the grabens filled with the non-magnetic sediments. As a result, the locally north-south-trending magnetic highs separated by magnetic lows which reflect the Basin and Range structures can also be seen within the broad eastward-trending region of the magnetic

highs.

To the south of lat 38°00' N, the trend of the magnetic features lies in a northeastward direction approximately over the present study area, with scattered magnetic highs. At about lat 37°30' N, a less prominent eastward-trending belt of magnetic highs overlies the intensive volcanic region of the east-west-trending Delamar-Iron Springs igneous belt.

The local magnetic patterns within the present survey area apparently reveal the near-surface structural variations throughout the region, in which the northeastward-trending intrusive bodies and the Basin and Range structural horsts and grabens (covered with various thicknesses of valley fill sediments and/or volcanic rocks) dominate the structural feature. The specific aeromagnetic anomalies and their relation to the geologic structures will be discussed in the later sections.

Comparison of Gravity and Magnetic Features

The similarity of the local gravity features and the aeromagnetic trends can be seen in the study area, although there does exist a major east-west-trending aeromagnetic feature that is different from the gravity trends beyond the study area on the north. This east-west-trending feature dominates the area along the Pioche-Marysvale intrusive belt. The study area lies within the southern portion of the extensive volcanic structural complex in southwestern Utah. The reason for the similarity in gravity and aeromagnetic trends may be related to the fact that the volcanism which occurred during the later period of

igneous activity in southwestern Utah was closely followed or accompanied by the Basin and Range tectonism. The features of the faulting and volcanism may have been much influenced by the older eastward-trending structure.

GEOLOGIC CONTROL

For the surface geology of the survey area, the geologic map of southwestern Utah by Hintze (1963) was used (Fig. 3). The survey area is covered mostly with alluvium in the valleys and volcanics over the high regions. The sedimentary rocks (most of which are Mesozoic in age) are exposed only around the intrusive belt of the Iron Spring district and in the Red Hills and Hurricane Cliffs areas. However, except in and near the intrusive belt, rocks of Paleozoic age are believed to exist in the basement throughout the study area. Therefore the densities of the rocks in the nearby areas, measured by other investigators, are necessarily used for the gravity interpretation. The density measurements made by Schmoker (1972), Carrier (1979), Serpa (1980), and Gabbert (1980) were especially studied to determine the densities of the rocks in this area. The magnetic susceptibility measurements made by Schmoker (1972) were also used for the brief analysis of the aeromagnetic map.

Sample Collection and Density Measurement

Rock samples of the common types were collected in the study area, and dry and wet density measurements were made. The dry density is actually the density of the exposed rock on the surface. However, the densities used in the gravity modeling should represent the densities of the rocks in the subsurface generally beneath the water table. (The water table is generally at a depth of about 200 ft (61 m) in the

valleys within the study area). Consequently, the rocks below the water table are under hydrostatic pressure at depth, and are considered to be essentially saturated with water. Moreover, it is believed that the measured wet density of the saturated rock measured represents better that of the rock at depth in the field. Therefore the wet densities of the saturated rock samples were measured in the laboratory to help evaluate the average density of certain rock types used in the gravity modeling. The methods and results of the dry and wet density measurements of the rock samples are described in Appendix C.

Drill Hole Information

The locations of all drill holes used for geologic control in this report are shown on Figures 3 and 4. Pertinent lithologic information of these drill holes, including abbreviated well logs, if available, is summarized in Appendix B.

An abandoned oil and gas well Little Salt Lake #1, drilled by Mountain Fuel Supply Company in 1963, is in the Red Hills area. The complete lithologic log of the well is available, and was used to help control the geologic cross section along profile D-D'. Another abandoned oil and gas well Fee #1-B, which is in the Escalante Desert near Table Butte, was drilled by Pan American Petroleum Corporation in 1971. The lithologic log of the well is partly available and can be used only qualitatively in the gravity map interpretation. An abandoned oil and gas well Shurtz Creek #1, in the Hurricane Cliffs area south of Cedar City, was drilled by Mountain Fuel Supply Company in 1973. The complete lithologic log of the well is used to help

control the geologic cross section along profile B-B'.

The geothermal test wells DeArman #1, State #1, and Jones #1, all of which are in the Escalante Desert, were drilled jointly by the McCulloch Oil Corporation, Incorporated, Geothermal Kinetics, Inc., and the Utah Power and Light Company in 1976. The complete well logs are available for the wells DeArman #1 and State #1; but only an abbreviated well log was made available to the author for the well Jones #1. The log of well State #1 is used to help control the geologic cross section of profile B-B'. The abbreviated log of well Jones #1 is used as a main control for the geologic cross section of profile C''-C'''. The log of well DeArman #1, which shows the geological subsurface feature which is difficult to correlate directly with that along the profile B-B', can be used only qualitatively in the interpretation of the gravity map.

DATA ACQUISITION, REDUCTION, AND COMPILATION

Gravity Data

During the summers of 1978 and 1979, a regional gravity survey was made with LaCoste and Romberg gravity meter No. 264 in the southern part of the Escalante Desert and vicinity. The survey consisted of 486 stations, including 50 stations coincident with those taken in the previous surveys. In addition to the 436 new stations, 917 other stations taken by Hardman (1964), the University of Utah GG521 gravity classes of 1965 and 1975, Selk (1974), Montgomery (1973), Kuennemann (1978), Gabbert (1980), and Green (1980) were used in this study. Table 1 shows the number of stations from each of these sources. A listing of all stations is given in Appendix A.

The sensitivity of the gravity meter is 1.05746 mgal/dial division and the reading can be obtained with an accuracy of 0.001 dial division with a repeatable precision of about 0.003 mgal. The U.S. Geological Survey 7-1/2-minute topographic quadrangle maps with a scale of 1:24,000 were used for horizontal control. Latitudes and longitudes were located within 0.01 min of arc, giving a location accuracy of about 50 ft (15 m).

Vertical control was obtained from bench marks and spot elevations on the topographic quadrangle maps where available, and a Wallace and Tiernan altimeter model No. 185 was used otherwise. About 70 percent of the elevations of the stations taken during the survey were controlled by bench marks or spot elevations. The altimeter was used to obtain the elevations of only about 30 percent of the stations. The altimeter was read to the

Table 1. Source of gravity data for gravity map (Fig. 4).

Station Designation	Area	Investigator	Year(s) of Survey	Approximate No. of Stations
AA000	Area A	Eckhard Kuennemann	1978	200
EH000	Eastern Escalante Desert	Elwood Hardman	1963-64	470
LU000	Lund	Donald Selk	1974	110
RG000	Enterprise	Ronald Green	1980	25
SG000	Wah Wah Range	Stephen Gabbert	1980	80
WP000	Escalante Desert	Win Pe	1980	480
WU000	Escalante Desert	Jerry Montgomery	1973	60
65B00	Minersville	GG521 Class*	1965	8
75200	Lund	GG521 Class*	1975	5

*University of Utah

nearest foot; and the altimeter drift was obtained by reading the instrument at stations with known elevation (bench mark or spot elevation) at approximately 1-hour intervals. It should be emphasized that taking altimeter readings was avoided during the early afternoon, when the atmospheric pressure usually changes rapidly.

The accuracy of the elevations of the stations are estimated to be generally as follows: a) 1 ft (0.3 m) (or corresponding to about 0.06 mgal) for the bench marks; b) 4 ft (1.2 m) (or about 0.24 mgal) for the spot elevations (i.e., 10 percent of the contour interval); and c) 10 ft (3 m) (or about 0.6 mgal) for the stations using the altimeter. It should be noted that the elevations of all altimeter stations were also independently estimated directly from the topograhic maps by interpolation between the topogrpahic contours and compared with the elevations obtained with the altimeter technique. The differences in elevation were generally within the range of 0 to 10 ft (0-3 m).

The Cedar City base station, which is one of the main base stations in the Utah gravity base station network and which has a published absolute gravity value of 979,429.16 mgal (Cook et al., 1971), was used as the main base for the entire survey. All of the stations were tied directly to this station. The Enterprise base station was not used during the survey. The observed gravity values at the 50 coincident stations were generally found to be within ± 0.5 mgal of the values observed in the previous surveys.

Using the University of Utah UNIVAC 1108 digital computer, the observed gravity values were drift-corrected (assuming linear drift) and reduced to give simple Bouguer gravity anomaly values. In the reduction, the International Gravity Formula (Swick, 1942) was used to obtain the

theoretical gravity at mean sea level. Then a total terrain correction of 0.05999 mgal/ft, which assumes a mean rock density of 2.67 gm/cc, was used. The tidal correction, which may be as large as 0.3 mgal, was not applied independently; but it would be partly taken into account in the assumed-linear drift corrections, previously mentioned.

Terrain corrections out to a radial distance of 166.7 km (100 miles) from each station (herein designated the "total terrain correction") were made using a computer program provided by the U.S. Geological Survey and modified for use on the University of Utah UNIVAC 1108 digital computer by Serpa (1980). For the program description, the reader is referred to Serpa and Cook (1980). The total terrain corrections for a total of 1,403 gravity stations in the study area were made with this program. For 156 of these stations, the total terrain corrections, as done by the computer, were greater than 3 mgal; and for these 156 stations only, therefore, the inner-zone terrain corrections to a radial distance of 0.895 km were separately calculated by hand, using the Hammer (1939) zone chart. For these same 156 stations only, the terrain corrections from a radial distance of 0.895 km to 166.7 km were separately calculated by the terrain-correction program. For a station within very rugged topography, the terrain correction out to a radial distance of 0.895 km from a station done by hand is believed to be more accurate than that done with the computer. For those stations with the total terrain corrections less than 3 mgal, which were calculated using only the computer, the difference between the inner-zone corrections computed by hand and those calculated by the computer was found to be within 0.02 mgal. This conclusion was based on about 20 judiciously selected stations with the total terrain corrections just less

than 3 mgal.

For the stations that lie in the flat areas, which constitute about 70 percent of the total 1,403 stations, the accuracy of the terrain corrections is probably within 0.05 mgal; however, the accuracy for the remaining 30 percent of the total 1,403 stations, which lie in steeper terrain, is probably within 0.1 mgal, except for a few stations in very rugged areas (Hurricane Cliffs area, for instance), where the maximum error may be possibly as large as 0.2 mgal. Accounting for the errors introduced by the inaccuarcy of the elevation of the station itself, by the tidal variation, by the terrain correction technique, by the possible density variation of the surface rocks from 2.67 g/cc (used in the Bouguer and terrain corrections), and by the instrumental drift, the total error in the complete Bouguer gravity anomaly values for about 70 percent of the total stations is probably within 0.4 mgal; and the error for the remaining stations (about 30 percent) is probably within 0.7 mgal.

Finally, the complete Bouguer gravity anomaly values (i.e., those that have been terrain corrected out to a radial distance of 166.7 km from each station) of 1,403 stations were plotted on the map using the UNIVAC 1108 digital computer and contoured by hand with a 2-mgal contour interval. Only one station was omitted from the complete Bouguer gravity anomaly map because its value was considered unreasonable and was probably caused by a reading error in the field.

Aeromagnetic Data

The aeromagnetic map of the study area (Fig. 5) was taken from the total intensity aeromagnetic map of southwestern Utah with a scale of

1:250,000 (U.S. Geologic survey, 1972 a, b, area labeled with L' in Aeromagnetic Map of Utah, Zietz, et al., 1976). The aeromagnetic survey was conducted by Scintrex Mineral Survey, Inc. at an altitude of 9,000 ft (2,744 m) barometric, with 2-mile (3.2-km) spacing of the flight lines in an north-south direction. The total intensity magnetic field on the map was drawn relative to an arbitary datum with contour intervals of 20 gammas in areas of small magnetic relief and 100 gammas (heavy lines) in areas of large magnetic relief. The accuracy of the observed magnetic field intensity values, which mainly depends on the correctness in location of the aircraft, is estimated to be within ± 10 gammas.

INTERPRETATION OF COMPLETE BOUGUER GRAVITY ANOMALY MAP

General Features

On the complete Bouguer gravity anomaly map (Fig. 4), the dominant trend of the gravity contours is approximately northeastward throughout most of the survey area. This trend is parallel to that of the Laramide folds and faults in the region and indicates that the Laramide orogeny has largely determined the trend of the dominant geologic structures in this part of the transition zone. Except for a few gravity features in the western part of the study area, the general appearance of the gravity map is one of elongate northeast-trending gravity troughs separated by gravity highs.

The Bouguer gravity anomaly values range from a high of about -182 mgal over the area lying west of Enterprise, to a low of about -230 mgal over Hamblin Valley. As discussed previously, the variation of the regional gravity over the broad gravity saddle that overlies the study area, is assumed to be negligible except in the easternmost part of the area. Near the western boundary of the Colorado Plateau, which is approximately between longitudes 112°45'W and 113°00'W in this area, the regional gravity anomaly values gradually decrease eastward with a gradient of about 0.4 mgal/km. A widespread region with relatively high Bouguer gravity anomaly values of about -190 mgal overlies (1) the belt of quartz monzonite intrusions in the Iron Springs district, (2) the Beryl and Table Butte areas in the Escalante Desert, (3) Mount

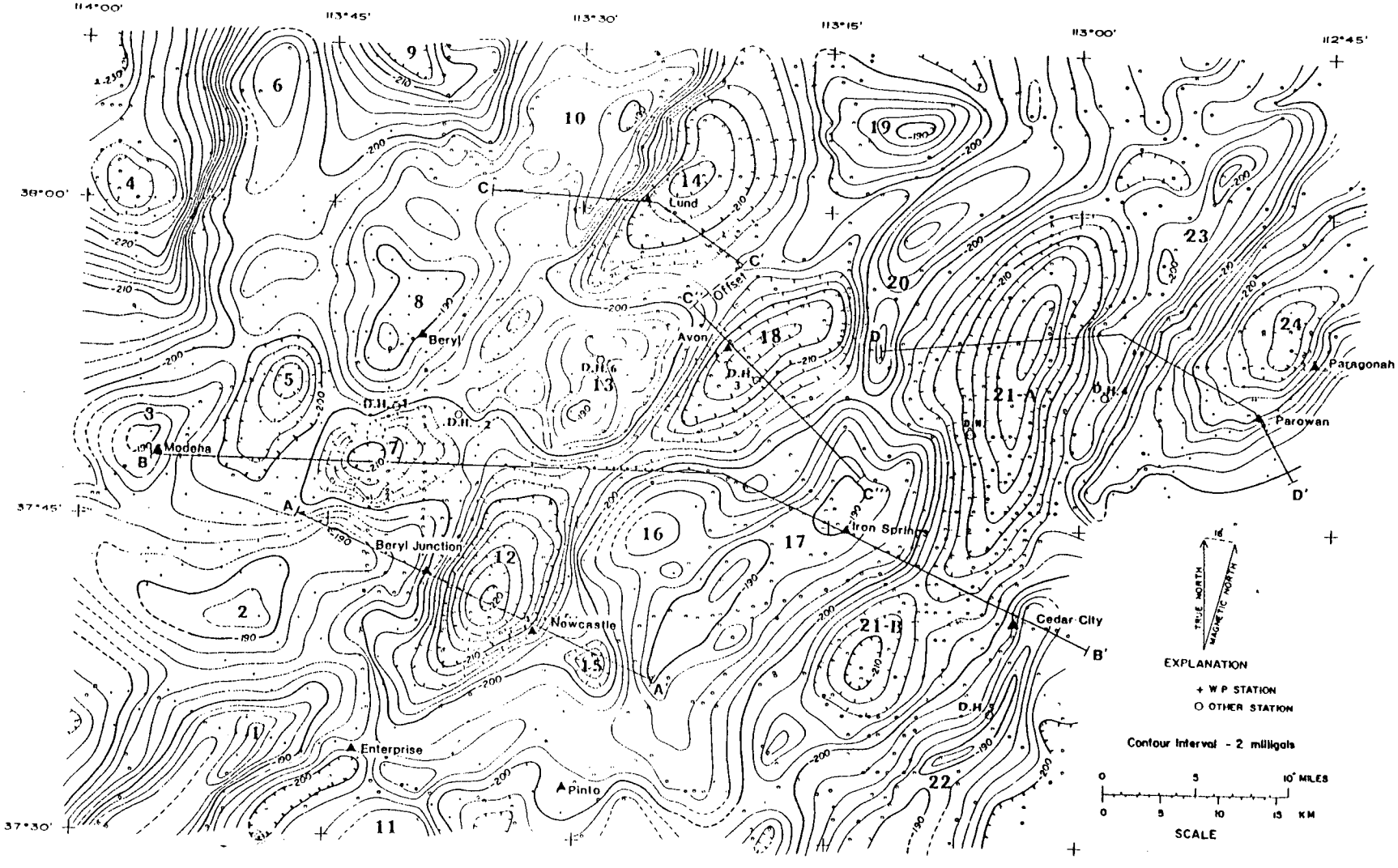

Figure 4. Complete Bouguer gravity anomaly map of the Escalante Desert and vicinity, Iron and Washington Counties, Utah.

Table 2. Identification and characteristics of gravity anomalies in Fig. 4.

No. of Area Designated in Fig. 4	Name of Gravity Anomaly	Amount of Closure (mgal)	Length of Anomaly (km)	Width of Anomaly (km)
1	Enterprise Reservoir gravity high	2	19	6
2	Mount Escalante gravity high	4	16	9
3	Modena gravity high	4	6	6
4	Hamblin Valley gravity low			
5	East Modena gravity low	6	13	6
6	Needle Range gravity high	2	12	5
7	South Beryl gravity low	8	12	8
8	Beryl gravity high	4	12	6
9	Pine Valley gravity low			
10	Wah Wah Range gravity high			
11	Big Mountain gravity high			
12	Newcastle gravity low	14	22	6
13	Table Butte gravity high	6	15	11
14	Lund gravity low	8	22	10
15	Pinto gravity low	4	4	4
16	Antelope gravity high	1	9	6
17	Iron Springs gravity high	4	30	10
18	Avon gravity low	8	19	9
19	Black Mountains gravity high	10	12	9
20	Gravity ridge north of The Three Peaks			
21-A	Cedar Valley gravity low (north)	12	31	11
21-B	Cedar Valley gravity low (south)	4	12	8
22	Gravity ridge over Hurricane Cliffs			
23	Red Hills gravity high	4	35	5
24	Parowan Valley gravity low	2	22	12

Escalante and the vicinity west of Enterprise, (4) the western portion of the Black Mountains, and (5) Cedar Mountain. The major gravity lows, which overlie Hamblin Valley, the Escalante Desert, Cedar Valley, and Parowan Valley, range from about -210 mgal to -230 mgal. A detailed discussion of individual gravity anomalies will be made in the following sections.

Iron Springs Gravity High

In the Iron Springs area, a northeastward-trending gravity high, approximately 30 km long, with about 6-mgal closure, coincides approximately with the aligned intrusive bodies (quartz monzonite porphyry) of Stoddard Mountain, Iron Mountain, Granite Mountain, and The Three Peaks (area 17, Fig. 4). The contrast in average density of 2.7 g/cc for the intrusive rocks and 2.5 g/cc for the surrounding Mesozoic and Tertiary sedimentary rocks, results in the correlation of the gravity highs with the intrusive bodies. The southern end of the gravity high, over Stoddard Mountain, is apparently offset to the southeast from the main alignment. This left-lateral offset of the gravity anomaly may indicate a major fault system between Iron Mountain and Stoddard Mountain. Such a fault system, if present, could possibly exert structural control on the emplacement of the iron ore. It should be noted that the Stoddard Mountain quartz monzonite body, unlike the three others to the north, is barren of iron ore, whereas the others are associated with replacement iron ore bodies. The continuity of the elongate gravity high, with a closure of about 2 mgal, over the alluvium-covered area between Iron Mountain and Granite Mountain

indicates the continuity also of the quartz monzonite at relatively shallow depth in this area. The continuity of the quartz monzonite in this area at shallow depth (about 900 ft (274 m)) has been confirmed by aeromagnetic surveys (Blank and Mackin, 1967) and by deep drilling (K. L. Cook, 1980, personal communication).

The continuous gravity high about 30 km (19 mi) in length which extends over and beyond the Iron Springs district (Fig. 4), and other geological, geophysical, and drill data indicate that: (1) a great quartz monzonite porphyry mass is probably not only continuous at relatively shallow depth between each of four individual intrusions, but also extends widespread in the subsurface through at a larger area in southwestern Utah; (2) the now-exposed intrusions which were formed along Laramide zones of weakness constitute only a small part of the entire igneous mass at depth (Cook and Hardman, 1967).

Furthermore, Cook and Hardman (1967) emphasized that the crest of the gravity ridge is generally centered west or northwest of the outcropping intrusions and that therefore the main mass of quartz monzonite porphyry is probably buried at relatively shallow depth to the west and northwest of the exposures of porphyry, and that this interpretation is consistent with two separate magnetic high anomalies with northeastward alignment about 2 mi (3.2 km) west of the main magnetic high anomalies over the intrusive rock exposures on the aeromagnetic map by Blank and Mackin (1967).

A prominent gravity high centered over the Antelope Range, which lies northwest of Iron Mountain, appears as an offshoot of the belt of the gravity anomalies approximately over the intrusions. Although the

gravity stations in the Antelope Range area are sparse due to inaccessiblity over the central area of this anomaly, the data around its flank are sufficient to define the high. Two possibilities for the causative body of the Antelope Range gravity high suggested by Hardman (1964) are: (1) the extension of the monzonite intrusion northwestward from Iron Mountain to the Antelope Range area; (2) the northwestward extension of a great structural block throughout the Iron Springs district that is bounded by faults and thick alluvium and/or volcanics at its margin.

The second possibility seems less likely for the following reasons: (1) the gravity high of about -192 mgal is probably caused only by rock with high density (2.7 to 2.8 g/cc), such as intrusive igneous rock or Paleozoic sedimentary rock, at shallow depth in the study area; (2) the main Laramide thrust sheet of such Paleozoic rocks which may exist at shallow depth, probably does not extend far enough southeastward in the Iron Springs district; (3) the structural block of upper Mesozoic rock might exist underneath the Antelope Range, but an exposed Mesozoic structural block in the Red Hills area contributes a maximum gravity high of only about -198 mgal.

The first possibility, that the gravity high may be attributed to an igneous mass with high density at shallow depth under the Antelope Range, now seems more probable. A small magnetic high (of about 20-gammas closure) also occurs over the northern part of the Antelope Range on the aeromagnetic map (Fig. 5). Therefore, it is conceivable that an intrusive igneous body occurs beneath the volcanic rock of the Antelope Range at shallow depth, which may have the same origin as the

Iron Springs intrusions.

Newcastle and Pinto Grabens

A large negative gravity anomaly exists in the Escalante Desert west of Newcastle (area 12, Fig. 4). The anomaly indicates as a northwest-trending graben which represents one of the dominant Basin and Range features previously controlled by the Laramide structure in this area. This graben is herein designated the "Newcastle graben".

On the east side of the graben, the trend of the pronounced gravity gradient coincides with the northeastward-trending margin of the desert floor on the west side of the Antelope Range north of Newcastle. However, at Newcastle the trend of the gravity gradient changes from south-southwest (S20°W) to southwest (S45°W); and this change in gravity trend indicates an abrupt change in the direction of faulting. The abrupt change in trend of the fault zone suggests a triple junction of faults, with one of the faults trending southeastward. The southeastward-trending fault probably extends from Newcastle southeastward along the southwestern margin of a small gravity low, which is located about 6 km east of Newcastle (area 15, Fig. 4). This circular gravity low may be caused by a small graben possibly resulting from gravity sliding near the Iron Springs intrusion. This graben is herein designated the "Pinto graben". The above-mentioned southeastward-trending fault zone probably extends southeastward to the area along Little Pinto Creek, which lies on the southwest side of Stoddard Mountain.

Lund and Avon Grabens

A northeast-trending gravity low (area 14, Fig. 4) exists in the Escalante Desert near Lund. The gravity low indicates a northeastward-trending graben, which was designated the "Lund graben" by Cook and Hardman (1967). A northeastward-trending late Pleistocene fault zone was independently mapped by Anderson and Miller (1979) along the area that corresponds with the gravity gradient on the west side of this gravity low.

Another northeastward-trending gravity low, approximately equal in size to the Lund gravity low, exists in the Escalante Desert near Avon (area 18, Fig. 4). The gravity low is separated from the Lund gravity low by a gravity ridge which extends between Table Butte gravity high and the Black Mountains gravity high (to be discussed later). The gravity low indicates a northeastward-trending Basin and Range-type graben, which was designated the "Avon graben" by Cook and Hardman (1967). Geothermal test well Jones #1 is located within the gravity low about 3 km south of its center. The drill failed to reach bedrock after penetrating a total thickness of 5,855 ft (1,785 m) of Cenozoic sediments and volcanics. A Schlumberger resistivity sounding survey in this area by Geothermal Kinetics, Inc., indicates that the bedrock is probably located at a depth of about 6,000 to 7,000 ft (1,829 to 2,134 m) (Dr. Norman Harthill, 1980, personal communication). The Newcastle gravity low is separated on the south from the Avon gravity low by a gravity ridge which lies between the Table Butte gravity high and the Antelope Range gravity high. Two northeastward-trending late Pleistocene faults were independently mapped by Anderson and Miller

(1979) along the area that corresponds approximately with the gravity gradient between the Antelope Range gravity high and the Avon gravity low.

East Modena and South Beryl Grabens

In the Escalante Desert, two intermediate gravity lows exist between the Modena gravity high (discussed later) on the west and the Newcastle gravity low on the east. One gravity low, which lies east of the Modena gravity high (area 5, Fig. 4), is herein designated the "East Modena gravity low". The gravity low is bounded on the north by a small, northward-trending gravity high over the Needle Range and on the south by the elongate, approximately east-west-trending Mount Escalante gravity high (discussed later).

The only eastward-trending gravity low in the study area lies east of the East Modena gravity low (area 7, Fig. 4). The gravity low, herein designated the "South Beryl gravity low," is bounded on the north by the Beryl gravity high (discussed later) and on the south by the Mount Escalante gravity high.

Because these two gravity lows, with abnormal trend and character, are located within the unusual environment of the gravity patterns, the subsurface geological features that cause these anomalies are assumed to be different from those of the northeastward-trending gravity lows which generally correspond with the Basin and Range grabens in the study area. It is commonly accepted that the northward-to northeastward-trending Basin and Range fault system in the study area is apparently the result of tectonic activity associated with

approximately east-west extension in southwestern Utah (Stewart, 1978). Consequently, the South Beryl gravity low, which shows an eastward alignment, was probably caused by an east-west-trending graben as a result of the tectonic system associated with north-south extension. If so, this tectonic system probably occurred before the period of intensive Basin and Range tectonic activity (with east-west extension). Consequently, the east-west-trending graben causing the gravity low, was probably activated during the time of the east-west trending igneous activity which started before the Basin and Range tectonism.

Another subsurface geologic feature that possibly causes the South Beryl gravity low is the vent of a collapsed caldera which was subsequently filled with low-density volcanic materials. Crosby (1973) has postulated a possible caldera in this general area. However, according to the drill data of geothermal test well DeArman #1, which is located about 5 km north of the center of the South Beryl gravity low, this possibility is obscure. Test well DeArman #1 penetrated sedimentary rock of Paleozoic (?) age after passing through about 1,600 ft (488 m) of late Cenozoic sedimentry rock and about 3,000 ft (915 m) of overlying volcanics. Conceivably, the South Beryl gravity low may be merely attributed to a down-faulted basement block of sedimentary rock, surrounded by the belt of igneous intrusions.

The subsurface geologic feature that causes the East Modena gravity low may be similar to that postulated above as causing the South Beryl gravity low. However, the graben which causes this gravity low seems to be slightly affected by the Laramide thrusting activity because of its northward trend. The northward-trending

gravity ridge between these two gravity lows is possibly caused by thrusted sedimentary rock underlain by a zone of igneous intrusion.

Table Butte Horst

In the Escalante Desert, a gravity high overlies Table Butte and the adjacent area (area 13, Fig. 4). Cook and Hardman (1967) interpreted this gravity high as caused by a horst that they designated the "Table Butte horst". Two separate small gravity highs, with northward trend and alignment, exist within the main Table Butte gravity high. One gravity high, with the smaller amplitude, is located about 2 km west of Table Butte proper; and the other, with the larger amplitude, is located about 6 km southwest of Table Butte. A gravity nose extends southwestward from the Table Butte gravity high toward the South Beryl gravity low. The Table Butte gravity high is herein interpreted as caused by an intrusive body, and the branches of this body may extend southwestward and southeastward at relatively greater depth. The quartz monzonite that was penetrated in geothermal test well State #1 is probably the southwestward extension of this body. This interpretation depends on the detailed petrologic log of the quartz monzonite penetrated in that well, which indicated that the drill failed to penetrate the main quartz monzonite mass, but rather apparently penetrated the edge of a major intrusive body located nearby.

The two separate northward-trending gravity highs are probably caused by two separate intrusions at shallow depth, which are cupolas or offshoots from the main quartz monzonite mass at greater depth. It

should be emphasized that in test well State #1, quartz monzonite was penetrated at a depth of 1,890 ft (576 m), which was immediately below the late Cenozoic sedimentary rocks. These drilling results suggest that in this area, deep erosion occurred after the quartz monzonite had intruded. An abandoned oil and gas well Fee #1-B is located between the two separate gravity highs just west of Table Butte. Although the complete drill data are not available, it was learned that the Claron Formation was penetrated at a depth of about 2,900 ft (884 m). This information suggests that the Claron Formation may exist on the flank of a dipping sedimentary series arched up by the intrusion. Furthermore, if there is a connection of the intrusive bodies under Table Butte and Antelope Range, then the connecting mass probably supports the horst underneath between the Newcastle graben and Avon graben.

Beryl Horst

A gravity high over the Beryl area (area 8, Fig. 4), is herein designated the "Beryl gravity high." The Beryl gravity high is probably caused by a complex structural high at shallow depth composed of pre-Tertiary sedimentary rocks associated with igneous intrusive bodies. The northeastward extension of the gravity high from the Beryl area to the southern end of the Wah Wah Range is probably caused by basement sedimentary rock at shallow depth with the possible northeastward-trending boundary on the east side. The Beryl gravity high is bounded on the south by a high gravity gradient, located between the Beryl high and the South Beryl gravity low. The total

gravity relief across the slope (peak to trough) of this gradient is about 22 mgal within a distance of 11 km and is possibly caused by a series of parallel faults downthrown on the south. In geothermal test well DeArman #1, which is approximately at the midpoint of this slope, the drill penetrated a fracture zone in the basement sedimentary rocks at a depth of between 7,710 ft (2,354 m) and 8,465 ft (2,581 m), and slickensides were found occasionally at a depth of between 7,000 ft (2,134 m) and 9,500 ft (2,896 m). This information partly supports the interpretation of a series of faults located on the north side of the South Beryl graben. The small gravity low between the Beryl gravity high and Table Butte gravity high may be caused by a northeastward-trending graben (or valley) which possibly forms the southwestward-extension of the Lund graben.

Black Mountains Gravity Highs

A pronounced gravity high exists near the eastern margin of the Escalante Desert over the western part of the Black Mountains (area 19, Fig. 4). The anomaly appears to be nearly circular-shaped, or oval-shaped with an easterly trending elongate pattern. Because it is recognized that in the study area the eastward-trending gravity anomalies are probably not related to the subsurface geologic features that were principally formed by the Laramide tectonic activity, this gravity high may represent a structural block at relatively shallow depth, disrupted by one or more deeply rooted igneous masses. Thus, the gravity high may indicate an area of volcanic eruptive vents lying under the Black Mountains. As there is no pronounced high magnetic

anomaly observed directly over the area of this gravity high, the upper part of the main causative igneous body (if one exists) may be composed of silicic volcanic materials. A series of northeast-trending suspected Quaternary faults was independently mapped by Rowley (1977) along the area that corresponds approximately with the southeast margin of this gravity high.

A narrow belt of gravity highs trending in approximately northwestward alignment is located along (or near) the east side of the gravity high discussed above. The gravity belt, which is about 6 km in width, extends northward from the northern end of the Iron Springs gravity high, then bends northeastward along the northwestern boundary of the Cedar Valley gravity low, and then continues northward again over the Black Mountains and beyond the study area. The gravity ridge is possibly caused by a northward-trending narrow horst composed of the pre-Tertiary sedimentary rocks possibly shaped by the minor thrusting in front of the main Laramide thrust. A zone of northward- to northeastward-trending late Pleistocene and suspected Quaternary faults were mapped by Anderson and others (1978) along the area that corresponds approximately with the eastern flank of this gravity ridge.

Gravity Anomalies over the Needle Range Area

An approximately circular gravity high over Modena and vicinity (area 3, Fig. 4) is probably caused by a block of Paleozoic sedimentary rock at shallow depth.

A northward-trending small gravity high was observed over the southern end of the Needle Range despite the sparse gravity data in

this rugged area (area 6, Fig. 4). The gravity high is probably caused by Paleozoic sedimentary rocks beneath the volcanic cover at shallow depth. The Needle Range was interpreted by Gabbert (1980) as a northward-trending horst which has been tilted east.

The gravity anomaly values decrease to about -230 mgal over Hamblin Valley. Even though the gravity data were taken only in the southeastern part of the valley and the gravity anomaly is not closed on the gravity map, the gravity low is probably caused by a Basin and Range-type graben (Gabbert, 1980). A steep gravity gradient, with an average value of about 4 mgal/km, overlies the eastern margin of the southern end of Hamblin Valley. The gravity gradient indicates a steeply dipping normal fault, with downthrow on the west, which separates the Hamblin Valley graben from the Needle Range horst. The gravity data indicate a total vertical throw of approximately 11,400 ft (3,475 m) along the zone (Gabbert, 1980).

A gravity low was observed over the southern end of Pine Valley (area 9, Fig. 4). This gravity low, which is bounded on the east by the Wah Wah gravity high and on the west by the Needle Range gravity high, indicates a graben (Gabbert, 1980). For the interpretation of the gravity anomalies over the major portion of this region beyond the study area to the north, the reader is referred to the M.S. thesis by Gabbert (1980).

Enterprise Reservoir Gravity High

A northeastward-trending gravity high overlies the area about 10 km west of Enterprise (area 1, Fig. 4). The feature is herein

designated the "Enterprise Reservoir gravity high." As the gravity stations are sparse in this area, the contours on the southern part of the anomaly (near the southern margin of the survey area) are inferred. However, the gravity gradients on the east, north, and west margins of the anomaly shows the prominent northeastward-trending gravity high which overlies this area. The gravity high is interpreted as caused by a northeastward-trending structural high in the near-surface basement rocks resulting mainly from the Laramide orogenic activity. The steep gravity gradient on the southeast side of the anomaly may indicate a steeply dipping fault which was formed at the western margin of the Reservoir trough during the period of the Basin and Range tectonism after the Reservoir trough was formed accompanying the Bull Valley- Big Mountain intrusion (Blank, 1959). The gravity gradient on the west side of the anomaly may be interpreted as caused by a northeastward-trending normal fault with downthrow on the west. Nevertheless, the relatively small gradient on the north side of the anomaly may be caused by density contrasts related to a different tectonism, which will be discussed in the interpretation of the Mount Escalante gravity high.

The northeastward-trending small gravity low which lies on the southeast side of the Enterprise Reservoir gravity high, was observed near Enterprise. This gravity low is probably caused by the low-density sediments within the Reservoir trough. Although there are a few rhyolitic and basaltic intrusions and uplifted blocks within the Reservoir trough region (Blank, 1959), the differences of the density distribution in the region may not be high enough to give the separate

gravity features.

Big Mountain Gravity High

A small gravity high exists over Big Mountain, about 7 km southeast of Enterprise; however, there is no closure of the gravity contours within the mapped area (area 11, Fig. 4). The high is herein designated the "Big Mountain gravity high". The gravity high is possibly caused by the doming of the Mesozoic sedimentary rocks by the igneous intrusion along the Bull Valley-Big Mountain Laramide structure, which may be the southwestward extension of the Iron Springs intrusion (Blank, 1959). The small northeastward-trending gravity high, with 2-mgal closure, which is located immediately north of the Big Mountain gravity high, is probably caused by a structural high (in the basement rocks) that is a northward extension of the Big Mountain intrusive arch.

A small gravity low, without any mapped closure on the gravity map, exists on the east side of the Big Mountain gravity high and is probably caused by a structural low (in the basement rocks) that is filled with low-density volcanics and/or sediments. A small gravity high, without closure, which occurs near the southern boundary of the survey area immediately southwest of Stoddard Mountain, may represent a structural high (in the basement rocks) that is probably related to Iron Springs doming-up structure.

Mount Escalante Gravity High

A broad, eastward-trending gravity high overlies Mount Escalante and vicinity, (area 2, Fig. 4). Despite the sparse gravity data over

the western part of this area, the pronounced gravity high, with a maximum gravity anomaly value of about -188 mgal, clearly exists over this region. The gravity high is herein designated the "Mount Escalante gravity high". The gravity high is apparently located within the surrounding gravity anomalies, the features of which seem to be incompatible with this high at the center. The isolation of the trend of the gravity high from that of the surrounding gravity anomalies suggests the possibility of major structural breaks between the causative body and the surrounding structures. One possibility of the cause of the gravity high is a block of basement sedimentary rock, located at shallow depth, which has been displaced laterally by a strike-slip fault system. If so, it is conceivable that this structural block was previously the continuation of the northeastward-trending Enterprise Reservoir basement structure that was later displaced by a left-lateral movement along the eastward-trending strike-slip fault. The eastward extension of this postulated left-lateral fault possibly coincides with the corresponding left-lateral offset of Stoddard Mountain from the main alignment of the belt of Iron Springs intrusions. If such a strike-slip fault exists, its horizontal displacement may be as large as about 8 km. However, the alignment of the Bull Valley-Big Mountain intrusive arch (south of Enterprise beyond the study area, along the dominant trend of the Iron Springs intrusive belt, as postulated by Blank (1959)) can be seen without pronounced offset on the aeromagnetic map of Utah (Zietz et al., 1976). Consequently, this inference seems to be unfavorable.

A second possibility of the cause of the Mount Escalante gravity

high is an igneous body composed of dense silicic volcanic materials at shallow depth. Moreover, the aeromagnetic map does not show a pronounced broad magnetic high over this area probably because of the absence of basic intrusive materials in the upper portion of the igneous body. The gravity ridge between the South Beryl graben and Newcastle graben may represent a horst supported by a linking of the igneous intrusion between the intrusive body beneath the Table Butte area (previously postulated) and the postulated igneous body under the Mount Escalante gravity high at a certain depth.

Cedar Valley and Parowan Valley Grabens

Two northeastward- to northward-trending gravity lows extend across the Cedar Valley area (area 21, Fig. 4). The more pronounced gravity low coincides with Cedar Valley approximately between Cedar City and the southern foothills of the Black Mountains (area 21-A, Fig. 4). This anomaly indicates a graben. The gravity gradients on either side of the anomaly indicate that the graben is bounded on the west by a pronounced fault zone and on the east by a fault zone butted against the west side of Red Hills structural block. Water wells and an abandoned oil and gas well, which have been drilled in Cedar Valley, indicate that the thickness of the valley fill is greater than 960 ft (295 m), which is the depth of the deepest well in the valley for which data are available (Hardman, 1964).

The other gravity low, on the south, with a closure of about 4 mgal, is separated by a small gravity ridge near Cedar City from the gravity low described above (area 21-B, Fig. 4). This gravity low is

located over Quichapa Lake area in the southern part of the Cedar Valley area, between Cedar City and the Harmony Mountains. The gravity low also indicates a graben.

The trend of the gravity lows over Cedar Valley extends southwestward generally parallel to the Hurricane Cliffs, through the New Harmony area, Grass Valley and beyond (Cook and Hardman, 1967). The two above-discussed grabens were designated jointly as the "Cedar Valley graben" by Cook and Hardman (1967). However, the graben probably comprises two separate structural blocks.

A northeastward-trending gravity low over Parowan Valley area exists with a minimum gravity value of about -228 mgal at the center (area 24, Fig. 4). Although the contours are not completely closed on the northeast part of the anomaly, the main portion of the anomaly lies within the survey area. The gravity low indicates a graben, herein designated the "Parowan Valley graben," between the Red Hills horst on the west and the structural high associated with a monocline (Threet, 1952a) on the southeast.

Red Hills Gravity High

A long, narrow, northeastward-trending gravity ridge overlies the Red Hills area (area 23, Fig. 4). The gravity ridge overlies exposures of Mesozoic sedimentary rock that form the structural block between the Cedar Valley graben on the west and the Parowan Valley graben (discussed later) on the east. According to the drill data of the Mountain Fuel Supply Company Little Salt Lake #1 well, located about 10 km southwest of Parowan Gap along the gravity ridge, quartz monzonite

was penetrated at a depth of about 3,490 ft (1,064 m). This quartz monzonite is possibly a northeastward extension of the Iron Springs intrusion. The discontinuity of the high gravity trend over the region between The Three Peaks and the Red Hills area is probably due to the domination of the gravity effect caused by the Basin and Range faulting over that of the igneous intrusion. For a more comprehensive discussion of the gravity discontinuity over the valley, the reader is referred to Cook and Hardman (1967).

Gravity Ridge over the Hurricane Fault Zone

The northern end of the Hurricane fault zone extends for a distance of about 24 km from Cedar City to the southeastern margin of the study area (area 22, Fig. 4). In this portion of the fault zone, it is conceivable that the steep gravity ridge corresponds mainly with Black Ridge, which is an upthrown faulted narrow block composed primarily of Paleozoic sedimentary rocks, covered with a relatively thin layer of lower Mesozoic units and (in some places) Quaternary basalt at the top. This interpretation is suggested by the abandoned oil and gas well Schurtz Creek #1 (located about 8 km south of Cedar City over the Black Ridge) that penetrated Paleozoic sedimentary rock at a shallow depth of about 746 ft (227 m) after passing through Mesozoic sedimentary rocks.

Trend Analysis of Gravity Map

Northward to northeastward trends.--On the eastern portion of the survey area (Fig. 4), a northeastward trend of gravity highs overlies the Hurricane fault zone and continues northeastward along the Red

Hills gravity ridge. The fact that this trend of gravity highs lies aproximately along a straight line in a northeastward direction, may indicate that the underlying geologic structures occur mainly as a result of the Basin and Range faulting system along the Laramide zone of weakness, and under less influence of the igneous intrusion in this region. A north- to northeastward-trending zone of gravity lows occurs along Cedar Valley on the west side of the above-mentioned gravity high trend. Within this zone of gravity lows, the trend of the gravity low on the west side of the Red Hills is approximately northward, whereas the overall trend of the zone is northeastward. This change in trend of the gravity lows may indicate that the northern part of the Cedar Valley graben was formed primarily under the influence of the regional north-south-trending Basin and Range faulting system.

Another gravity high with northeastward trend occurs over the Iron Springs intrusive bodies and extends northeastward along a narrow high gravity zone on the west side of the northern part of the Cedar Valley graben. The overall high gravity trend includes the relatively irregular individual gravity highs. This fact probably suggests that the subsurface structures along the different parts of the trend, have undergone different tectonic activities. In other words, the entire gravity high trend may represent a weak zone of minor thrusted sedimentary structure in front of the main Laramide thrust; however, at later periods, the southern portion of the trend was probably modified by the Iron Springs igneous intrusion, and the northern portion, without intrusion at shallow depth, is probably more influenced by the Basin and Range tectonism.

Another northeastward-trending gravity feature, on the west side of the Iron Springs gravity high, contains both high and low gravity anomalies. This trend includes the Newcastle gravity low, the Lund gravity low, and the Table Butte gravity high in the middle. In this case, the Avon gravity low is assumed to be excluded from this northeastward-trending alignment, although the underlying Avon graben resembles a Basin and Range structure. The Avon graben was apparently formed within a limited region during the Basin and Range tectonism among the complex structural features associated with the igneous intrusions, rather than formed along the general trend under Basin and Range structural control. Along the northeastward-trending gravity alignment, it should be noted that steep gravity gradients occur along the west side of the Lund gravity low, the Newcastle gravity low, and the small gravity low (located on the east side of the Enterprise Reservoir gravity high). The geologic structures along this trend were probably shaped by the locally intensive Basin and Range tectonism along the northeastward- trending narrow zone, located near the east side of the main Laramide thrust.

Eastward to southeastward trends.--Three relatively pronounced trends of the boundaries of the gravity anomalies, with a southeast direction (approximately S 60° E), exist on the gravity map (Fig. 4). The first (and northermost) trend extends southeastward from the southern end of the Pine Valley gravity low to approximately the southern end of the Red Hills gravity high, across the northern boundaries of the Beryl gravity high and the Table Butte gravity high,

the center of the Avon gravity low, and the northern end of the Iron Springs gravity high.

The second (and middle) trend extends over the approximate northern boundaries of the East Modena gravity low, the South Beryl gravity low, the Newcastle gravity low, the Antelope gravity high, and the small gravity saddle between The Three Peaks gravity high and the Granite Mountain gravity high, and continues over the small gravity ridge across Cedar Valley near Cedar City.

The third (and southern) trend lies along the approximate southern boundaries of the East Modena gravity low and the South Beryl gravity low, and extends southeastward across the center of the Newcastle gravity low, the town of Newcastle, and continues over the southern end of the Iron Mountain gravity high, the southern margin of the gravity low in the southern part of Cedar Valley, and extends over the offset of the gravity ridge in the Murie Creek fault area (Cook and Hardman, 1967) within the Hurricane fault zone.

The southeastward-trending zone of the gravity features within these three trends probably corresponds with the subsurface geological variations. These features are partly shaped by a southeastward-trending structural control which may be related to a belt of minor igneous intrusion across the Escalante Desert (which will be discussed later).

REGIONAL FEATURES OF THE AEROMAGNETIC MAP

The aeromagnetic data were taken at a constant barometric elevation of 9,000 ft (2,744m), along north-south flight lines with a separation of 2 mi (3.2 km). The contour intervals are 100 gammas (heavy lines) and 20 gammas (thin lines) on the aeromagnetic map (Fig. 5). The earth's magnetic field in this region has an approximate declinaton of 16°E, an inclination of 64°N, and a total field strength of approximately 54,000 gammas (Vestine and others, 1947). A plane regional magnetic field corresponding to the gradient of the earth's main magnetic field of about 9.0 gammas per mi (5.63 gammas per km), increasing about N30°E has been removed on the aeromagnetic map. The elevations of the area range from about 5,000 ft (1,524 m) on the desert floor to about 8,000 ft (2,439 m) on the peaks of the high mountains. Consequently, the aeromagnetic anomalies are possibly attributed to the topography to a large extent; and therefore in this report, only the general trends and characteristics of the large regional magnetic anomalies, rather than the small local magnetic anomalies, will be discussed.

The overall character of the aeromagnetic map shows regions of magnetic highs over the Needle Range area and the Black Mountains. These high magnetic regions may correspond mainly with the regional magnetic anomaly and the topographic anomalies, even though there may be other magnetic regional effects due to deeper structures.

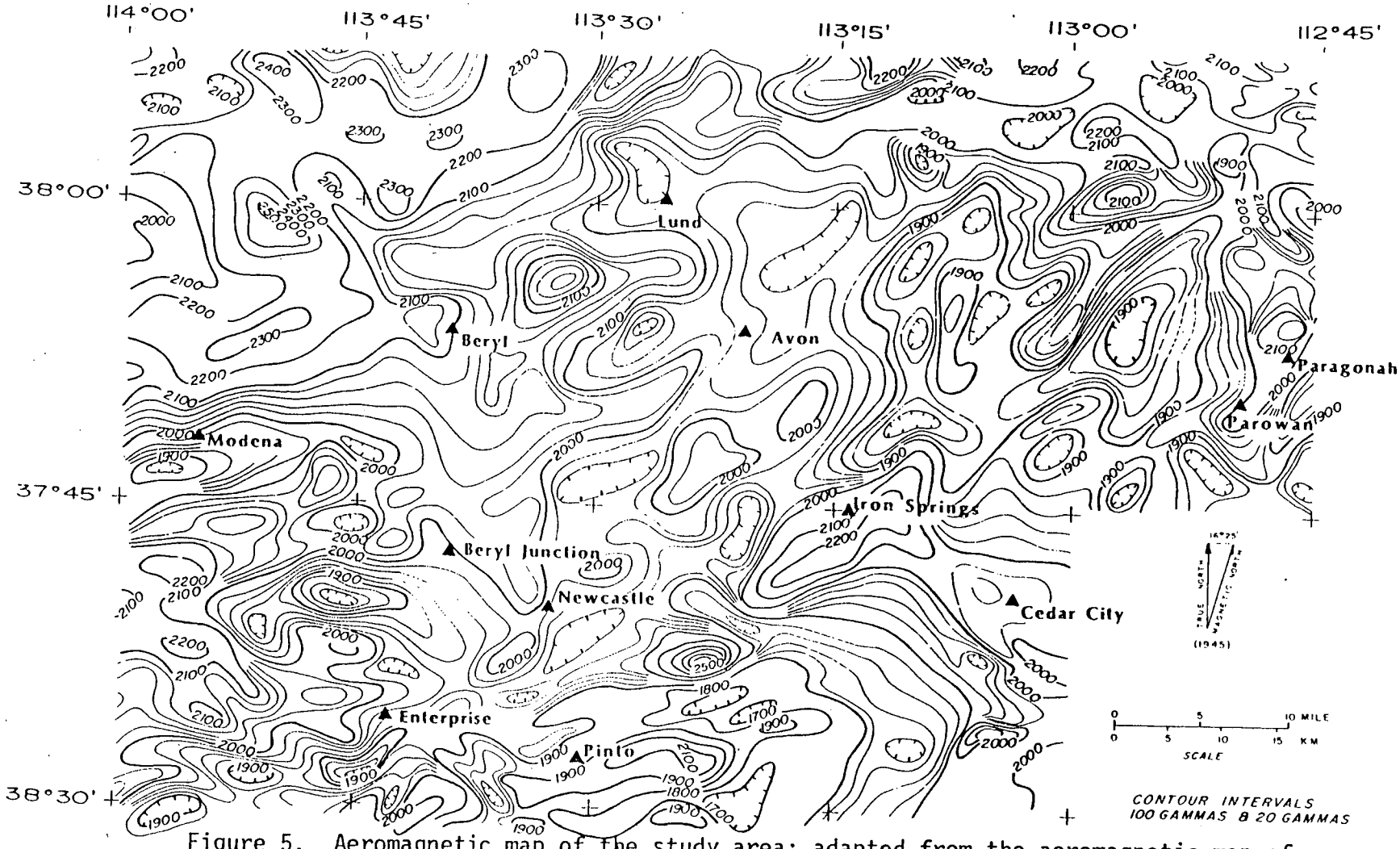

Figure 5. Aeromagnetic map of the study area; adapted from the aeromagnetic map of parts of the Richfield and Cedar City 1° by 2° quadrangles, Utah, with a scale of 1:250,000 (U.S. Geological Survey, 1972 a, b, area labeled with L' in Aeromagnetic Map of Utah, Zietz et al., 1976).

A zone of prominent magnetic highs and lows, which overlies the hilly region near Enterprise and the Iron Springs district, extends northeastward to join the region of the magnetic highs over the Black Mountains. Magnetic contours with only gentle magnetic relief overlie most of the flat surface of the valley areas, where there is little or no local magnetic disturbance.

Eastward- to Northeastward-Trending Magnetic Features

The most pronounced northeastward-trending belt of magnetic anomalies in the study area overlies the belt of the Iron Springs quartz monzonite intrusive bodies. The average high magnetic susceptibility values of 0.00345 cgs units for the intrusive rocks, in contrast with that of 0.00028 cgs units for the alluvium (Schmoker, 1972), causes the high magnetic anomalies over the intrusions. These magnetic susceptibility values were taken by Schmoker (1972) from the measurements of samples of quartz monzonite from the San Francisco Mountains and vicinity, located about 20 km north of the northern margin of the present survey area. The elongate magnetic high over Granite Mountain and The Three Peaks has a closure of about 100 gammas. The magnetic high is partly caused by the high topography of the mountains. This suggestion is supported by the isolated magnetic high, with a closure of about 400 gammas, over Iron Mountain, which is about 1,000 ft (305 m) higher in elevation than the other two.

The possible northward extension of the elongate magnetic high over Granite Mountain and The Three Peaks is found in Cedar Valley, in the area lying west of the Red Hills, after a gap of about 6 mi (10

km). From this area, a magnetic ridge extends northeastward and merges into the magnetic high over the Black Mountains. The continuation of the magnetic ridge, west of the Red Hills, may correspond with the extension of the quartz monzonite body at shallow depth beneath this area. The magnetic low over the Red Hills is consistent with the lower average magnetic susceptibility of 0.00004 cgs units for consolidated sedimentary rocks and the relatively higher average magnetic susceptibility of 0.00028 cgs units for alluvium (Schmoker, 1972).

Similarly, the northward-trending belt of magnetic lows, which extends northward from the northern end of the Iron Springs magnetic high to the western portion of the Black Mountains, is possibly caused by a northward-trending ridge, composed of sedimentary rocks with low magnetic susceptibility at shallow depth. Across the southern part of Cedar Valley, a magnetic ridge, which extends southeastward from the Iron Springs magnetic high to Cedar City, coincides with the gravity ridge between the two northeastward-trending gravity lows in Cedar Valley. Therefore, the eastward-trending horst between the two grabens in Cedar Valley may be a structural high related to the less silicic igneous material.

Eastward-trending magnetic anomalies overlie the region west of Enterprise. Although the magnetic highs are partly due to high topography, the anomalies may be interpreted as caused mainly by the eastward-trending igneous-related structures, possibly unrelated to the northeastward-trending Laramide geologic features. A prominent eastward-trending magnetic low (with a closure of about 100 gammas and with its center located about 12 km northwest of Enterprise) and an

adjacent magnetic high (with approximately equal amplitude and located immediately south of the above-mentioned magnetic low) occur over this relatively low topographic region. This pair of magnetic anomalies (high and low) may indicate an east-west-trending magnetic body with a large component of transverse polarization in a north-south direction.

It should be noted that the high magnetic anomaly values over the region near Mount Escalante are approximately equal to those over Granite Mountain and The Three Peaks, in the Iron Springs district. These two areas have approximately the same topographic features. Although there may be a magnetic regional that is different from the plane regional due to the geomagnetic gradient, the causative magnetic bodies under the area near Mount Escalante may have approximately the same magnetic characteristics as those of the Iron Springs intrusive bodies. If so, the rocks beneath the area near Mount Escalante may be intrusive rocks at shallow depth.

It should also be noted that the prominent magnetic low near Modena is bounded on the north with a steep magnetic gradient of about 200 gammas per 3 mi (4.8 km). Because most of this magnetic gradient is located over the flat region of the Escalante Desert near Modena, the northward-trending mountain ranges lying north of Modena may not be primarily responsible for this steep magnetic gradient. However, the magnetic low may be interpreted as an eastward-trending basement sedimentary structure which generally has lower magnetic susceptibility than that of the surrounding alluvium and extrusive volcanic rocks with high silica content (Schmoker, 1972). Moreover, the Modena gravity high, which is located about 2 km north of Modena, overlies the steep

magnetic gradient. Therefore, the steep magnetic gradient between the magnetic high on the north and the magnetic low on the south suggests the alternative qualitative interpretation that an east-west-trending elongate body exists with its center located approximately 1 km north of Modena. If so, this body is probably an igneous body at shallow depth, with reverse polarization. This interpretation seems more consistent with the location of the causative body corresponding with the Modena gravity high.

Southeastward-Trending Magnetic Feature

Over the Escalante Desert, approximately between the Antelope Range on the east and the foothills of the southern end of the Needle Range (north of Beryl) on the west, the abrupt terminations of the northeastward-trending magnetic anomalies with relatively small amplitudes, on both the northeast and southwest sides, are approximately located along the trends in a southeastward direction. The width of the southeastward-trending zone of the magnetic anomalies between the two lines which apparently confine the northeastward extent of the anomalies, is about 15 km. The zone of the magnetic anomalies apparently extends southeastward to the magnetic high over Granite Mountain and The Three Peaks. The zone of the magnetic anomalies (most of which are high anomalies), approximately coincides with the southeastward-trending belt of the gravity anomalies, which includes the gravity highs over the Beryl area, Table Butte area, Antelope Range, and Iron Springs area, from northwest to southeast (see Fig. 4). The belt is interpreted as caused by a southeastward-trending

igneous-related structure, probably a minor intrusive belt joining the two major easterly trending igneous belts on the north and south. The trends of the magnetic pattern over this region are obviously not related to topographic effects. About 12 km northeast of Beryl, an approximately circular magnetic high, with a closure of about 100 gammas within the belt, is probably due to an offshoot of an intrusion at shallow depth, possibly within the shallow basement sedimentary rock, under the alluvium of the Escalante Desert.

GRAVITY PROFILES AND INTERPRETATIVE MODELS

Four gravity profiles, extending approxmately in an east-west direction, were chosen in the survey area (Figs. 3 and 4), to be modeled using a 2-1/2 dimensional gravity modeling program. This program was developed by Snow (1978), using 2-1/2 dimenisonal gravity computation algorithm (Talwani, et al., 1959).

Except for the eastern part of the profile D-D', the regional gravity for all profiles was assumed to be zero (as previously discussed). Each profile was modeled assuming a three-layer subsurface geologic model. The top layer, with an assumed density of 2.2 g/cc, represents alluvium and late-Tertiary sediments, the maximum thickness of which is assumed to be about 3,000 ft (912 m). At greater depth, late-Tertiary sediments may exist, but the density of the sediments is assumed to be greater. This assumption is based on the density-depth curve for Tertiary sediments, as given by Grant and West (1965, p. 194). The top layer may be composed of claystone, siltstone, shale, and loose conglomerate. The second layer, with an assumed average density of 2.45 g/cc or 2.5 g/cc, may represent late-Cenozoic sediments at a depth of greater than about 3,000 ft (912 m), volcanics, the Claron Formation, and possibly the upper portion of Mesozoic sedimentary rocks (for instance, the Iron Springs Formation). The third, and bottom, layer with an assumed average density of 2.7 g/cc, may represent lower Mesozoic rocks, Paleozoic rocks, and intrusive

igneous rocks all of which are herein collectively designated as "basement rock" or "bedrock".

The gravity profiles were modeled with the assumption that the earth's surface is horizontal. Thus the depths to the rock layers shown in the models and discussed in the text of this report are with respect to the surface elevation. Models for each profile were constrained using (1) known surface geology, (2) sample density measurements, and (3) drill hole information, where available. The three-layer interpretative geologic cross sections shown are not unique, but are considered more realistic for the geologic setting than two-layer geologic cross sections. In some of the models along the margin of a graben, only a single, steeply dipping fault is shown; however, it should be emphasized that a larger number of smaller step faults may actually occur that would give essentially the same gravity anomaly.

Profile A-A'

Profile A-A' (Fig. 6) extends southeastward approximately 30 km from a place (located about 8 km northwest of Beryl Junction in the Escalante Desert), along Utah highway 56, across Newcastle, and terminates at a point about 2 km southwest of Iron Mountain. From northwest to southeast, the profile is located over the alluvium of the Escalante Desert for about 18 km, over exposed volcanics (in the area lying east of Newcastle) for about 2 km, and over alluvium again for about 10 km. The complete Bouguer gravity anomaly values range from approximately -190 mgal over both ends of the profile, to about -220

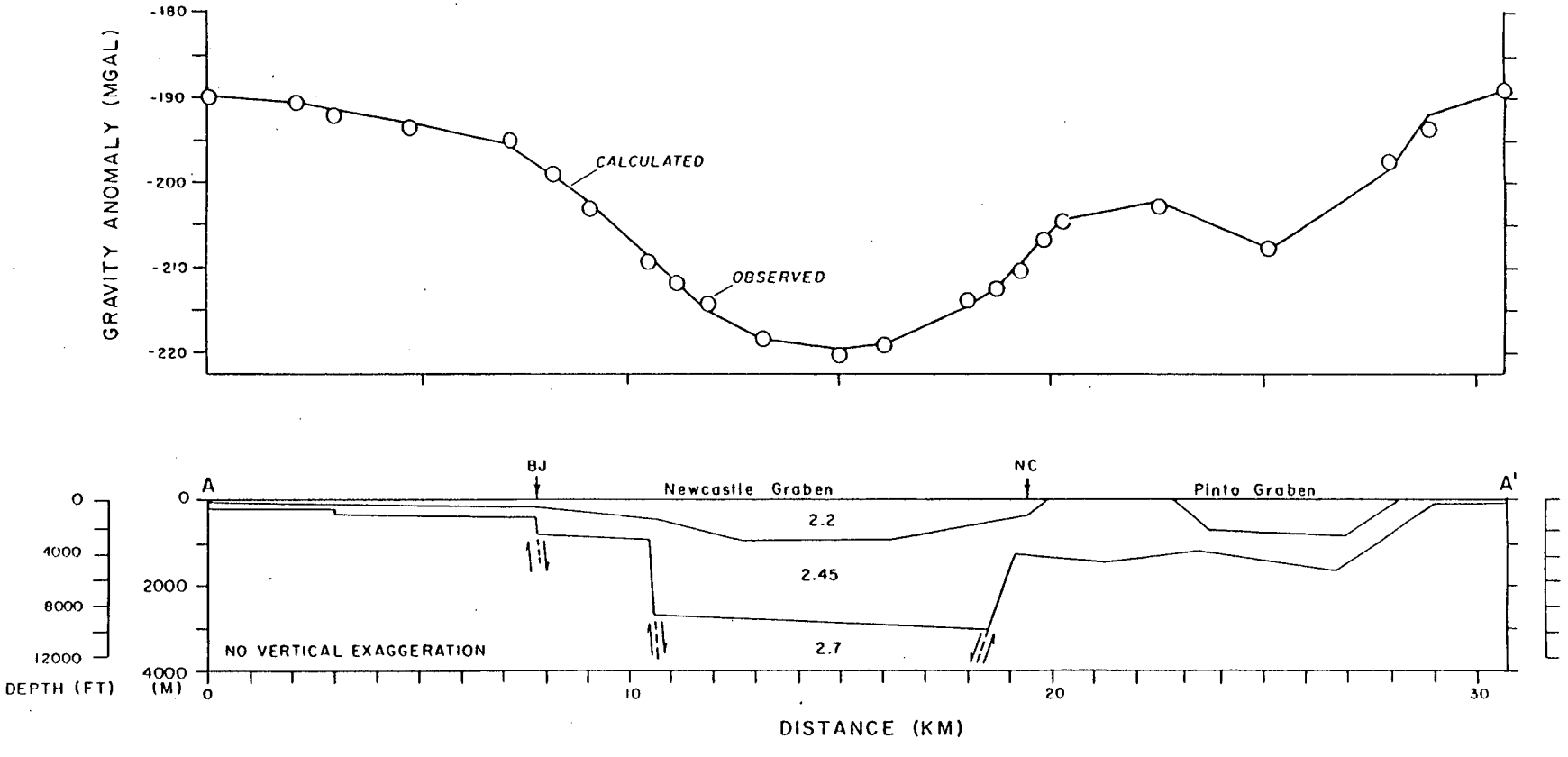

Figure 6. Interpretative geologic cross section along gravity profile AA'. The number is the density (in g/cc) of the layer. Designations: BJ = Beryl Junction; and NC = Newcastle.

mgal in the middle of the anomaly about 4 km west of Newcastle. Along profile A-A' west of Newcastle, the subsurface geology is interpreted as a deep graben (Newcastle graben) tilted east, and bounded on both the east and west margins by steeply dipping faults or fault zones. The top layer is modeled as bowl-shaped at the bottom, with a maximum thickness of 3,000 ft (920 m) at the center; and the deepest part of the bedrock near the eastern boundary of the graben is modeled at a depth of about 10,000 ft (3,050 m). The steeply dipping fault zone that forms the eastern margin of the Newcastle graben, may extend to a great depth and serve as a conduit for the circulation of hot water. Therefore, in the Newcastle area, the hot water with a temperature of about 220° F (104°C) observed near the surface, possibly originates from a deep heat source.

A small graben (i.e., the Pinto graben) is modeled near the east end of profile A-A', with tilted bedrock at a depth of about 5,000 ft (1,600 m), and with the near-surface valley-fill thickness of about 2,600 ft (800 m). The subsurface geologic model between the two grabens seems to be complex: the underlying basement may be either the westward extension of the intrusive igneous rock or possibly sedimentary rocks of lower Mesozic age. The basement at the easternmost end of the profile, near the Iron Mountain intrusion, is assumed to be shallow; and consequently, the basement at the westernmost end of the profile is also assumed to be shallow.

Profile B-B'

Profile B-B' (Fig. 7) extends for about 84 km approximately in an

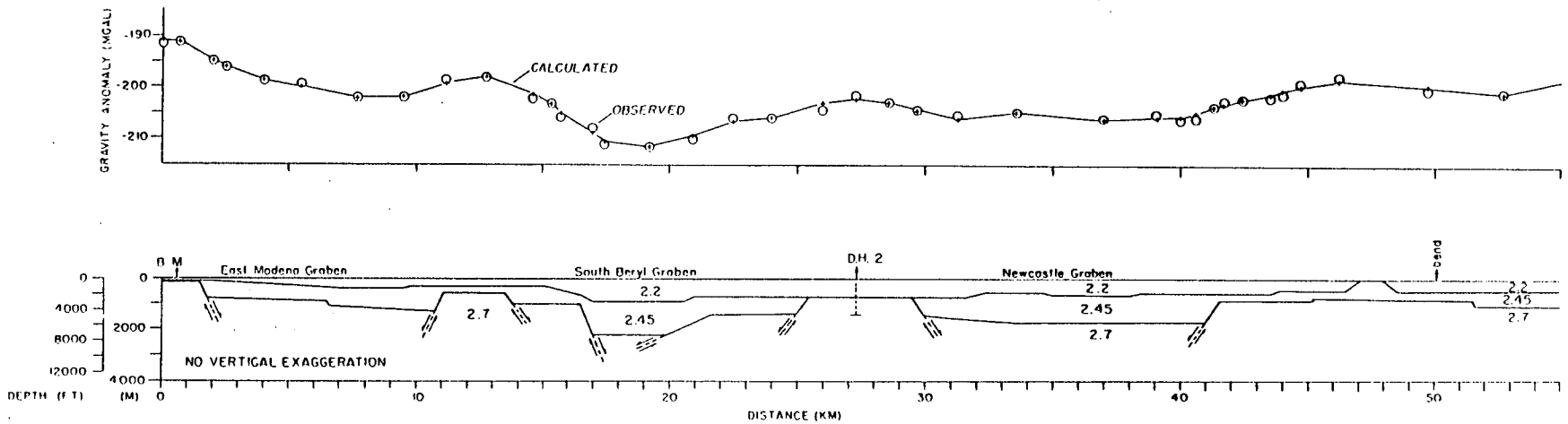

Figure 7. Interpretative geologic cross section along gravity profile B-B'. The number is the density (in g/cc) of the layer. Designations: M = Modena; DH2 = Well State #1 (projected); IS = Iron Springs; F = mapped fault; CC = Cedar City; and DH5 = Well Shurtz Creek #1 (projected).

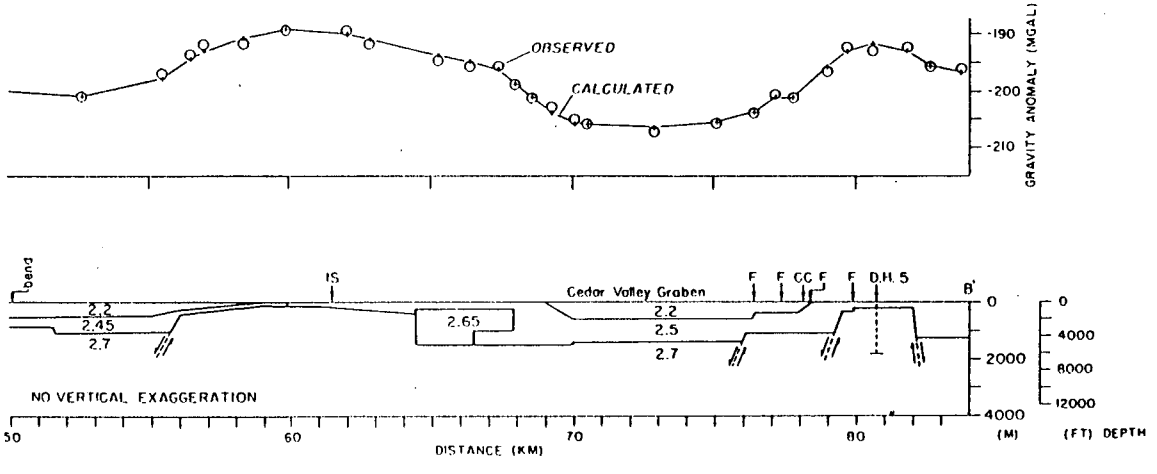

Figure 7. Continued.

east-west direction, across the entire study area, with a bend at a point north of the Antelope Range. The profile extends from Modena across the Escalante Desert for about 45 km to the northern edge of the Antelope Range, then continues southeastward along Antelope Road to Iron Springs and across Cedar Valley to Cedar City, and terminates in Coal Creek Canyon at a point about 6 km east of Cedar City. The profile overlies a few volcanic exposures north of the Antelope Range, lies near some exposures of volcanics, Mesozoic rocks, and intrusive rocks in the Iron Springs district, and overlies exposures of Mesozoic sedimentary rocks in Coal Creek Canyon, east of Cedar City. The gravity anomaly values range from about -190 magal near The Three Peaks intrusion to about -210 mgal over the South Beryl graben.

Along the western portion of profile B-B', in the Escalante Desert, the subsurface geology is interpreted as a sequence of horsts and grabens. Four relatively wide grabens are modeled here. In this area, the basement rock is probably Paleozoic rocks associated with intrusive igneous rock; and the density of the middle layer is herein assumed to be 2.45 g/cc because of the large thickness of the volcanics.

In the eastern part of profile B-B', the basement at shallow depth is modeled beneath the Iron Springs district. Although the density of the basement rock (assumed as the main igneous mass) beneath the point of the highest gravity anomaly is assumed to be 2.7 g/cc, the density of the quartz monzonite in the outcropping bodies is assumed to be 2.65 g/cc.

In the eastern part of the profile, a graben (Cedar Valley graben)

is modeled within Cedar Valley. The density value of the middle layer beneath Cedar Valley is assumed to be 2.5 g/cc, instead of 2.45 g/cc (which was the value assumed in the area lying west of the Iron Springs intrusion), because of the smaller thickness of volcanics near the area of the Hurricane Cliffs.

Along profile B-B', from west to east, the bedrock of the Modena horst is modeled to lie at a depth of about 656 ft (200 m), whereas the basement of the southern portion of the East Modena graben is modeled as tilted east at a depth of about 4,000 ft (1,300 m) and overlain by a top layer with an assumed thickness of about 1,000 ft (305 m). The maximum depth to bedrock in the South Beryl graben is modeled as about 7,000 ft (2,134 m), with an assumed thickness of 3,000 ft (920 m) for the near-surface alluvium and sediments.

The bedrock beneath the structural high between the South Beryl graben and the northern part of the Newcastle graben is modeled at a depth of approximately 2,300 ft (700 m), i.e., immediately beneath the top layer. This bedrock depth is inferred from the log of the geothermal test well State #1, located about 4 km north of profile B-B' (Fig. 4), which penetrated quartz monzonite beneath the late Cenozoic sediments with a thickness of about 1,900 ft (580 m).

Along profile B-B', the basement of the northern edge of the Newcastle graben is modeled at a depth of about 5,300 ft (1,630 m); and the thickness of the middle layer, which partly represents the exposed volcanics at the northern end of the Antelope Range, is modeled as about 2,300 ft (700 m). A small graben, located west of The Three Peaks, is modeled with a depth of about 3,280 ft (1,000 m) to the

basement.

The basement under the peak of the Iron Springs gravity high along profile B-B' is modeled at a depth of about 328 ft (100 m). In the area between Granite Mountain and The Three Peaks, the depth to the top of the quartz monzonite mass is shown as 800 ft (244 m), based on the log of U.S. Bureau of Mines drill hole No. 20, which was drilled during 1944-45 (Cook, 1950). The depth to the bottom of the eastern edge of the exposed monzonite belt (with the assumed density of 2.65 g/cc) is modeled as 3,280 ft (1,000 m) on this profile. The basement beneath the Cedar Valley graben is modeled at a depth of about 4,592 ft (1,400 m), and with an assumed thickness of 2,165 ft (660 m) for the top layer.

The existence of Paleozoic rock (bedrock) at shallow depth beneath the gravity ridge in the Hurricane Cliffs area, near Cedar City, is inferred by the log of the well Schurtz Creek #1 located about 9 km south of the profile, which penetrated Paleozoic rock at a depth of about 746 ft (227 m) under the exposed lower Mesozoic rocks. On the profile, in the area east of Cedar City, the thickness of the Mesozoic rock is modeled with about 800 ft (244 m).

A regional gravity, with gravity values decreasing eastward, may exist over the eastern part of profie B-B' near the Hurricane fault zone. However, it is assumed that the density of some of the Paleozoic rocks at shallow depth in the Hurricane Cliffs area is possibly greater than 2.7 g/cc (which is the density value used for the basement in the model) and therefore may contribute to the higher gravity anomaly values which may compensate for the decrease of the regional gravity,

to a certain extent. Therefore, the net regional gravity, after compensating for the difference between the observed and calculated gravity anomaly (if the correct and higher density were used specifically for the bedrock in the Hurricane Cliffs, on the profile), is assumed to be zero over the area near Cedar City.

Profile C-C'''

Profile C-C''' (Fig. 8), which comprises two separate segments C-C' and C''-C''', extends eastward for about 42 km from a point near the southern edge of the Wah Wah Range, to a point north of The Three Peaks in the Iron Springs district, with an offset of about 5 km near Avon, and with a bend at a point near Lund in the first segment C-C'. The entire profile overlies alluvium of the Escalante Desert except for a few exposures of volcanics near the west end of the profile and at a place about 6 km west of Lund. The gravity anomaly values are about -194 mgal near the volcanic outcrops on the westernmost end of the profile and about -191 mgal near The Three Peaks quartz monzonite outcrop on the eastern end. A gravity anomaly difference of about 2 mgal occurs over the north-south offset of the profile between points C' and C''. The gravity anomaly values decrease to about -213 mgal and -215 mgal in the middle of the Lund gravity low and the Avon gravity low, respectively. Each segment of the profile is modeled separately and presented in a composite profile with the location of the offset (between points C' and C'') at a point about 23.2 km from the west end of the profile.

The first segment C-C' is modeled with a small graben in the area

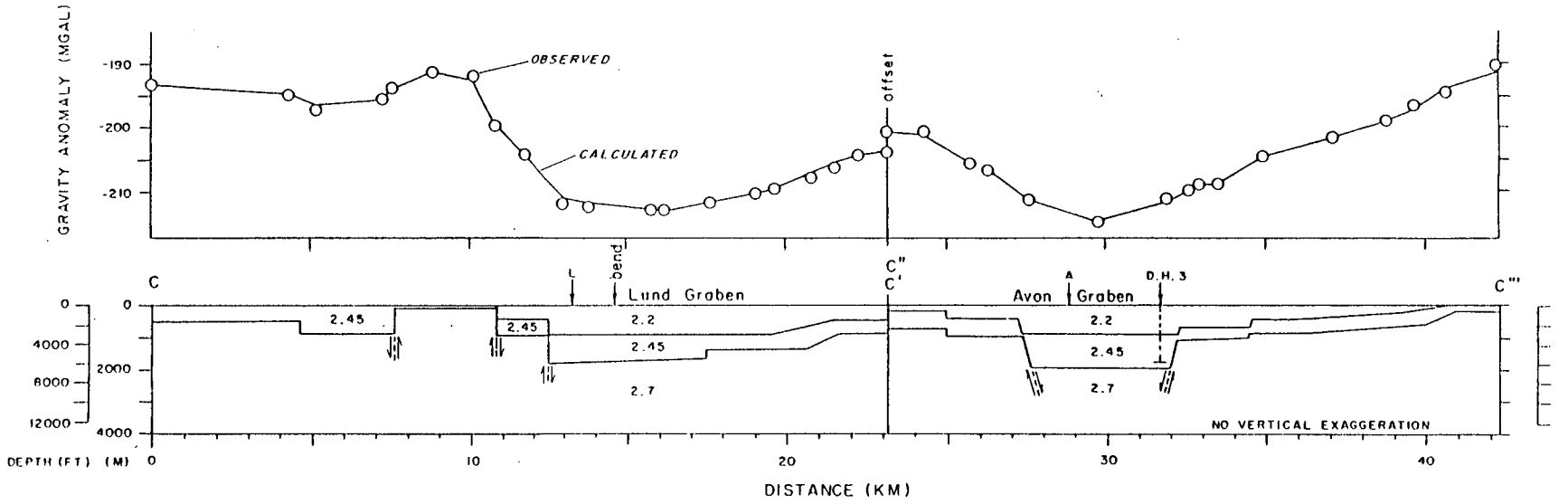

Figure 8. Interpretative geologic cross section along gravity profile C-C'''. The number is the density (in g/cc) of the layer. Designations: L = Lund; A = Avon; and DH3 = Well Jones #1.

lying west of Lund and a large deep graben (Lund graben) in the area east of Lund. Because no drill hole data are available on this segment of the profile to help control the geologic cross section, the bedrock at a point about 4 km west of Lund is assumed to be located at shallow depth. Moreover, along the profile in the area west of Lund, the alluvium is assumed to be too thin to model. The small graben in the area west of Lund is modeled with a depth to bedrock of about 2,952 ft (900 m), and with the bedrock overlain by volcanics. On the profile, the Lund graben is modeled with a depth to basement of about 5,900 ft (1,800 m) and with a thickness of 3,000 ft (915 m) for the top layer. In the model, the graben is bounded on the west by two steeply dipping step faults and on the east by a step fault and a gently dipping fault.

The second segment C''-C''' is modeled with a deep graben (Avon graben), with a depth to bedrock of 6,500 ft (1,982 m). Geothermal test well Jones #1 is located approximately on the profile, about 2 km east of the center of the graben (see Fig. 4). This test well, with a bottom depth of 5,855 ft (1,785 m), failed to reach bedrock. This fact, together with the results of the electrical depth sounding survey in this area (Dr. Norman Harthill, 1980, personal communication) were used to model the bedrock at an assumed depth of 6,500 ft (1,982 m). The Avon graben is modeled with a steep fault bounding each side of the graben, and the thickness of the top layer is assumed to be a maximum value of about 3,000 ft (915 m). A series of step faults may exist between The Three Peaks basement structural high and the Avon graben, although only two step faults are modeled on this side of the graben. The top of the basement (assuming it is composed of intrusive rock)

near The Three Peaks is modeled at a depth of about 558 ft (170 m).

Profile D-D'

Profile D-D' (Fig. 9) extends eastward for about 40 km from a point about 14 km north of The Three Peaks, across Cedar Valley, through Parowan Gap, across Parowan Valley to the town of Parowan, and then continues southeastward approximately along Utah highway 14 for about 7 km (within the deep canyons) to the Hurricane Cliffs area. There are two bends in the profile, one at Parowan Gap and the other near Parowan. The profile overlies alluvium in Cedar Valley for about 17 km, exposures of Mesozoic rocks in the Parowan Gap area (including the Red Hills) for about 4 km, alluvium in Parowan Valley for about 11 km, and exposures of volcanics and Mesozoic rocks in the Hurricane Cliffs area, near Parowan, for about 7 km.

The gravity anomaly values on the profile range from about -195 mgal at the west end of the profile to about -223 mgal in Parowan Valley. Although the regional gravity is assumed to be zero along the profile west of the Red Hills, it is assumed that the regional gravity is decreasing eastward over Parowan Valley and the Hurricane Cliffs area. An eastward-lowering gravity regional, with a rate of approximately 0.4 mgal/km, is obtained from the calculated model assuming that (1) the depth to the Moho is 25 km on the west side of the western boundary of the Colorado Plateau (assumed to be located near the town of Parowan), (2) the depth to the Moho is 40 km on the east side of the boundary, (3) the boundary is dipping 45° E, and (4) the density contrast between the crust and mantle is 0.1 g/cc.

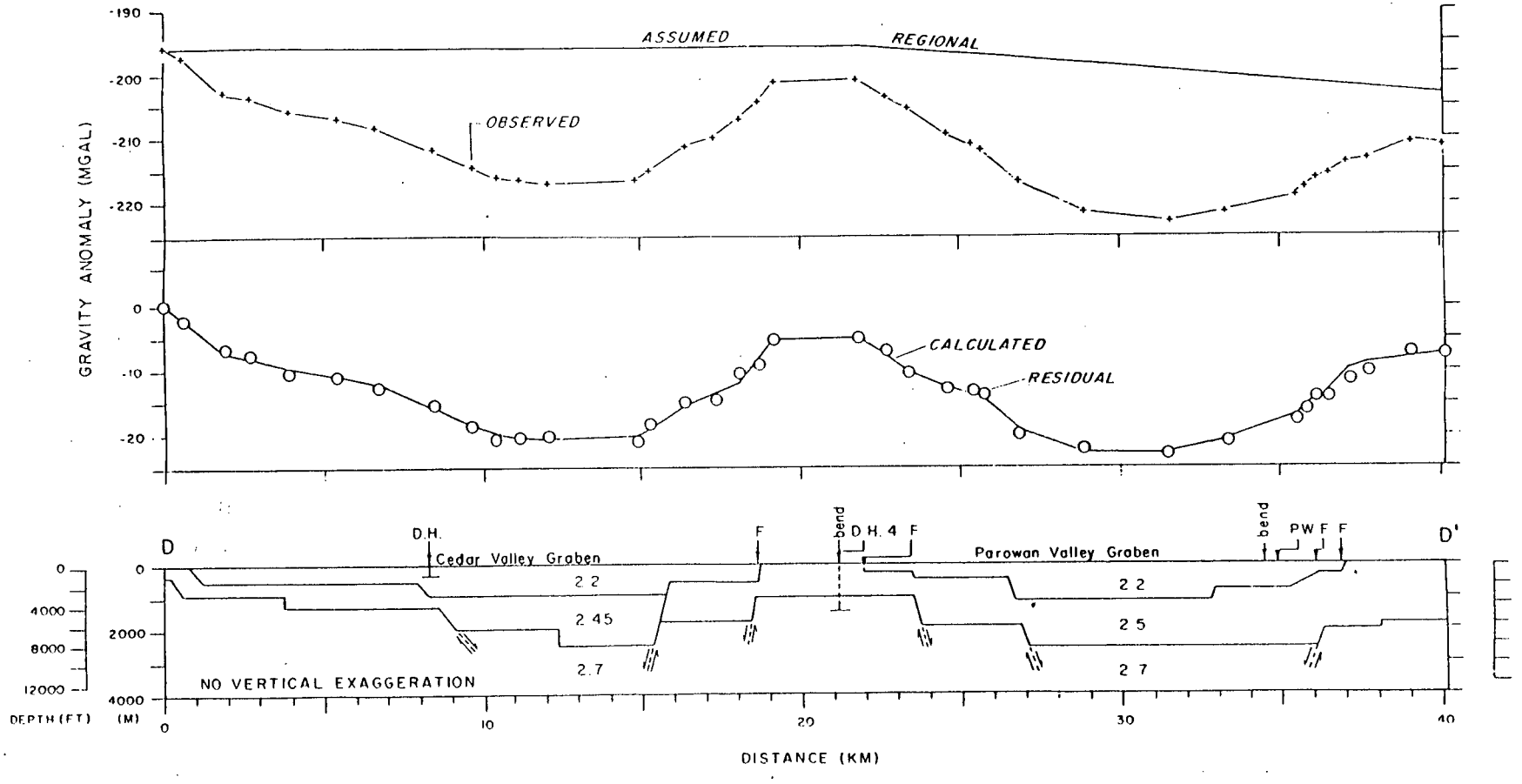

Figure 9. Interpretative geologic cross section along gravity profile D-D'. The number is the density (in g/cc) of the layer. Designations: DH = Well Rush Lake (projected); F = mapped fault; DH4 = Well Little Salt Lake #1 (projected); and PW = Parowan.

The density of the middle layer is assumed to be 2.45 g/cc in the area on the west side of the Red Hills and 2.5 g/cc on the east side. This difference in the density values of the middle layer is assumed from the fact that the Hurricane Cliffs area has been deeply eroded. The bedrock in the deepest part of the Cedar Valley graben is modeled with a depth of about 8,200 ft (2,500 m). In the model a series of four step faults is shown on the west side of the Cedar Valley graben and two step faults are shown on the east side. The basement rock in the Cedar valley graben is believed to be quartz monzonite that forms the northeastward extension of the quartz monzonite body in the Iron Springs district.

The drill data of well Little Salt Lake #1, located over the Red Hills about 6 km south of the profile, was used for geologic control of the cross section. In accordance with the well log, the basement rock (known to be quartz monzonite) is modeled at the known depth of 3,490 ft (1,064 m) and is overlain by the middle layer that in this area is actually the Mesozoic rocks penetrated in the drill hole and exposed at the surface. Beneath the Parowan Valley graben, the depth to the basement is modeled as about 8,397 ft (2,560 m). In the basement, two steeply dipping faults are modeled on the west side of the graben and two step faults are modeled on the east side of the graben.

The bedrock beneath Parowan Valley may not be the extension of the intrusive body. Instead, it is probably Paleozoic rock underlying the thick sequence of Cenozoic and Mesozoic sedimentary rocks. In the model, the maximum thickness of the top layer is assumed to be 3,700 ft (1,128 m) in the middle of Parowan Valley and 3,000 ft (915 m), in the

middle of Cedar Valley.

Relationships between Gravity Features and Geothermal Systems in Study Area

The gravity method is generally used in geothermal prospecting. In some areas, the gravity data indicate the causative feature which is directly related to the geothermal system. A gravity high may indicate an anomalous region in which the density of the host rock or sediments is greater than the surrounding area due to the densification process by geothermal hot fluid. A relatively broad gravity low may indicate directly the heat source of the geothermal system (magma chamber at shallow depth). In some KGRA's the gravity method is used indirectly in geothermal prospecting to locate the subsurface structure associated with the geothermal system. For instance, a large gravity gradient may indicate a steeply dipping fault or fault zone with a large normal slip; and such a fault zone is often associated with fractures and openings (in the rock) that play an important role either the formation of a geothermal reservoir or in the movement of the geofluid, or both.

Within the Newcastle KGRA is a large gravity gradient which bounds the Newcastle gravity low on the east (area 12, Fig. 4). The gradient indicates a steeply dipping fault zone on the eastern margin of the Newcastle graben with a downthrow of about 3 km on the west (see profile A-A', Fig. 6). The fault zone may serve as a conduit for the hot water to rise from a deep source. Because the occurrence of hot water (up to 220° F) is confined within a small area near Newcastle (Clement, 1980), the geothermal system may be partly controlled by

another easterly trending fault system. The previously proposed triple junction fault system near Newcastle may be an important structural feature for the plumbing system of the hot water in the Newcastle KGRA. For a more detailed discussion of the geothermal activity, the circulation system of the hot water, and the possible heat source in this area, the reader is referred to the M.S. thesis of Clement (1980).

Within the Lund KGRA is also a large gravity gradient which bounds the Lund gravity low on the west (area 14, Fig. 4). The gradient indicates a steeply dipping fault zone on the western margin of the Lund graben with a downthrow of about 1 km on the east. The warm water in the shallow wells in this area may be related to the movement of the ground water partly controlled by the fault zone.

SUMMARY AND CONCLUSIONS

The survey area is located within the transition zone between the Colorado Plateau and Basin and Range provinces. The western margin of the transition zone extends in a northeastward direction on the west side of the Escalante Desert near the western margin of the survey area. The Wasatch Line and the eastern margin of the main Laramide thrust also extend similarly across the study area.

The study area has been influenced by four significant geologic events. The first event was a period of large-scale thrusting of Sevier age. The northeastward-trending folds, faults, and minor thrusts occurred in front of the main Laramide* thrust throughout the study area. The intensity of thrusting gradually decreases to the southeast. The second event was probably an episode of east-west-trending igneous activity (possibly of deep origin in the crust), which started about 43 to 34 m.y. ago. The easterly trending Pioche-Marysvale igneous belt on the north, and the Delamar Iron Springs igneous belt on the south of the survey area are possibly caused by this igneous activity. The third event, which occurred more or less concurrently with the eastward-trending igneous activity, was a period of Basin and Range tectonism. The northeastward-trending horsts and grabens were formed during this period. The forth event was a

*The term "Laramide" is generally used for the structures including those developed during the Sevier orogeny.

period of intensive volcanism with associated intrusive activity. The last three geologic events probably overlapped each other.

Geophysically, the study area lies approximately at the junction of the north-south-trending Intermountain Siesmic Belt and an easterly trending secondary seismic zone which extends westward from southwestern Utah to southern Nevada. The smooth Bouguer gravity anomaly map of Montgomery (1973) shows that the survey area overlies the eastward-trending broad regional gravity saddle between the Sevier gravity high on the north and the St. George-Kanab gravity high on the southwest. The aeromagnetic map of Utah (Zietz, et al., 1976) shows a broad easterly trending band of prominent magnetic highs on the north side of the study area, and a relatively less prominent easterly trending belt of magnetic highs which bounds the study area on the south. The magnetic highs are typically caused by the igneous intrusive bodies lying at relatively shallow depth.

The complete Bouguer gravity anomaly map of the study area with a 2-mgal contour interval, shows the dominant features of the gravity contours to be in a northeastward direction, which indicate that the Basin and Range structures are partly controlled by the northeastward-trending features of Laramide age.

The horizontal extent of the Basin and Range grabens, horsts, and igneous-related structures at shallow depth, the characteristics of the faults which bounds the horsts and the grabens, and the vertical extent of the grabens are estimated qualitatively in the interpretation of the complete Bouguer gravity anomaly map. Furthermore, the locations of the bounding faults, the depths to the bottom of the grabens and to the

top of the horsts below the surface are interpreted quantiatively by modeling four gravity profiles selected on the gravity map. The easterly trending gravity highs and lows are interpreted as caused by the subsurface structural highs and lows, which were possibly modified or formed under the geologic control which may be related to the east-west-trending igneous activity, that started prior to the Basin and Range tectonic activity. The interpretation of these structures is also made qualitatively and quantitatively.

The northeastward-trending large gravity lows in the Escalante Desert indicate the Newcastle graben, Lund graben, and Avon graben. These grabens are characterized mainly by the Basin and Range activity. The gravity low over the Newcastle graben, with a total relief of about 20 mgal, indicates a depth to bedrock of about 3 km in the modeling of profile A-A'. The gravity low over the Lund graben, with a total relief of about 13 mgal on profile C-C', indicates a depth to bedrock of about 1.8 km. The gravity low over the Avon graben, with a total relief of about 15 mgal, indicates a depth to basement of about 2 km in the modeling of profile C''-C'''.

Two intermediate gravity lows in the Escalante Desert indicate the South Beryl and East Modena grabens, which are probably shaped to a large extent by the east-west trending pre-Basin and Range igneous activity. The basement beneath the South Beryl graben is believed to be pre-Tertiary sedimentary rock, in accordance with the log of geothermal test well DeArman #1, which penetrated the basement sedimentary rock at a depth of about 4,600 ft (1,402 m). On profile B-B', the depth to basement beneath the South Beryl graben is

calculated as about 2.2 km, and that beneath the East Modena graben is calculated as about 1.2 km.

Two northward- to northeastward-trending gravity lows along Cedar Valley indicate two typical intermontane down-faulted grabens that form contiguous blocks that are herein jointly designated the "Cedar Valley graben". The depth to bedrock beneath the northern part of the Cedar Valley graben, near the Red Hills, is calculated as about 2.5 km in the modeling of profile D-D'. A northeastward-trending gravity low over the Parowan Valley graben, with a total relief of about 20 mgal, indicates a depth to basement of about 2.5 km in the modeling of profile D-D', which extends across the southern part of the graben.

In the Iron Springs area, a northeastward-trending gravity high, approximately 30 km long, corresponds approximately with the belt of four intrusive bodies, which, from southwest to northeast, are: Stoddard Mountain, Iron Mountain, Granite Mountain, and The Three Peaks. The relatively high average density of 2.7 g/cc of the intrusive rock probably causes the gravity high. A gravity high over the Antelope Range, northwest of Iron Mountain, is interpreted as caused by an igneous mass at shallow depth which may have the same origin as the Iron Springs intrusions. The gravity high (without closure on the gravity map) over Big Mountain, south of Enterprise, probably indicates the southwestward continuation of the Iron Springs intrusive belt. The belt of gravity highs extending northward from The Three Peaks area to the Black Mountains, surprisingly corresponds with the belt of <u>low</u> magnetic anomalies on the acromagnetic map. This correlation possibly indicates that the northward-trending ridge of

basement sedimentary rock at shallow depth probably has a lower magnetic susceptibility than the surrounding alluvium.

The northeastward-trending gravity highs over the Hurricane Cliffs near Cedar City, the Red Hills, and the Enterprise Reservoir area, are interpreted as caused by the uplifted pre-Tertiary sedimentary blocks developed along the Laramide zones of weakness during the period of the Basin and Range tectonism. The easterly trending elongate gravity highs over the western portion of the Black Mountains and Mount Escalante area are provisionally interpreted as caused by basement structures of sedimentary rock that has been intruded by eastward-trending vein-like igneous intrusions at shallow depth. A small gravity high over Modena is probably caused either by an eastward-trending basement structural block or an elongate igneous body at shallow depth. This gravity high approximately coincides with an east-west-trending pronounced magnetic low.

A gravity high over the Beryl area probably indicates bedrock that has been complexly deformed by the igneous intrusions at shallow depth. The northeastward extension of the Beryl gravity high to the area west of Lund and beyond, is interpreted as caused by a basement structure which may correspond with the eastern margin of the main Laramide thrust. The gravity high over the Table Butte area probably indicates an igneous intrusive body at shallow depth. This interpretation is partly supported by the drill data of geothermal test well State #1, which penetrated quartz monzonite at a depth of about 1,900 ft (579 m).

The Beryl gravity high, Table Butte gravity high, Antelope Range gravity high, and Iron Springs gravity high are located along a

southeastward alignment. The alignment coincides approximately with a belt of high aeromagnetic anomalies that extends across the Escalante Desert in a southeastward direction. Therefore, this belt of gravity highs may indicate a southeastward-trending minor igneous belt which resembles a bridge between the easterly trending Pioche-Marysvale igneous belt on the north and Delamar-Iron Springs igneous belt on the south.

Even though no gravity anomaly that indicates a geologic feature directly related to the geothermal process or heat source (such as a magma chamber), is observed in the study area, the gravity survey delineates well the steeply dipping faults or fault zones which bound the deep grabens and associated structures that may control the geothermal systems in this area. In particular, in the Newcastle and Lund KGRA's the gravity data indicate that steeply dipping fault zones along the east (with a downthrow of about 3 km) and west (with a downthrow of about 1 km) margins of the Newcastle and Lund grabens, respectively, probably form conduits for the upward circulation of hot water observed at shallow depth near Newcastle (220° F) and Lund. According to Clement (1980), the water in the Newcastle KGRA is probably heated by the geothermal gradient in this region and probably originates at a depth of about 3 km.

In addition, the gravity survey probably reveals some possible igneous bodies (probably young in age), associated with complexly deformed basement structure in the study area. The possible easterly trending igneous features in the Mount Escalante area and the western portion of the Black Mountains are worthwhile for further study to evaluate the geothermal potential of these regions.

APPENDIX A

PRINCIPAL FACTS OF GRAVITY STATIONS

Notes: 1) Units are as follows:

	Units
Latitude	degrees, minutes
Longitude	degrees, minutes
Elevation	feet
Observed gravity	milligal
Theoretical gravity #	milligal
Free-air gravity anomaly value	milligal
Simple Bouguer gravity anomaly value*	milligal
Terrain correction (T.C.)*	milligal
Terrain-corrected Bouguer gravity anomaly value*	milligal

2) Coding is as follows:

WP 000 - Number designation of gravity station taken by Win Pe.

AA 000 - Number designation of gravity station taken by Eckhard Kuennemann during 1978.

EH 000 - Number designation of gravity station taken by Hardman (1964).

LU 000 - Number designation of gravity station taken by Donald Selk during 1967.

WU 000 - Number designation of gravity station taken by Montgomery (1973).

65B 00 - Number designation of gravity station taken by GG 521 gravity classes, University of Utah, during 1965.

752 00 - Number designation of gravity station taken by GG 521 gravity classes, University of Utah, during 1975.

SG 000 - Number designation of gravity station taken by Gabbert (1980).

RG 000 - Number designation of gravity station taken by Green (1980).

Theoretical gravity at mean sea level, using the International gravity formula (Swick, 1942)

* A density contrast of 2.67 g/cc was assumed for both the Bouguer and terrain corrections. Terrain-correction values were obtained (1) for the inner zone (out to a radial distance of 0.895 km from the station) by hand using a Hammer zone chart, and for the outer zones (out to a radial distance of 166.7 km from the station) by using the terrain-correction program of Serpa (1980) on the UNIVAC 1108 digital computer, at the University of Utah.

Note: All data are referred to the Cedar City base station which has a published absolute gravity value of 979,429.16 mgal (Cook et al., 1971).

STAT.	LATITUDE	LONGITUDE	ELEV.	OBSERVED GRAVITY	THEOR. GRAVITY	FREE-AIR	SIMPLE BOUGUER	T.C	T.C. BOUGUER
WP240	37. 40.29	113. 29.14	5722.	979429.07	979975.37	-8.09	-202.98	1.30	-201.68
WP241	37. 40.33	113. 32.89	5293.	979444.87	979975.42	-32.69	-212.97	.60	-212.37
WP242	37. 41.49	113. 36.32	5192.	979446.84	979977.12	-41.92	-218.76	.25	-218.51
WP243	37. 42.45	113. 37.42	5173.	979455.91	979978.52	-36.04	-212.23	.19	-212.04
WP244	37. 42.43	113. 36.32	5177.	979450.71	979978.49	-40.84	-217.17	.21	-216.96
WP245	37. 42.44	113. 35.19	5184.	979448.02	979978.50	-42.88	-219.44	.24	-219.20
WP246	37. 43.30	113. 34.91	5171.	979451.73	979979.76	-41.65	-217.77	.22	-217.55
WP247	37. 43.30	113. 36.01	5172.	979454.55	979979.76	-38.73	-214.89	.19	-214.70
WP248	37. 43.31	113. 37.15	5166.	979460.77	979979.77	-33.10	-209.06	.17	-208.89
WP249	37. 43.31	113. 38.21	5168.	979466.66	979979.77	-27.02	-203.05	.16	-202.89
WP250	37. 43.32	113. 39.31	5172.	979472.55	979979.79	-20.76	-196.91	.16	-196.75
WP251	37. 44.20	113. 39.32	5165.	979474.76	979981.05	-20.49	-196.41	.13	-196.28
WP252	37. 44.20	113. 38.21	5162.	979471.61	979981.05	-23.92	-199.74	.14	-199.60
WP253	37. 44.19	113. 37.12	5163.	979467.45	979981.04	-27.97	-203.82	.15	-203.67
WP254	37. 44.18	113. 36.01	5159.	979461.04	979981.02	-34.74	-210.46	.17	-210.29
WP255	37. 44.20	113. 34.92	5154.	979456.36	979981.05	-39.92	-215.46	.19	-215.27
WP256	37. 44.18	113. 34.10	5167.	979455.66	979981.02	-39.36	-215.35	.22	-215.13
WP257	37. 44.18	113. 32.70	5161.	979455.18	979981.02	-40.41	-216.19	.32	-215.87
WP258	37. 45.06	113. 33.89	5150.	979459.32	979982.30	-38.58	-213.99	.19	-213.80
WP259	37. 45.06	113. 35.47	5149.	979462.29	979982.30	-35.71	-211.08	.15	-210.93
WP260	37. 45.06	113. 37.66	5156.	979472.45	979982.30	-24.89	-200.51	.12	-200.39
WP261	37. 45.06	113. 39.32	5159.	979475.70	979982.30	-21.36	-197.08	.12	-196.96
WP262	37. 45.95	113. 39.32	5152.	979473.93	979983.60	-25.08	-200.56	.10	-200.46
WP263	37. 45.94	113. 38.21	5153.	979474.14	979983.59	-24.76	-200.27	.10	-200.17
WP264	37. 45.94	113. 37.12	5151.	979473.29	979983.59	-25.80	-201.24	.11	-201.13
WP265	37. 45.93	113. 36.02	5151.	979468.95	979983.57	-30.12	-205.57	.12	-205.45
WP266	37. 45.92	113. 34.93	5141.	979464.59	979983.55	-35.41	-210.52	.14	-210.38
WP267	37. 45.93	113. 32.71	5144.	979463.22	979983.57	-36.51	-211.71	.20	-211.51
WP268	37. 45.94	113. 31.62	5146.	979463.51	979983.59	-36.05	-211.32	.28	-211.04
WP269	37. 46.81	113. 31.62	5137.	979468.66	979984.85	-33.01	-207.98	.21	-207.77
WP270	37. 46.80	113. 32.72	5135.	979468.30	979984.84	-33.55	-208.45	.17	-208.28
WP271	37. 46.81	113. 33.82	5137.	979467.69	979984.85	-33.99	-208.96	.14	-208.82

STAT.	LATITUDE	LONGITUDE	ELEV.	OBSERVED GRAVITY	THEOR. GRAVITY	FREE-AIR	SIMPLE BOUGUER	T.C	T.C. BOUGUER
WP272	37. 46.81	113. 34.92	5136.	979469.31	979984.85	-32.46	-207.39	.12	-207.27
WP273	37. 46.81	113. 36.01	5140.	979473.05	979984.85	-28.34	-203.40	.11	-203.29
WP274	37. 46.81	113. 37.12	5144.	979475.39	979984.85	-25.62	-200.83	.10	-200.73
WP275	37. 46.82	113. 38.21	5147.	979474.66	979984.87	-26.09	-201.40	.09	-201.31
WP276	37. 47.68	113. 39.32	5143.	979472.14	979986.12	-30.24	-205.41	.09	-205.32
WP277	37. 47.67	113. 37.95	5141.	979474.01	979986.11	-28.55	-203.66	.09	-203.57
WP278	37. 47.68	113. 37.12	5143.	979475.51	979986.12	-26.87	-202.04	.09	-201.95
WP279	37. 47.68	113. 34.42	5133.	979472.34	979986.12	-30.99	-205.82	.11	-205.71
WP280	37. 48.00	113. 34.92	5133.	979474.36	979986.59	-29.43	-204.26	.09	-204.17
WP281	37. 48.08	113. 36.17	5135.	979475.91	979986.70	-27.81	-202.71	.09	-202.62
WP282	37. 48.55	113. 36.02	5134.	979476.01	979987.39	-28.49	-203.35	.09	-203.26
WP283	37. 48.52	113. 32.79	5127.	979478.95	979987.34	-26.15	-200.78	.11	-200.67
WP284	37. 48.51	113. 31.69	5128.	979483.40	979987.33	-21.60	-196.26	.13	-196.13
WP285	37. 48.50	113. 30.55	5128.	979481.19	979987.31	-23.79	-198.45	.15	-198.30
WP286	37. 48.55	113. 39.32	5138.	979473.22	979987.39	-30.90	-205.90	.09	-205.81
WP287	37. 48.56	113. 38.21	5136.	979475.30	979987.41	-29.03	-203.97	.09	-203.88
WP288	37. 49.43	113. 38.22	5132.	979479.23	979988.67	-26.73	-201.53	.11	-201.42
WP289	37. 49.43	113. 39.32	5134.	979476.32	979988.67	-29.46	-204.32	.10	-204.22
WP290	37. 49.43	113. 40.43	5137.	979474.37	979988.67	-31.12	-206.08	.12	-205.96
WP291	37. 48.56	113. 40.43	5139.	979471.29	979987.41	-32.75	-207.79	.12	-207.67
WP292	37. 47.68	113. 40.41	5144.	979470.65	979986.12	-31.64	-206.84	.11	-206.73
WP293	37. 50.31	113. 39.33	5131.	979479.65	979989.95	-27.69	-202.45	.10	-202.35
WP294	37. 50.31	113. 38.23	5128.	979481.48	979989.95	-26.14	-200.80	.11	-200.69
WP295	37. 50.30	113. 37.12	5124.	979482.37	979989.94	-25.61	-200.13	.13	-200.00
WP296	37. 50.29	113. 36.02	5122.	979485.03	979989.92	-23.12	-197.58	.10	-197.48
WP297	37. 49.42	113. 36.02	5128.	979479.74	979988.66	-26.58	-201.24	.08	-201.16
WP298	37. 49.87	113. 34.92	5124.	979479.74	979989.31	-27.61	-202.13	.08	-202.05
WP299	37. 50.30	113. 34.92	5123.	979482.52	979989.94	-25.55	-200.04	.08	-199.96
WP300	37. 50.30	113. 33.84	5118.	979483.59	979989.94	-24.95	-199.27	.08	-199.19
WP301	37. 50.30	113. 32.75	5117.	979484.66	979989.94	-23.98	-198.26	.10	-198.16
WP302	37. 49.41	113. 32.76	5122.	979482.74	979988.64	-24.13	-198.59	.10	-198.49
WP303	37. 50.29	113. 30.54	5117.	979493.21	979989.92	-15.41	-189.70	.12	-189.58

STAT.	LATITUDE	LONGITUDE	ELEV.	OBSERVED GRAVITY	THEOR. GRAVITY	FREE-AIR	SIMPLE BOUGUER	T.C	T.C. BOUGUER
WP304	37. 50.29	113. 31.64	5116.	979488.63	979989.92	-20.08	-194.33	.10	-194.23
WP305	37. 51.16	113. 30.53	5113.	979490.30	979991.20	-19.98	-194.13	.10	-194.03
WP306	37. 52.04	113. 30.53	5109.	979492.43	979992.48	-19.50	-193.51	.08	-193.43
WP307	37. 51.17	113. 31.84	5110.	979488.46	979991.21	-22.11	-196.16	.12	-196.04
WP308	37. 51.17	113. 32.76	5113.	979488.59	979991.21	-21.70	-195.85	.17	-195.68
WP309	37. 51.17	113. 33.86	5116.	979489.48	979991.21	-20.52	-194.77	.11	-194.66
WP310	37. 51.17	113. 34.92	5119.	979487.10	979991.21	-22.62	-196.97	.08	-196.89
WP311	37. 51.17	113. 36.02	5121.	979486.01	979991.21	-23.53	-197.95	.11	-197.84
WP312	37. 52.05	113. 36.02	5122.	979485.61	979992.49	-25.11	-199.56	.11	-199.45
WP313	37. 52.05	113. 34.91	5118.	979486.50	979992.49	-24.60	-198.92	.09	-198.83
WP314	37. 52.92	113. 34.96	5126.	979485.83	979993.77	-25.79	-200.39	.09	-200.30
WP315	37. 53.75	113. 34.96	5138.	979485.53	979994.95	-26.15	-201.15	.11	-201.04
WP316	37. 54.66	113. 34.96	5172.	979486.49	979996.28	-23.32	-199.48	.09	-199.39
WP317	37. 54.66	113. 37.16	5163.	979492.57	979996.28	-18.09	-193.95	.15	-193.80
WP318	37. 55.52	113. 34.78	5202.	979487.54	979997.53	-20.70	-197.88	.12	-197.76
WP319	37. 54.66	113. 33.81	5151.	979483.88	979996.28	-27.90	-203.35	.10	-203.25
WP320	37. 55.91	113. 33.81	5198.	979487.96	979998.10	-21.22	-198.27	.13	-198.14
WP321	37. 57.26	113. 30.50	5159.	979488.48	980000.07	-26.34	-202.05	.17	-201.88
WP322	37. 57.61	113. 29.71	5149.	979486.24	980000.59	-30.04	-205.41	.15	-205.26
WP323	37. 56.39	113. 29.41	5112.	979484.87	979998.80	-33.10	-207.22	.08	-207.14
WP324	37. 58.17	113. 30.50	5222.	979491.99	980001.41	-18.24	-196.10	.20	-195.90
WP325	37. 58.14	113. 31.60	5265.	979487.84	980001.37	-18.31	-197.63	.22	-197.41
WP326	37. 58.14	113. 32.70	5285.	979486.46	980001.37	-17.81	-197.82	.29	-197.53
WP327	37. 58.13	113. 33.80	5334.	979483.20	980001.35	-16.45	-198.12	.22	-197.90
WP328	37. 58.13	113. 34.79	5341.	979484.72	980001.35	-14.27	-196.19	.24	-195.95
WP329	37. 58.82	113. 34.79	5392.	979481.78	980002.36	-13.42	-197.07	.28	-196.79
WP330	37. 59.87	113. 34.77	5468.	979479.77	980003.89	-9.82	-196.06	.38	-195.68
WP331	37. 59.72	113. 30.50	5353.	979488.48	980003.66	-11.69	-194.02	.32	-193.70
WP332	37. 57.30	113. 34.96	5287.	979488.04	980000.12	-14.80	-194.87	.21	-194.66
WP333	37. 56.40	113. 34.96	5237.	979488.57	979998.81	-17.66	-196.03	.16	-195.87
WP334	37. 55.53	113. 36.05	5196.	979490.86	979997.55	-17.96	-194.94	.15	-194.79
WP335	37. 56.40	113. 36.60	5215.	979494.90	979998.81	-13.40	-191.02	.26	-190.76

STAT.	LATITUDE	LONGITUDE	ELEV.	OBSERVED GRAVITY	THEOR. GRAVITY	FREE-AIR	SIMPLE BOUGUER	T.C	T.C. BOUGUER
WP336	37. 55.53	113. 37.15	5181.	979494.70	979997.55	-15.53	-192.00	.19	-191.81
WP337	37. 53.78	113. 39.36	5143.	979494.52	979995.00	-16.73	-191.90	.19	-191.71
WP338	37. 53.77	113. 40.45	5163.	979495.73	979994.98	-13.63	-189.48	.19	-189.29
WP339	37. 54.65	113. 40.45	5200.	979495.55	979996.27	-11.61	-188.72	.24	-188.48
WP340	37. 55.51	113. 40.45	5233.	979494.32	979997.52	-10.99	-189.22	.31	-188.91
WP341	37. 56.38	113. 40.45	5291.	979491.40	979998.79	-9.73	-189.95	.38	-189.57
WP342	37. 56.38	113. 39.35	5263.	979493.75	979998.79	-10.01	-189.27	.39	-188.88
WP343	37. 56.39	113. 38.24	5225.	979496.88	979998.80	-10.46	-188.42	.35	-188.07
WP344	37. 57.25	113. 40.44	5403.	979484.84	980000.05	-7.02	-191.05	.42	-190.63
WP345	37. 58.07	113. 39.24	5575.	979472.63	980001.27	-4.25	-194.13	.50	-193.63
WP346	37. 58.98	113. 39.30	5692.	979468.59	980002.59	1.39	-192.48	.68	-191.80
WP347	37. 59.68	113. 37.69	5666.	979470.48	980003.61	-.19	-193.17	.71	-192.46
WP348	37. 58.42	113. 42.80	5658.	979470.35	980001.77	.77	-191.94	.80	-191.14
WP349	37. 58.71	113. 44.11	5715.	979462.68	980002.20	-1.98	-196.63	.98	-195.65
WP350	37. 57.01	113. 44.24	5537.	979472.63	979999.70	-6.27	-194.86	.56	-194.30
WP351	37. 57.25	113. 42.64	5461.	979481.48	980000.05	-4.92	-190.92	.51	-190.41
WP352	37. 57.26	113. 41.53	5430.	979484.67	980000.07	-4.66	-189.61	.46	-189.15
WP353	37. 56.38	113. 41.53	5330.	979488.09	979998.79	-9.37	-190.91	.39	-190.52
WP354	37. 55.51	113. 41.54	5271.	979490.85	979997.52	-10.88	-190.41	.33	-190.08
WP355	37. 54.64	113. 41.54	5218.	979493.91	979996.25	-11.54	-189.26	.30	-188.96
WP356	37. 53.77	113. 41.54	5173.	979497.10	979994.98	-11.32	-187.51	.23	-187.28
WP357	37. 53.78	113. 43.74	5215.	979488.75	979995.00	-15.74	-193.37	.29	-193.08
WP358	37. 53.78	113. 44.83	5232.	979484.90	979995.00	-17.99	-196.19	.34	-195.85
WP359	37. 54.65	113. 44.83	5307.	979482.51	979996.27	-14.59	-195.35	.41	-194.94
WP360	37. 55.51	113. 44.83	5393.	979478.07	979997.52	-12.19	-195.87	.48	-195.39
WP361	37. 56.39	113. 44.85	5493.	979472.05	979998.80	-10.09	-197.19	.55	-196.64
WP362	37. 53.83	113. 42.96	5210.	979491.50	979995.07	-13.53	-190.98	.26	-190.72
WP363	37. 52.91	113. 39.34	5138.	979491.96	979993.75	-18.52	-193.52	.15	-193.37
WP364	37. 52.91	113. 40.43	5146.	979494.71	979993.75	-15.01	-190.29	.17	-190.12
WP365	37. 52.90	113. 41.54	5157.	979495.61	979993.73	-13.07	-188.72	.18	-188.54
WP366	37. 52.58	113. 42.78	5156.	979493.99	979993.27	-14.31	-189.92	.20	-189.72
WP367	37. 51.15	113. 44.82	5169.	979482.30	979991.18	-22.69	-198.75	.19	-198.56

STAT.	LATITUDE	LONGITUDE	ELEV.	OBSERVED GRAVITY	THEOR. GRAVITY	FREE-AIR	SIMPLE BOUGUER	T.C	T.C. BOUGUER
WP368	37. 48.56	113. 44.81	5184.	979473.25	979987.41	-26.56	-203.13	.13	-203.00
WP369	37. 48.57	113. 43.72	5168.	979468.98	979987.42	-32.35	-208.37	.11	-208.26
WP370	37. 48.57	113. 42.61	5156.	979467.95	979987.42	-34.51	-210.12	.11	-210.01
WP371	37. 49.43	113. 42.61	5153.	979475.73	979988.67	-28.25	-203.77	.11	-203.66
WP372	37. 49.44	113. 43.72	5163.	979477.26	979988.69	-25.81	-201.66	.12	-201.54
WP373	37. 45.94	113. 42.62	5264.	979470.52	979983.59	-17.95	-197.25	.26	-196.99
WP374	37. 45.06	113. 43.72	5182.	979476.52	979982.30	-18.38	-194.88	.14	-194.74
WP375	37. 45.93	113. 43.71	5175.	979472.41	979983.57	-24.41	-200.67	.13	-200.54
WP376	37. 51.18	113. 41.52	5142.	979488.80	979991.22	-18.77	-193.91	.15	-193.76
WP377	37. 52.05	113. 41.54	5146.	979493.62	979992.49	-14.85	-190.12	.16	-189.96
WP378	37. 52.05	113. 38.22	5130.	979487.07	979992.49	-22.90	-197.63	.12	-197.51
WP379	37. 36.81	113. 31.06	5679.	979431.81	979970.31	-4.34	-197.77	1.00	-196.77
WP380	37. 36.07	113. 30.66	5636.	979432.93	979969.23	-6.19	-198.15	1.39	-196.76
WP381	37. 32.27	113. 30.95	6052.	979400.12	979963.72	5.65	-200.48	1.70	-198.78
WP382	37. 34.66	113. 31.68	5798.	979419.74	979967.19	-2.09	-199.57	2.07	-197.50
WP383	37. 31.23	113. 30.72	6168.	979390.95	979962.21	8.90	-201.19	1.77	-199.42
WP384	37. 31.18	113. 33.66	6530.	979363.82	979962.13	15.90	-206.51	2.12	-204.39
WP385	37. 31.78	113. 36.78	5797.	979412.12	979963.01	-5.62	-203.06	1.10	-201.96
WP386	37. 30.87	113. 37.39	5818.	979409.99	979961.68	-4.46	-202.62	1.52	-201.10
WP387	37. 34.00	113. 37.30	5528.	979436.56	979966.24	-9.72	-198.01	1.49	-196.52
WP388	37. 36.25	113. 37.99	5341.	979447.28	979969.49	-19.85	-201.77	.64	-201.13
WP389	37. 38.91	113. 39.63	5218.	979454.94	979973.37	-27.63	-205.36	.32	-205.04
WP390	37. 38.04	113. 39.63	5231.	979451.52	979972.10	-28.57	-206.74	.38	-206.36
WP391	37. 37.15	113. 39.62	5253.	979449.52	979970.80	-27.19	-206.11	.43	-205.68
WP392	37. 36.29	113. 39.63	5288.	979447.72	979969.55	-24.46	-204.57	.51	-204.06
WP393	37. 35.10	113. 40.75	5323.	979447.91	979967.81	-19.22	-200.52	.69	-199.83
WP394	37. 34.52	113. 41.86	5367.	979446.40	979966.98	-15.78	-198.58	.65	-197.93
WP395	37. 33.33	113. 41.31	5532.	979438.50	979965.27	-6.43	-194.85	1.27	-193.58
WP396	37. 32.41	113. 39.97	5836.	979419.74	979963.92	4.75	-194.03	1.29	-192.74
WP397	37. 31.48	113. 38.47	6034.	979398.46	979962.57	3.45	-202.06	2.07	-199.99
WP398	37. 30.26	113. 37.99	5900.	979406.29	979960.80	.45	-200.50	1.89	-198.61
WP399	37. 33.64	113. 42.94	5392.	979441.61	979965.72	-16.95	-200.61	.78	-199.83

STAT.	LATITUDE	LONGITUDE	ELEV.	OBSERVED GRAVITY	THEOR. GRAVITY	FREE-AIR	SIMPLE BOUGUER	T.C	T.C. BOUGUER
WP400	37. 32.57	113. 43.61	5418.	979436.64	979964.16	-17.92	-202.46	1.66	-200.80
WP401	37. 32.23	113. 44.65	5576.	979427.65	979963.66	-11.54	-201.46	1.17	-200.29
WP402	37. 34.41	113. 44.30	5321.	979449.70	979966.82	-16.63	-197.87	1.40	-196.47
WP403	37. 35.04	113. 43.05	5305.	979454.16	979967.75	-14.61	-195.29	.74	-194.55
WP404	37. 36.01	113. 42.77	5296.	979455.84	979969.14	-15.17	-195.55	.79	-194.76
WP405	37. 36.73	113. 42.63	5312.	979456.53	979970.20	-14.03	-194.95	.60	-194.35
WP406	37. 37.15	113. 41.53	5255.	979455.44	979970.80	-21.09	-200.08	.44	-199.64
WP407	37. 37.17	113. 37.97	5282.	979446.75	979970.84	-27.27	-207.17	.54	-206.63
WP408	37. 38.04	113. 37.98	5245.	979447.51	979972.10	-31.25	-209.89	.46	-209.43
WP409	37. 38.92	113. 37.97	5214.	979448.94	979973.38	-34.03	-211.62	.36	-211.26
WP410	37. 44.41	113. 44.49	5191.	979479.77	979981.36	-13.34	-190.15	.19	-189.96
WP411	37. 41.87	113. 44.01	5425.	979458.20	979977.67	-9.20	-193.98	.32	-193.66
WP412	37. 39.78	113. 42.96	5251.	979459.27	979974.62	-21.45	-200.30	.81	-199.49
WP413	37. 38.49	113. 42.96	5264.	979460.43	979972.76	-17.21	-196.50	.67	-195.83
WP414	37. 38.48	113. 41.87	5238.	979455.69	979972.74	-24.38	-202.79	.42	-202.37
WP415	37. 38.92	113. 40.72	5223.	979455.61	979973.38	-26.50	-204.39	.31	-204.08
WP416	37. 39.79	113. 40.72	5216.	979459.80	979974.63	-24.22	-201.88	.27	-201.61
WP417	37. 38.04	113. 40.72	5233.	979453.53	979972.10	-26.36	-204.60	.35	-204.25
WP418	37. 45.22	113. 46.51	5223.	979470.37	979982.54	-20.90	-198.79	.20	-198.59
WP419	37. 45.07	113. 48.12	5246.	979469.75	979982.32	-19.14	-197.82	.22	-197.60
WP420	37. 45.07	113. 49.23	5261.	979468.87	979982.32	-18.61	-197.80	.31	-197.49
WP421	37. 45.07	113. 50.33	5283.	979467.84	979982.32	-17.57	-197.51	.31	-197.20
WP422	37. 45.07	113. 51.42	5303.	979466.71	979982.32	-16.82	-197.45	.30	-197.15
WP423	37. 46.05	113. 48.56	5261.	979468.48	979983.74	-20.42	-199.61	.22	-199.39
WP424	37. 45.93	113. 47.02	5226.	979470.09	979983.57	-21.93	-199.93	.17	-199.76
WP425	37. 45.92	113. 45.94	5204.	979470.26	979983.55	-23.82	-201.07	.16	-200.91
WP426	37. 46.81	113. 45.91	5206.	979470.75	979984.85	-24.43	-201.74	.15	-201.59
WP427	37. 46.81	113. 47.02	5223.	979473.11	979984.85	-20.47	-198.37	.17	-198.20
WP428	37. 46.81	113. 48.12	5241.	979471.30	979984.85	-20.59	-199.10	.19	-198.91
WP429	37. 46.82	113. 49.22	5261.	979468.37	979984.87	-21.65	-200.84	.22	-200.62
WP430	37. 47.68	113. 49.22	5263.	979467.75	979986.12	-23.35	-202.61	.22	-202.39
WP431	37. 47.68	113. 48.11	5238.	979472.49	979986.12	-20.96	-199.37	.19	-199.18

STAT.	LATITUDE	LONGITUDE	ELEV.	OBSERVED GRAVITY	THEOR. GRAVITY	FREE-AIR	SIMPLE BOUGUER	T.C	T.C. BOUGUER
WP432	37. 47.69	113. 47.01	5219.	979474.69	979986.13	-20.55	-198.31	.17	-198.14
WP433	37. 48.56	113. 47.02	5213.	979474.63	979987.41	-22.45	-200.00	.18	-199.82
WP434	37. 49.42	113. 45.55	5185.	979477.84	979988.66	-23.12	-199.72	.15	-199.57
WP435	37. 49.43	113. 47.02	5202.	979474.03	979988.67	-25.35	-202.53	.19	-202.34
WP436	37. 51.00	113. 47.01	5199.	979472.23	979990.96	-29.72	-206.80	.26	-206.54
WP437	37. 50.30	113. 48.12	5219.	979470.95	979989.94	-28.10	-205.86	.27	-205.59
WP438	37. 49.43	113. 48.12	5227.	979470.80	979988.67	-26.22	-204.26	.23	-204.03
WP439	37. 48.56	113. 48.12	5234.	979471.65	979987.41	-23.46	-201.73	.20	-201.53
WP440	37. 49.43	113. 49.21	5251.	979469.58	979988.67	-25.19	-204.04	.26	-203.78
WP441	37. 49.43	113. 50.31	5268.	979470.09	979988.67	-23.08	-202.51	.31	-202.20
WP442	37. 48.57	113. 50.32	5289.	979467.15	979987.42	-22.80	-202.94	.27	-202.67
WP443	37. 47.69	113. 50.31	5293.	979466.34	979986.13	-21.94	-202.22	.25	-201.97
WP444	37. 48.56	113. 51.42	5312.	979468.60	979987.41	-19.17	-200.10	.30	-199.80
WP445	37. 49.43	113. 51.42	5303.	979471.31	979988.67	-18.57	-199.19	.35	-198.84
WP446	37. 47.69	113. 51.97	5346.	979465.42	979986.13	-17.87	-199.96	.31	-199.65
WP447	37. 51.42	113. 49.86	5269.	979473.56	979991.57	-22.41	-201.88	.42	-201.46
WP449	37. 50.93	113. 51.67	5322.	979475.29	979990.86	-14.99	-196.26	.50	-195.76
WP448	37. 51.65	113. 49.06	5248.	979472.95	979991.91	-25.33	-204.07	.41	-203.66
WP450	37. 51.98	113. 47.02	5198.	979473.89	979992.39	-29.58	-206.62	.31	-206.31
WP451	37. 51.87	113. 45.18	5176.	979481.70	979992.23	-23.68	-199.97	.23	-199.74
WP452	37. 53.79	113. 47.03	5245.	979480.94	979995.02	-20.74	-199.39	.51	-198.88
WP453	37. 52.92	113. 47.02	5209.	979478.16	979993.77	-25.66	-203.08	.40	-202.68
WP454	37. 53.81	113. 48.23	5295.	979478.34	979995.05	-18.67	-199.02	.60	-198.42
WP455	37. 53.82	113. 49.35	5380.	979474.29	979995.06	-14.74	-197.98	.70	-197.28
WP456	37. 52.95	113. 50.32	5383.	979470.97	979993.79	-16.50	-199.85	.64	-199.21
WP457	37. 53.52	113. 51.99	5589.	979457.24	979994.62	-11.68	-202.04	1.05	-200.99
WP458	37. 54.33	113. 50.45	5534.	979465.21	979995.80	-10.07	-198.56	.98	-197.58
WP459	37. 55.56	113. 50.45	5780.	979453.55	979997.59	-.39	-197.25	1.52	-195.73
WP460	37. 54.97	113. 49.22	5518.	979468.13	979996.73	-9.59	-197.54	.99	-196.55
WP461	37. 55.35	113. 48.48	5505.	979468.90	979997.29	-10.60	-198.10	1.03	-197.07
WP462	37. 56.71	113. 49.18	5926.	979446.63	979999.27	4.76	-197.10	2.21	-194.89
WP463	37. 58.38	113. 45.82	5822.	979453.41	980001.72	-.69	-198.98	1.07	-197.91

STAT.	LATITUDE	LONGITUDE	ELEV.	OBSERVED GRAVITY	THEOR. GRAVITY	FREE-AIR	SIMPLE BOUGUER	T.C	T.C. BOUGUER
WP464	37. 59.49	113. 46.93	6039.	979440.53	980003.34	5.22	-200.47	1.61	-198.86
WP465	37. 57.06	113. 46.74	5652.	979464.11	979999.77	-4.04	-196.55	1.67	-194.88
WP466	37. 56.67	113. 45.92	5500.	979472.12	979999.21	-9.76	-197.09	.85	-196.24
WP467	37. 55.09	113. 45.93	5341.	979478.45	979996.91	-16.09	-198.01	.56	-197.45
WP468	37. 50.06	113. 53.27	5378.	979472.07	979989.59	-11.67	-194.84	.62	-194.22
WP469	37. 48.99	113. 53.52	5420.	979467.66	979988.03	-10.57	-195.18	.46	-194.72
WP470	37. 48.16	113. 55.24	5482.	979466.04	979986.82	-5.15	-191.87	.68	-191.19
WP471	37. 47.67	113. 54.00	5410.	979464.82	979986.11	-12.43	-196.70	.42	-196.28
WP472	37. 45.94	113. 53.63	5371.	979463.19	979983.59	-15.21	-198.15	.48	-197.67
WP473	37. 46.86	113. 54.80	5430.	979463.65	979984.93	-10.54	-195.49	.63	-194.86
WP474	37. 45.85	113. 56.76	5594.	979452.52	979983.45	-4.77	-195.31	.93	-194.38
WP475	37. 46.81	113. 57.92	5502.	979459.23	979984.85	-8.11	-195.51	.81	-194.70
WP476	37. 46.07	113. 58.43	5519.	979455.82	979983.77	-8.85	-196.83	.67	-196.16
WP477	37. 47.11	113. 59.45	5550.	979451.47	979985.30	-11.80	-200.83	1.24	-199.59
WP478	37. 48.80	113. 55.76	5554.	979464.02	979987.75	-1.33	-190.50	1.02	-189.48
WP479	37. 52.05	113. 53.37	5607.	979455.92	979992.49	-9.18	-200.15	.92	-199.23
WP480	37. 52.83	113. 53.33	5673.	979452.11	979993.62	-7.92	-201.14	1.08	-200.06
WP481	37. 49.59	113. 56.21	5644.	979457.74	979988.91	-.30	-192.53	1.28	-191.25
WP482	37. 50.49	113. 56.42	5751.	979448.76	979990.22	-.53	-196.41	1.07	-195.34
WP483	37. 51.32	113. 56.50	5865.	979439.90	979991.43	.13	-199.63	1.15	-198.48
WP484	37. 52.23	113. 56.52	5990.	979429.42	979992.76	.08	-203.94	1.37	-202.57
WP485	37. 53.16	113. 56.38	6071.	979422.48	979994.09	-.59	-207.37	1.59	-205.78
WP486	37. 54.01	113. 56.54	6155.	979417.20	979995.34	.80	-208.84	1.60	-207.24
WP487	37. 54.69	113. 56.93	6255.	979410.60	979996.33	2.62	-210.43	2.00	-208.43
WP488	37. 55.52	113. 56.84	6330.	979405.52	979997.53	3.39	-212.21	2.33	-209.88
WP489	37. 56.33	113. 57.06	6465.	979393.75	979998.71	3.14	-217.05	1.50	-215.55
WP490	37. 57.14	113. 56.97	6589.	979384.59	979999.90	4.46	-219.96	1.04	-218.92
WP491	37. 57.84	113. 57.04	6641.	979381.29	980000.93	5.01	-221.18	1.00	-220.18
WP492	37. 59.04	113. 57.03	6627.	979378.23	980002.68	-1.12	-226.83	.95	-225.88
WP493	37. 59.03	113. 58.14	6710.	979372.99	980002.66	1.47	-227.07	1.22	-225.85
WP494	37. 59.28	113. 59.00	6812.	979368.26	980003.02	5.97	-226.05	1.55	-224.50
WP495	37. 59.95	113. 59.95	6905.	979362.80	980004.00	8.28	-226.90	1.61	-225.29

STAT.	LATITUDE	LONGITUDE	ELEV.	OBSERVED GRAVITY	THEOR. GRAVITY	FREE-AIR	SIMPLE BOUGUER	T.C	T.C. BOUGUER
WP496	37. 59.91	113. 58.13	6715.	979370.90	980003.95	-1.44	-230.15	1.11	-229.04
WP497	37. 59.90	113. 57.04	6624.	979376.68	980003.93	-4.21	-229.83	.93	-228.90
WP498	37. 59.91	113. 55.93	6552.	979382.27	980003.95	-5.41	-228.58	.85	-227.73
WP499	37. 59.90	113. 54.84	6509.	979386.40	980003.93	-5.30	-227.00	.84	-226.16
WP500	37. 59.91	113. 53.76	6523.	979391.09	980003.95	.70	-221.47	.89	-220.58
WP501	37. 59.91	113. 52.29	6650.	979402.55	980003.95	24.10	-202.40	1.54	-200.86
WP502	37. 43.76	113. 49.21	5244.	979471.23	979980.43	-15.96	-194.57	.35	-194.22
WP503	37. 44.01	113. 47.38	5219.	979473.87	979980.77	-16.01	-193.77	.24	-193.53
WP504	37. 42.67	113. 47.86	5249.	979474.39	979978.84	-10.73	-189.51	.49	-189.02
WP505	37. 42.25	113. 50.21	5289.	979470.37	979978.22	-10.38	-190.53	.60	-189.93
WP506	37. 44.15	113. 52.23	5295.	979467.81	979980.98	-15.12	-195.46	.47	-194.99
WP507	37. 44.78	113. 45.49	5206.	979475.21	979981.90	-17.02	-194.34	.18	-194.16
WP508	37. 43.33	113. 51.42	5277.	979469.45	979979.80	-14.01	-193.75	.44	-193.31
WP509	37. 43.34	113. 50.32	5249.	979471.70	979979.81	-14.40	-193.18	.39	-192.79
WP510	37. 42.45	113. 51.42	5351.	979464.97	979978.52	-10.24	-192.49	.52	-191.97
WP511	37. 41.48	113. 49.50	5386.	979464.95	979977.10	-5.55	-189.00	.77	-188.23
WP512	37. 41.07	113. 49.01	5440.	979461.35	979976.51	-3.48	-188.76	.74	-188.02
WP513	37. 40.21	113. 49.09	5580.	979452.68	979975.26	2.28	-187.77	.82	-186.95
WP514	37. 39.01	113. 47.91	5600.	979445.27	979973.52	-1.51	-192.25	.59	-191.66
WP515	37. 39.23	113. 45.31	5375.	979455.22	979973.84	-13.05	-196.12	.90	-195.22
WP516	37. 40.24	113. 46.70	5466.	979453.58	979975.29	-7.59	-193.77	.79	-192.98
WP517	37. 43.32	113. 53.61	5376.	979463.20	979979.79	-10.93	-194.03	.48	-193.55
WP518	37. 44.20	113. 53.61	5342.	979465.00	979981.05	-13.60	-195.55	.59	-194.96
WP519	37. 43.32	113. 55.81	5487.	979457.63	979979.79	-6.06	-192.94	.58	-192.36
WP520	37. 43.32	113. 54.72	5432.	979460.28	979979.79	-8.58	-193.60	.52	-193.08
WP521	37. 42.68	113. 55.92	5566.	979452.83	979978.84	-2.49	-192.07	.67	-191.40
WP522	37. 41.57	113. 55.85	5794.	979439.05	979977.23	6.80	-190.55	1.11	-189.44
WP523	37. 42.03	113. 55.00	5625.	979448.36	979977.90	-.46	-192.05	.82	-191.23
WP524	37. 42.54	113. 53.77	5460.	979459.09	979978.65	-6.00	-191.97	.64	-191.33
WP525	37. 34.28	113. 45.27	5352.	979448.34	979966.64	-14.90	-197.19	1.38	-195.81
WP526	37. 33.91	113. 46.31	5388.	979448.93	979966.12	-10.40	-193.92	2.03	-191.89
WP527	37. 34.24	113. 47.31	5404.	979453.62	979966.58	-4.67	-188.73	2.07	-186.67

STAT.	LATITUDE	LONGITUDE	ELEV.	OBSERVED GRAVITY	THEOR. GRAVITY	FREE-AIR	SIMPLE BOUGUER	T.C	T.C. BOUGUER
WP528	37. 34.47	113. 48.16	5438.	979452.27	979966.91	-3.16	-188.38	3.69	-184.69
WP529	37. 34.63	113. 50.25	5506.	979451.73	979967.14	2.49	-185.05	1.04	-184.01
WP530	37. 34.85	113. 51.28	5518.	979451.10	979967.46	2.66	-185.29	1.04	-184.25
WP531	37. 30.88	113. 51.03	5715.	979422.92	979961.70	-1.23	-195.88	1.61	-194.27
WP532	37. 35.41	113. 49.67	5577.	979450.03	979968.27	6.34	-183.61	.73	-182.88
WP533	37. 36.75	113. 48.19	5812.	979428.02	979970.22	4.47	-193.48	1.16	-192.32
WP534	37. 36.88	113. 46.05	5640.	979440.35	979970.41	.44	-191.65	1.05	-190.60
WP535	37. 33.62	113. 50.17	5522.	979452.08	979965.69	5.79	-182.56	1.59	-180.97
WP536	37. 31.85	113. 50.88	5625.	979429.05	979963.11	-4.98	-196.57	4.09	-192.48
WP537	37. 35.63	113. 52.97	5598.	979441.22	979968.59	-.83	-191.50	.82	-190.68
WP538	37. 36.10	113. 54.01	5639.	979436.97	979969.27	-1.91	-193.97	.98	-192.99
WP539	37. 36.45	113. 55.78	5897.	979413.86	979969.78	-1.26	-199.59	.75	-198.84
WP540	37. 36.52	113. 56.77	5986.	979409.37	979969.89	2.52	-201.36	.85	-200.51
WP541	37. 36.44	113. 57.84	6095.	979402.48	979969.77	6.01	-201.58	.73	-200.85
WP542	37. 36.68	113. 58.86	5954.	979409.64	979970.12	-.45	-203.24	.64	-202.60
WP543	37. 35.67	113. 56.12	5950.	979413.36	979968.65	4.37	-198.29	.88	-197.41
WP544	37. 34.87	113. 57.56	6126.	979398.45	979967.49	7.17	-201.48	.83	-200.65
WP545	37. 40.55	113. 29.97	5592.	979436.86	979975.74	-12.91	-203.39	1.08	-202.31
WP546	37. 40.52	113. 30.36	5536.	979439.79	979975.70	-15.21	-203.76	.96	-202.80
WP547	37. 40.54	113. 30.68	5475.	979443.24	979975.73	-17.52	-203.98	.91	-203.07
WP548	37. 40.52	113. 31.06	5434.	979445.39	979975.70	-19.20	-204.28	.79	-203.49
WP549	37. 40.48	113. 31.46	5376.	979448.11	979975.64	-21.87	-204.96	.77	-204.19
WP550	37. 40.43	113. 31.90	5320.	979449.12	979975.58	-26.06	-207.26	.78	-206.48
WP551	37. 40.35	113. 32.38	5313.	979445.87	979975.45	-29.85	-210.81	.66	-210.15
WP552	37. 40.39	113. 33.24	5275.	979444.19	979975.52	-35.17	-214.84	.55	-214.29
WP553	37. 40.83	113. 34.50	5226.	979442.99	979976.16	-41.61	-219.61	.42	-219.19
WP554	37. 41.09	113. 35.21	5207.	979443.65	979976.54	-43.13	-220.48	.33	-220.15
WP555	37. 41.79	113. 37.12	5183.	979451.45	979977.55	-38.60	-215.14	.22	-214.92
WP556	37. 41.71	113. 31.22	5286.	979451.97	979977.44	-28.28	-208.32	.94	-207.38
WP557	37. 42.44	113. 30.51	5237.	979457.23	979978.50	-28.69	-207.06	1.65	-205.41
WP558	37. 47.64	113. 25.01	5383.	979463.49	979986.06	-16.25	-199.60	.42	-199.18
WP559	37. 47.61	113. 25.62	5349.	979464.63	979986.02	-18.26	-200.45	.46	-199.99

STAT.	LATITUDE	LONGITUDE	ELEV.	OBSERVED GRAVITY	THEOR. GRAVITY	FREE-AIR	SIMPLE BOUGUER	T.C	T.C. BOUGUER
WP560	37. 47.62	113. 26.04	5300.	979466.44	979986.03	-21.08	-201.59	.49	-201.10
WP561	37. 47.66	113. 26.59	5239.	979469.44	979986.09	-23.89	-202.34	.51	-201.83
WP562	37. 47.66	113. 27.14	5173.	979472.75	979986.09	-26.78	-202.97	.54	-202.43
WP563	37. 47.64	113. 27.46	5151.	979472.55	979986.06	-29.02	-204.46	.53	-203.93
WP564	37. 47.66	113. 27.91	5130.	979472.19	979986.09	-31.39	-206.09	.49	-205.60
WP565	37. 47.65	113. 28.34	5128.	979472.29	979986.08	-31.46	-206.12	.43	-205.69
WP566	37. 47.66	113. 29.08	5129.	979472.58	979986.09	-31.09	-205.78	.32	-205.46
WP567	37. 47.69	113. 31.06	5133.	979473.82	979986.13	-29.51	-204.34	.18	-204.16
WP568	37. 47.69	113. 32.80	5130.	979473.57	979986.13	-30.04	-204.77	.13	-204.64
WP569	37. 47.69	113. 41.51	5151.	979467.34	979986.13	-34.30	-209.75	.11	-209.64
WP570	37. 47.69	113. 42.61	5160.	979464.70	979986.13	-36.09	-211.84	.11	-211.73
WP571	37. 47.69	113. 43.72	5169.	979464.88	979986.13	-35.06	-211.11	.12	-210.99
WP572	37. 47.67	113. 30.00	5133.	979471.91	979986.11	-31.40	-206.24	.24	-206.00
WP573	37. 50.12	113. 25.64	5148.	979476.80	979989.68	-28.66	-204.00	.14	-203.86
WP574	37. 50.61	113. 24.66	5153.	979474.23	979990.39	-31.48	-207.00	.11	-206.89
WP575	37. 51.08	113. 25.99	5164.	979484.61	979991.08	-20.75	-196.64	.16	-196.48
WP576	37. 51.92	113. 25.76	5197.	979484.74	979992.30	-18.73	-195.72	.23	-195.49
WP577	37. 52.90	113. 22.81	5169.	979475.38	979993.73	-32.16	-208.22	.05	-208.17
WP578	37. 52.90	113. 23.11	5162.	979478.23	979993.73	-29.97	-205.80	.04	-205.76
WP579	37. 52.90	113. 23.92	5163.	979482.88	979993.73	-25.23	-201.08	.04	-201.04
WP580	37. 52.90	113. 24.45	5164.	979484.30	979993.73	-23.72	-199.61	.05	-199.56
WP581	37. 52.89	113. 25.00	5149.	979486.43	979993.72	-22.98	-198.36	.06	-198.30
WP582	37. 52.92	113. 25.55	5161.	979488.52	979993.77	-19.81	-195.59	.11	-195.48
WP583	37. 52.96	113. 26.15	5237.	979485.27	979993.80	-15.95	-194.34	.26	-194.08
WP584	37. 53.26	113. 26.63	5181.	979489.66	979994.24	-17.26	-193.74	.14	-193.60
WP585	38. .36	113. 27.48	5088.	979494.44	980004.60	-31.60	-204.90	.35	-204.55
WP586	38. .39	113. 28.60	5265.	979496.02	980004.64	-13.41	-192.73	.39	-192.34
WP587	38. .08	113. 29.60	5306.	979493.87	980004.20	-11.25	-191.98	.41	-191.57
WP588	38. .06	113. 31.56	5381.	979484.12	980004.16	-13.92	-197.19	.40	-196.79
WP589	38. .39	113. 32.66	5480.	979478.43	980004.64	-10.77	-197.42	.35	-197.07
WP590	38. .69	113. 33.80	5524.	979479.35	980005.09	-6.15	-194.30	.39	-193.91
WP591	38. .68	113. 34.75	5514.	979479.48	980005.07	-6.95	-194.75	.45	-194.30

STAT.	LATITUDE	LONGITUDE	ELEV.	OBSERVED GRAVITY	THEOR. GRAVITY	FREE-AIR	SIMPLE BOUGUER	T.C	T.C. BOUGUER
WP592	37. 43.76	113. 42.62	5170.	979478.23	979980.43	-15.91	-192.00	.19	-191.81
WP593	37. 43.37	113. 41.52	5176.	979475.50	979979.85	-17.50	-193.79	.16	-193.63
WP594	37. 42.97	113. 40.43	5179.	979473.95	979979.27	-18.19	-194.59	.16	-194.43
WP595	37. 42.57	113. 39.33	5180.	979468.98	979978.69	-22.49	-198.92	.18	-198.74
WP596	37. 42.08	113. 37.96	5179.	979457.73	979977.98	-33.11	-209.51	.19	-209.32
WP597	37. 54.21	113. 1.84	5510.	979450.05	979995.62	-27.32	-214.99	.49	-214.50
WP598	37. 54.47	113. .73	5515.	979453.34	979996.01	-23.94	-211.80	.57	-211.23
WP599	37. 54.63	113. .01	5528.	979454.98	979996.23	-21.29	-209.58	.65	-208.93
WP600	37. 54.66	112. 59.56	5535.	979456.35	979996.28	-19.32	-207.84	.82	-207.02
WP601	37. 54.89	112. 59.54	5565.	979454.16	979996.62	-19.03	-208.58	.71	-207.87
WP602	37. 54.65	112. 59.22	5540.	979458.20	979996.27	-16.99	-205.68	1.13	-204.55
WP603	37. 54.48	112. 58.88	5556.	979459.70	979996.02	-13.73	-202.96	1.57	-201.39
WP604	37. 54.29	112. 53.40	5573.	979459.41	979995.74	-12.14	-201.95	2.18	-199.77
WP605	37. 54.04	112. 57.41	5646.	979452.52	979995.38	-11.80	-204.10	3.17	-200.93
WP606	37. 53.73	112. 56.81	5719.	979446.31	979994.92	-10.69	-205.48	2.34	-203.14
WP607	37. 53.63	112. 56.36	5691.	979445.98	979994.78	-13.51	-207.34	1.89	-205.45
WP608	37. 52.95	112. 55.48	5687.	979440.17	979993.79	-18.71	-212.42	1.21	-211.21
WP609	37. 53.17	112. 54.93	5719.	979437.85	979994.11	-18.34	-213.13	1.09	-212.04
WP610	37. 52.95	112. 54.21	5697.	979433.87	979993.79	-24.07	-218.09	1.30	-216.79
WP611	37. 52.99	112. 44.12	6465.	979384.19	979993.84	-1.57	-221.76	7.75	-214.01
WP612	37. 52.51	112. 44.56	6290.	979394.01	979993.16	-7.53	-221.77	9.76	-212.01
WP613	37. 52.54	112. 44.94	6197.	979399.55	979993.20	-10.77	-221.84	8.46	-213.38
WP614	37. 52.94	112. 45.88	5950.	979413.29	979993.79	-20.85	-223.51	3.52	-219.99
WP615	37. 53.00	112. 46.35	5892.	979415.22	979993.86	-24.45	-225.13	3.01	-222.12
WP616	37. 52.93	112. 46.77	5842.	979416.70	979993.77	-27.59	-226.57	2.84	-223.73
WP617	37. 52.92	112. 47.30	5803.	979416.98	979993.77	-30.96	-228.61	2.49	-226.12
WP618	37. 54.71	112. 45.34	5887.	979418.83	979996.36	-23.81	-224.32	2.62	-221.70
WP619	37. 55.60	112. 47.55	5713.	979423.54	979997.66	-36.76	-231.35	1.49	-229.86
WP620	37. 56.46	112. 49.19	5694.	979430.96	979998.91	-32.38	-226.31	1.37	-224.94
WP621	37. 55.57	112. 49.76	5704.	979427.96	979997.61	-33.14	-227.42	1.34	-226.08
WP622	37. 53.61	112. 50.59	5740.	979423.95	979994.75	-30.90	-226.40	1.32	-225.08
WP623	37. 47.88	112. 48.88	6615.	979370.59	979986.41	6.39	-218.91	7.92	-210.99

STAT.	LATITUDE	LONGITUDE	ELEV.	OBSERVED GRAVITY	THEOR. GRAVITY	FREE-AIR	SIMPLE BOUGUER	T.C	T.C. BOUGUER
WP625	37. 49.44	112. 48.62	6297.	979392.48	979988.69	-3.92	-218.39	5.40	-212.99
WP626	37. 49.69	112. 48.82	6215.	979397.79	979989.05	-6.69	-218.37	4.75	-213.62
WP627	37. 50.01	112. 48.94	6154.	979400.63	979989.52	-10.05	-219.67	4.18	-215.49
WP628	37. 50.20	112. 49.08	6106.	979403.70	979989.80	-11.77	-219.74	3.84	-215.90
WP629	37. 50.32	112. 49.14	6066.	979405.11	979989.97	-14.30	-220.90	3.52	-217.38
WP630	37. 50.53	112. 49.25	6028.	979406.70	979990.27	-16.59	-221.90	3.04	-218.86
WP631	37. 51.44	112. 49.64	5990.	979408.89	979991.60	-19.30	-223.32	2.14	-221.18
WP632	37. 51.95	112. 48.13	5853.	979414.30	979992.34	-27.52	-226.87	2.79	-224.08
WP633	37. 51.50	112. 47.56	5950.	979410.72	979991.69	-21.32	-223.98	4.15	-219.83
WP634	37. 50.98	112. 48.30	5942.	979410.65	979990.93	-21.39	-223.78	3.98	-219.80
WP635	37. 51.45	112. 49.77	5932.	979412.23	979991.62	-21.43	-223.47	2.08	-221.39
WP636	37. 50.32	112. 50.33	5950.	979410.04	979989.97	-20.28	-222.94	3.98	-219.80
WP637	37. 49.90	112. 51.14	5889.	979415.38	979989.36	-20.07	-220.64	3.73	-216.91
WP638	37. 49.73	112. 51.96	5872.	979416.98	979989.11	-19.81	-219.81	3.56	-216.25
WP639	37. 52.08	112. 50.32	5838.	979416.55	979992.53	-26.87	-225.71	1.69	-224.02
WP640	37. 52.08	112. 51.43	5801.	979420.08	979992.53	-26.82	-224.40	1.49	-222.91
WP641	37. 51.28	112. 51.41	5841.	979417.06	979991.37	-24.91	-223.85	1.83	-222.02
WP642	37. 51.85	112. 52.50	5769.	979424.16	979992.20	-25.42	-221.91	1.43	-220.48
WP643	37. 50.75	112. 52.11	5819.	979418.09	979990.59	-25.18	-223.38	2.04	-221.34
WP644	37. 51.39	112. 52.53	5778.	979422.73	979991.53	-25.33	-222.13	1.61	-220.52
WP645	37. 54.36	112. 54.19	5718.	979428.62	979995.84	-29.40	-224.15	1.07	-223.08
WP646	37. 51.84	112. 55.28	5703.	979434.12	979992.19	-21.65	-215.89	1.42	-214.47
WP647	37. 51.20	112. 55.21	5721.	979431.59	979991.25	-21.54	-216.40	1.48	-214.92
WP648	37. 50.31	112. 53.89	5788.	979425.41	979989.95	-20.13	-217.27	1.89	-215.38
WP649	37. 50.30	112. 52.51	5810.	979418.91	979989.94	-24.55	-222.44	2.35	-220.09
WP650	37. 48.64	112. 48.47	6437.	979380.36	979987.52	-1.71	-220.95	10.56	-210.39
WP651	37. 49.13	112. 53.88	5943.	979413.12	979988.24	-16.13	-218.55	2.90	-215.65
WP652	37. 48.62	112. 53.45	6148.	979401.24	979987.49	-7.98	-217.38	4.30	-213.08
WP653	37. 47.99	112. 54.40	6230.	979396.62	979986.58	-3.97	-216.16	5.06	-211.10
WP654	37. 47.21	112. 54.93	6313.	979394.27	979985.44	2.63	-212.39	6.70	-205.69
WP655	37. 46.79	112. 54.65	6667.	979372.20	979984.83	14.47	-212.61	5.58	-207.03
WP656	37. 48.27	112. 55.26	6017.	979410.44	979986.98	-10.59	-215.53	2.99	-212.54

STAT.	LATITUDE	LONGITUDE	ELEV.	OBSERVED GRAVITY	THEOR. GRAVITY	FREE-AIR	SIMPLE BOUGUER	T.C	T.C. BOUGUER
WP657	37. 48.06	112. 56.49	5952.	979414.70	979986.67	-12.14	-214.86	2.61	-212.25
WP658	37. 46.89	112. 57.97	6030.	979409.79	979984.98	-8.01	-213.39	3.78	-209.61
WP659	37. 47.23	112. 56.92	5952.	979412.50	979985.47	-13.13	-215.86	4.19	-211.67
WP660	37. 50.09	112. 55.27	5776.	979427.82	979989.63	-18.53	-215.26	1.69	-213.57
WP661	37. 49.63	112. 56.36	5808.	979425.40	979988.96	-17.27	-215.09	1.62	-213.47
WP662	37. 48.75	112. 55.92	5862.	979420.10	979987.68	-16.21	-215.87	2.31	-213.56
WP663	37. 47.46	112. 59.75	5857.	979423.50	979985.80	-11.40	-210.88	1.95	-208.93
WP664	37. 48.13	112. 57.75	5855.	979420.27	979986.78	-15.79	-215.22	2.11	-213.11
WP665	37. 50.54	112. 56.92	5753.	979432.10	979990.29	-17.07	-213.02	1.66	-211.36
WP666	37. 50.03	112. 57.38	5772.	979431.59	979989.55	-15.04	-211.63	1.69	-209.94
WP667	37. 49.21	112. 58.02	5790.	979428.34	979988.35	-15.42	-212.63	1.61	-211.02
WP668	37. 49.82	112. 58.59	5880.	979428.99	979989.24	-7.18	-207.45	1.43	-206.02
WP669	37. 49.24	112. 59.25	5702.	979440.74	979988.40	-11.33	-205.54	1.66	-203.88
WP670	37. 50.12	112. 59.46	5854.	979432.45	979989.68	-6.61	-206.00	1.24	-204.76
WP671	37. 51.28	112. 59.23	5950.	979428.26	979991.37	-3.46	-206.12	1.01	-205.11
WP672	37. 52.12	112. 58.96	5936.	979431.83	979992.59	-2.43	-204.61	.98	-203.63
WP673	38. 4.01	112. 41.35	5901.	979433.32	980009.92	-21.56	-222.55	1.69	-220.86
WP674	38. 3.47	112. 41.57	5871.	979434.41	980009.13	-22.51	-222.47	1.66	-220.81
WP675	38. .44	112. 43.23	5809.	979433.08	980004.72	-25.25	-223.10	1.41	-221.69
WP676	37. 39.41	113. 30.44	5623.	979433.55	979974.10	-11.65	-203.17	.69	-202.48
WP677	37. 38.73	113. 30.40	5474.	979441.35	979973.11	-16.88	-203.33	1.17	-202.16
WP678	37. 39.19	113. 31.73	5443.	979444.16	979973.78	-17.67	-203.06	1.48	-201.58
WP679	37. 37.97	113. 31.80	5833.	979421.48	979972.00	-1.87	-200.54	.93	-199.61
WP680	37. 35.13	113. 32.28	6350.	979385.00	979967.86	14.42	-201.86	4.28	-197.58
WP681	37. 31.91	113. 33.74	6695.	979356.16	979963.20	22.69	-205.34	3.07	-202.27
WP682	37. 33.48	113. 32.78	6245.	979389.14	979965.49	11.05	-201.65	1.43	-200.22
WP683	37. 32.22	113. 32.38	6415.	979376.74	979963.65	16.49	-202.01	1.28	-200.73
WP684	37. 33.47	113. 35.58	6398.	979384.09	979965.48	20.41	-197.51	2.63	-194.88
WP685	37. 40.65	113. 25.38	6262.	979407.53	979975.90	20.64	-192.64	1.46	-191.18
WP686	37. 41.93	113. 26.57	6889.	979366.36	979977.76	36.58	-198.06	2.48	-195.58
WP687	37. 42.72	113. 25.93	6825.	979374.07	979978.91	37.12	-195.34	2.19	-193.15
WP688	37. 42.71	113. 24.24	6670.	979380.81	979978.89	29.30	-197.88	2.61	-195.27

STAT.	LATITUDE	LONGITUDE	ELEV.	OBSERVED GRAVITY	THEOR. GRAVITY	FREE-AIR	SIMPLE BOUGUER	T.C	T.C. BOUGUER
WP689	37. 42.46	113. 22.61	6296.	979408.12	979978.52	21.79	-192.65	1.26	-191.39
WP690	37. 47.70	113. 23.45	5402.	979463.89	979986.15	-14.15	-198.15	.41	-197.74
WP691	37. 45.91	113. 22.98	5615.	979452.82	979983.54	-2.58	-193.83	.84	-192.99
WP692	37. 52.03	113. 27.22	5235.	979484.06	979992.47	-16.01	-194.31	.22	-194.09
WP693	38. 5.10	113. 38.64	5988.	979441.05	980011.51	-7.23	-211.18	2.02	-209.16
WP694	38. 5.95	113. 39.76	6168.	979425.76	980012.75	-6.84	-216.92	1.26	-215.66
WP695	38. 6.76	113. 41.65	6414.	979413.10	980013.93	2.47	-215.99	.78	-215.21
WP696	38. 6.86	113. 42.72	6458.	979414.25	980014.07	7.62	-212.34	1.05	-211.29
WP697	38. 6.50	113. 44.90	6750.	979401.34	980013.55	22.69	-207.21	1.69	-205.52
WP698	38. 2.13	113. 40.18	5976.	979453.80	980007.18	8.72	-194.82	.69	-194.13
WP699	38. 3.71	113. 42.67	6469.	979416.71	980009.48	15.70	-204.65	2.17	-202.48
WP700	38. 3.37	113. 41.78	6221.	979432.87	980008.99	9.02	-202.85	1.31	-201.54
WP701	38. 1.68	113. 42.29	6192.	979436.92	980006.52	12.82	-198.04	1.09	-196.95
WP702	38. .58	113. 43.61	6117.	979439.12	980004.92	9.56	-198.78	1.20	-197.58
WP703	37. 56.91	113. 44.83	5556.	979470.25	979999.56	-6.72	-195.95	.62	-195.33
WP704	37. 57.81	113. 45.23	5683.	979462.31	980000.89	-4.04	-197.61	.84	-196.77
WP705	37. 58.91	113. 46.29	5997.	979442.68	980002.49	4.26	-199.98	1.15	-198.83
WP706	38. .16	113. 46.97	6226.	979430.79	980004.31	12.10	-199.96	1.13	-198.83
WP707	37. 59.04	113. 55.93	6564.	979383.26	980002.68	-2.02	-225.59	.86	-224.73
WP708	37. 59.04	113. 54.82	6550.	979385.44	980002.68	-1.16	-224.26	.93	-223.33
WP709	37. 59.04	113. 53.76	6610.	979390.70	980002.68	9.75	-215.38	1.11	-214.27
WP710	37. 58.30	113. 53.50	6829.	979384.02	980001.60	24.75	-207.84	2.14	-205.70
WP711	37. 59.04	113. 52.95	6732.	979394.37	980002.68	24.90	-204.40	1.45	-202.95
WP712	37. 58.45	113. 52.96	7075.	979370.40	980001.82	34.05	-206.92	2.09	-204.83
WP713	37. 59.91	113. 51.75	6788.	979393.19	980003.95	27.72	-203.49	2.12	-201.37
WP714	37. 59.91	113. 52.97	6581.	979399.82	980003.95	14.89	-209.25	1.04	-208.21
WP715	37. 59.91	113. 54.30	6500.	979388.81	980003.95	-3.75	-225.15	.88	-224.27
WP716	37. 59.05	113. 51.68	6870.	979387.96	980002.70	31.46	-202.52	2.70	-199.82
WP717	37. 58.32	113. 51.46	7370.	979354.22	980001.62	45.82	-205.20	4.31	-200.89
WP718	38. .38	113. 51.92	6654.	979401.56	980004.63	22.81	-203.82	1.50	-202.32
WP719	38. 1.03	113. 51.11	6670.	979404.85	980005.58	26.65	-200.53	1.15	-199.38
WP720	38. .87	113. 50.45	6716.	979402.44	980005.34	28.80	-199.96	1.40	-198.56

STAT.	LATITUDE	LONGITUDE	ELEV.	OBSERVED GRAVITY	THEOR. GRAVITY	FREE-AIR	SIMPLE BOUGUER	T.C	T.C. BOUGUER
WP721	38. .73	113. 49.86	6767.	979400.45	980005.14	31.81	-198.66	1.64	-197.02
WP722	37. 37.45	113. 49.30	6217.	979401.34	979971.24	14.86	-196.89	1.41	-195.48
WP723	37. 38.11	113. 51.04	6217.	979404.66	979972.20	17.23	-194.52	.97	-193.55
WP724	37. 36.63	113. 54.43	5668.	979433.34	979970.05	-3.59	-196.64	.87	-195.77
WP725	37. 41.45	113. 45.73	5641.	979443.52	979977.05	-2.95	-195.09	.49	-194.60
AA020	38. .44	112. 43.23	5809.	979433.15	980004.72	-25.18	-223.03	1.41	-221.62
AA091	38. 7.37	112. 45.38	7558.	979342.89	980014.84	38.96	-218.47	2.76	-215.71
AA092	38. 6.39	112. 46.02	7883.	979319.79	980013.39	47.87	-220.62	3.37	-217.28
AA093	38. 6.08	112. 47.45	7653.	979341.05	980012.94	47.95	-212.71	2.70	-210.01
AA094	38. 4.74	112. 48.13	7326.	979364.74	980010.98	42.84	-206.68	2.94	-203.74
AA095	38. 3.99	112. 50.12	7033.	979382.21	980009.89	33.85	-205.69	1.70	-203.99
AA096	38. 4.93	112. 52.36	6805.	979395.50	980011.27	24.32	-207.46	1.18	-206.28
AA097	38. 6.21	112. 50.18	7496.	979355.58	980013.12	47.53	-207.79	2.43	-205.36
AA098	38. 7.42	112. 50.55	7328.	979369.11	980014.91	43.47	-206.12	1.94	-204.18
AA100	38. 6.25	112. 48.22	7525.	979352.02	980013.19	46.63	-209.67	2.83	-206.84
AA101	38. 5.51	112. 48.63	7838.	979328.77	980012.11	53.91	-213.05	2.99	-210.06
AA105	38. 1.52	112. 43.32	5778.	979440.91	980006.29	-21.90	-218.69	1.41	-217.28
AA106	38. 1.51	112. 44.08	5779.	979442.30	980006.27	-20.41	-217.23	1.37	-215.86
AA108	38. 1.27	112. 46.86	6036.	979427.56	980005.93	-10.63	-216.22	1.28	-214.94
AA109	38. .67	112. 47.44	5981.	979431.50	980005.05	-10.99	-214.70	1.13	-213.57
AA110	38. .50	112. 49.04	6118.	979429.83	980004.80	.48	-207.90	1.28	-206.62
AA111	38. 1.48	112. 50.16	6568.	979407.10	980006.23	18.65	-205.06	1.50	-203.56
AA112	38. 2.01	112. 51.60	6756.	979403.48	980007.01	31.94	-198.17	1.08	-197.09
AA113	38. .85	112. 51.16	6659.	979402.16	980005.31	23.20	-203.60	1.18	-202.42
AA114	38. .63	112. 52.13	6532.	979411.60	980004.99	21.01	-201.47	1.12	-200.35
AA115	38. .18	112. 45.30	5738.	979438.98	980004.34	-25.65	-221.09	1.26	-219.83
AA144	37. 58.24	112. 43.16	5860.	979423.13	980001.52	-27.20	-226.79	1.94	-224.85
AA145	37. 57.39	112. 44.01	5864.	979422.05	980000.27	-26.67	-226.40	1.75	-224.65
AA146	37. 57.60	112. 45.52	6120.	979413.24	980000.59	-11.71	-220.16	2.55	-217.61
AA147	37. 53.82	112. 46.45	5834.	979416.77	979995.06	-29.56	-228.26	2.29	-225.97
AA148	37. 53.83	112. 45.33	5880.	979417.81	979995.07	-24.19	-224.46	4.01	-220.45
AA149	37. 54.54	112. 44.87	5990.	979414.38	979996.10	-18.31	-222.33	5.02	-217.31

STAT.	LATITUDE	LONGITUDE	ELEV.	OBSERVED GRAVITY	THEOR. GRAVITY	FREE-AIR	SIMPLE BOUGUER	T.C	T.C. BOUGUER
AA150	37. 56.03	112. 44.48	5784.	979424.20	979998.28	-30.05	-227.05	2.77	-224.28
AA154	37. 53.30	112. 46.11	5897.	979415.41	979994.30	-24.23	-225.09	2.90	-222.19
AA155	37. 52.94	112. 45.46	6008.	979410.92	979993.79	-17.76	-222.40	4.82	-217.58
AA156	37. 52.99	112. 44.13	6465.	979384.10	979993.84	-1.65	-221.85	7.73	-214.12
AA157	37. 52.92	112. 47.84	5792.	979415.95	979993.77	-33.03	-230.31	2.20	-228.11
AA158	37. 52.95	112. 49.21	5798.	979417.13	979993.79	-31.30	-228.78	1.65	-227.13
AA159	37. 52.95	112. 50.29	5796.	979419.72	979993.79	-29.85	-226.92	1.43	-225.49
AA160	37. 52.94	112. 51.43	5758.	979423.42	979993.79	-28.78	-224.90	1.28	-223.62
AA161	37. 52.95	112. 52.48	5730.	979426.20	979993.79	-28.63	-223.79	1.20	-222.59
AA162	37. 52.95	112. 53.07	5709.	979428.62	979993.79	-28.19	-222.64	1.23	-221.41
AA164	37. 52.94	112. 56.03	5727.	979439.31	979993.79	-15.80	-210.86	1.23	-209.63
AA166	37. 54.61	112. 55.25	5770.	979439.42	979996.20	-14.07	-210.60	1.12	-209.48
AA167	37. 55.22	112. 54.79	5810.	979438.87	979997.09	-11.74	-209.63	1.00	-208.63
AA168	37. 55.59	112. 54.01	5897.	979435.37	979997.64	-7.61	-208.46	.96	-207.50
AA169	37. 54.80	112. 53.57	5699.	979441.32	979996.48	-19.12	-213.22	1.17	-212.05
AA170	37. 55.88	112. 53.21	5979.	979427.51	979998.05	-8.17	-211.81	1.25	-210.56
AA171	37. 57.33	112. 49.76	5721.	979435.87	980000.17	-26.18	-221.04	1.37	-219.67
AA172	37. 59.68	112. 49.16	6005.	979432.59	980003.61	-6.19	-210.72	1.27	-209.45
AA173	37. 58.86	112. 46.82	5737.	979437.48	980002.41	-25.32	-220.72	1.19	-219.53
AA174	37. 59.09	112. 45.76	5722.	979436.05	980002.75	-28.49	-223.38	1.28	-222.10
AA175	37. 54.70	112. 47.55	5735.	979421.03	979996.34	-35.89	-231.22	1.66	-229.56
AA176	37. 53.83	112. 47.54	5762.	979418.60	979995.07	-34.50	-230.76	1.89	-228.87
AA177	37. 54.70	112. 49.20	5718.	979425.19	979996.34	-33.33	-228.08	1.43	-226.65
AA178	37. 54.70	112. 50.56	5698.	979427.28	979996.34	-33.11	-227.18	1.36	-225.82
AA180	37. 55.95	112. 58.96	5670.	979447.08	979998.16	-17.77	-210.89	.60	-210.29
AA181	37. 57.15	112. 58.53	5817.	979441.30	979999.91	-11.48	-209.59	.48	-209.11
AA182	37. 58.38	112. 58.00	5965.	979435.36	980001.72	-5.30	-208.46	.56	-207.90
AA183	37. 59.53	112. 57.25	6040.	979435.95	980003.39	.68	-205.06	.51	-204.55
AA184	38. .14	112. 56.23	6111.	979434.23	980004.28	4.75	-203.39	.58	-202.81
AA185	38. .59	112. 55.32	6295.	979423.20	980004.94	10.36	-204.05	.70	-203.35
AA186	38. 1.70	112. 55.23	6292.	979424.11	980006.55	9.38	-204.93	.68	-204.25
AA187	38. 2.66	112. 54.03	6449.	979414.37	980007.94	13.03	-206.62	.78	-205.84

STAT.	LATITUDE	LONGITUDE	ELEV.	OBSERVED GRAVITY	THEOR. GRAVITY	FREE-AIR	SIMPLE BOUGUER	T.C	T.C. BOUGUER
AA188	38. 4.55	112. 57.42	6493.	979418.34	980010.71	18.36	-202.79	.71	-202.09
AA189	38. 4.75	112. 56.53	6606.	979410.95	980011.00	21.31	-203.69	.91	-202.78
AA190	38. 4.50	112. 55.56	6503.	979418.87	980010.64	19.91	-201.59	.75	-200.84
AA191	38. 5.04	112. 55.09	6583.	979413.49	980011.42	21.27	-202.95	.87	-202.08
AA192	38. 6.11	112. 54.13	6776.	979400.45	980012.98	24.81	-205.98	1.15	-204.83
AA193	38. 6.91	112. 56.66	6946.	979393.03	980014.15	32.22	-204.36	3.73	-200.63
AA194	38. 6.56	112. 53.24	6903.	979394.69	980013.64	30.34	-204.77	1.35	-203.42
AA195	38. 7.27	112. 52.69	7081.	979389.38	980014.69	40.73	-200.45	1.58	-198.87
AA196	38. 3.73	112. 55.12	6403.	979421.70	980009.52	14.45	-203.63	.68	-202.95
AA197	38. 3.73	112. 53.93	6500.	979413.71	980009.52	15.58	-205.81	.80	-205.01
AA198	38. 4.99	112. 53.35	6779.	979406.02	980011.35	32.30	-198.60	1.08	-197.52
AA199	38. 3.47	112. 53.18	6677.	979402.71	980009.13	21.61	-205.81	1.06	-204.75
AA200	38. 3.20	112. 56.48	6399.	979419.55	980008.74	12.69	-205.26	.65	-204.61
AA201	38. .83	112. 58.53	6160.	979430.58	980005.29	4.70	-205.11	.50	-204.61
AA202	38. 1.40	112. 59.84	6246.	979428.22	980006.12	9.60	-203.14	.56	-202.58
AA203	38. .74	112. 57.68	6148.	979431.54	980005.16	4.66	-204.75	.55	-204.20
AA204	38. 1.90	112. 57.74	6255.	979426.45	980006.84	7.96	-205.08	.57	-204.51
AA205	37. 55.97	112. 57.49	5872.	979442.34	979998.19	-3.53	-203.53	.66	-202.87
AA206	37. 55.26	112. 57.44	5962.	979436.66	979997.16	.29	-202.77	.87	-201.90
AA207	37. 54.98	112. 58.60	5690.	979451.09	979996.74	-10.46	-204.26	.80	-203.46
AA208	37. 55.78	112. 58.31	5724.	979447.79	979997.91	-11.73	-206.69	.70	-205.99
AA209	37. 56.20	112. 56.85	5945.	979438.15	979998.52	-1.20	-203.68	.70	-202.98
AA210	37. 56.38	112. 55.97	6090.	979430.83	979998.79	4.86	-202.56	.67	-201.89
AA211	37. 56.39	112. 55.18	6110.	979430.34	979998.80	6.25	-201.86	.76	-201.10
AA212	37. 57.72	112. 55.09	6200.	979428.91	980000.75	11.33	-199.84	.80	-199.04
AA213	37. 58.47	112. 54.45	6274.	979423.63	980001.85	11.91	-201.79	.95	-200.84
AA214	37. 59.20	112. 53.87	6372.	979416.87	980002.91	13.31	-203.72	1.00	-202.72
AA215	38. .04	112. 53.65	6315.	979421.43	980004.14	11.28	-203.81	1.22	-202.59
AA216	38. 5.00	112. 59.90	6658.	979409.98	980011.37	24.87	-201.90	1.09	-200.81
AA217	38. 3.83	112. 59.83	6445.	979422.31	980009.66	18.86	-200.66	.68	-199.98
AA218	38. 4.20	113. 1.41	6513.	979419.21	980010.20	21.63	-200.20	.80	-199.40
AA219	38. 4.67	113. 3.08	6591.	979418.48	980010.88	27.55	-196.94	1.31	-195.63

STAT.	LATITUDE	LONGITUDE	ELEV.	OBSERVED GRAVITY	THEOR. GRAVITY	FREE-AIR	SIMPLE BOUGUER	T.C	T.C. BOUGUER
AA220	38. 4.14	113. 3.20	6537.	979418.48	980010.11	23.24	-199.41	1.01	-198.40
AA221	38. 3.50	113. 3.51	6381.	979427.58	980009.18	18.60	-198.74	.76	-197.98
AA222	38. 3.21	113. 1.68	6742.	979405.67	980008.76	31.07	-198.57	1.42	-197.15
AA223	38. 5.77	113. 4.00	6174.	979442.78	980012.48	11.02	-199.26	.73	-198.53
AA224	38. 4.99	113. 5.98	5984.	979451.70	980011.35	3.21	-200.61	.58	-200.03
AA227	38. 6.01	113. .70	7494.	979353.01	980012.84	45.06	-210.19	10.30	-199.89
AA231	38. 7.15	113. 12.78	5107.	979506.69	980014.50	-27.46	-201.40	.37	-201.03
AA232	38. 6.23	113. 13.40	5089.	979508.48	980013.16	-26.02	-199.36	.51	-198.85
AA233	38. 6.51	113. 11.84	5353.	979492.21	980013.57	-17.86	-200.20	.85	-199.35
AA234	38. 6.88	113. 14.51	5076.	979510.49	980014.10	-26.17	-199.06	.17	-198.89
AA235	38. 6.11	113. 14.51	5084.	979510.34	980012.98	-24.46	-197.62	.31	-197.31
AA236	38. 5.13	113. 13.76	5172.	979505.22	980011.55	-19.86	-196.02	.55	-195.47
AA237	38. 4.25	113. 13.83	5234.	979501.56	980010.27	-16.41	-194.68	.50	-194.18
AA238	38. 3.17	113. 13.42	5269.	979496.97	980008.70	-16.14	-195.60	.60	-195.00
AA239	38. 3.39	113. 12.85	5369.	979491.89	980009.02	-12.13	-195.00	.75	-194.25
AA240	38. .90	113. 12.98	5202.	979493.72	980005.39	-22.38	-199.56	.24	-199.32
AA241	38. .90	113. 14.78	5150.	979496.27	980005.39	-24.72	-200.12	.10	-200.02
AA242	38. 1.68	113. 13.95	5157.	979499.83	980006.52	-21.64	-197.29	.23	-197.06
AA243	38. .90	113. 11.99	5276.	979485.68	980005.39	-23.46	-203.16	.31	-202.85
AA244	38. .80	113. 10.66	5367.	979478.24	980005.24	-22.19	-204.99	.28	-204.71
AA245	38. 1.65	113. 10.06	5519.	979474.83	980006.48	-12.55	-200.52	.43	-200.09
AA246	38. 2.70	113. 9.24	5685.	979470.39	980008.00	-2.89	-196.52	.62	-195.90
AA247	38. 4.01	113. 9.15	5960.	979460.02	980009.92	10.70	-192.30	1.45	-190.85
AA248	38. 2.11	113. 8.45	5570.	979472.37	980007.16	-10.88	-200.60	.56	-200.04
AA249	38. 5.12	113. 7.85	6150.	979447.02	980011.54	13.95	-195.52	.75	-194.77
AA254	38. 6.88	113. 15.16	5081.	979510.29	980014.10	-25.90	-198.96	.13	-198.83
AA255	38. 6.01	113. 16.22	5082.	979506.70	980012.84	-28.13	-201.22	.12	-201.10
AA256	38. 5.97	113. 17.31	5081.	979504.98	980012.77	-29.89	-202.94	.09	-202.85
AA257	38. 6.88	113. 17.36	5075.	979505.82	980014.10	-30.93	-203.79	.09	-203.70
AA258	38. 6.88	113. 16.26	5078.	979508.84	980014.10	-27.64	-200.60	.10	-200.50
AA259	38. 5.23	113. 15.66	5105.	979507.16	980011.70	-24.37	-198.25	.23	-198.02
AA260	38. 4.26	113. 15.16	5114.	979504.72	980010.29	-24.56	-198.74	.20	-198.54

STAT.	LATITUDE	LONGITUDE	ELEV.	OBSERVED GRAVITY	THEOR. GRAVITY	FREE-AIR	SIMPLE BOUGUER	T.C	T.C. BOUGUER
AA261	38. 3.39	113. 15.16	5118.	979505.21	980009.02	-22.42	-196.74	.21	-196.53
AA262	38. 3.39	113. 16.26	5111.	979499.99	980009.02	-28.30	-202.38	.09	-202.29
AA263	38. 3.38	113. 17.36	5111.	979496.52	980009.01	-31.75	-205.83	.05	-205.78
AA264	38. 3.38	113. 18.46	5094.	979495.54	980009.01	-34.33	-207.84	.04	-207.80
AA265	38. 3.37	113. 19.57	5093.	979493.87	980008.99	-36.08	-209.55	.05	-209.50
AA266	38. 3.37	113. 20.67	5088.	979492.52	980008.99	-37.90	-211.20	.08	-211.12
AA267	38. 1.63	113. 24.38	5077.	979486.16	980006.45	-42.75	-215.68	.14	-215.54
AA268	38. 1.64	113. 22.81	5087.	979486.26	980006.47	-41.74	-215.00	.09	-214.91
AA269	38. 1.63	113. 21.85	5091.	979487.75	980006.45	-39.85	-213.25	.05	-213.20
AA270	38. 1.62	113. 20.61	5095.	979489.66	980006.44	-37.54	-211.07	.03	-211.04
AA271	38. 1.62	113. 19.57	5103.	979490.27	980006.44	-36.18	-209.99	.03	-209.95
AA272	38. 1.63	113. 18.47	5111.	979491.62	980006.45	-34.10	-208.18	.03	-208.15
AA273	38. 1.63	113. 17.38	5123.	979494.05	980006.45	-30.54	-205.03	.04	-204.99
AA274	38. 1.64	113. 16.26	5132.	979497.62	980006.47	-26.14	-200.93	.06	-200.87
AA275	38. 1.65	113. 15.16	5141.	979498.87	980006.48	-24.07	-199.17	.10	-199.07
AA276	38. 2.52	113. 15.16	5129.	979498.77	980007.73	-26.54	-201.24	.14	-201.10
AA277	37. 58.55	113. 13.96	5179.	979486.18	980001.96	-28.65	-205.05	.09	-204.96
AA278	37. 59.53	113. 13.95	5175.	979489.15	980003.39	-27.49	-203.75	.10	-203.65
AA295	38. 6.11	113. 25.17	5431.	979489.61	980012.98	-12.54	-197.52	.65	-196.87
AA296	38. 4.25	113. 25.00	5186.	979493.09	980010.27	-29.40	-206.04	.38	-205.66
AA297	38. 4.24	113. 23.63	5177.	979488.04	980010.26	-35.28	-211.61	.22	-211.39
AA298	38. 4.24	113. 22.80	5158.	979487.65	980010.26	-37.46	-213.15	.19	-212.96
AA299	38. 3.95	113. 21.67	5107.	979490.69	980009.84	-38.79	-212.74	.13	-212.61
AA300	38. 5.19	113. 22.25	5196.	979489.34	980011.64	-33.57	-210.54	.20	-210.34
AA301	38. 6.03	113. 21.70	5189.	979493.54	980012.87	-31.26	-208.00	.20	-207.80
EH 1	37. 54.22	113. 1.84	5510.	979449.62	979995.64	-27.75	-215.42	.49	-214.93
EH 2	37. 55.61	113. 1.84	5616.	979445.16	979997.66	-24.28	-215.56	.41	-215.15
EH 3	37. 54.45	113. 1.84	5692.	979441.65	979995.98	-18.95	-212.82	.93	-211.89
EH 4	37. 57.31	113. 1.84	5762.	979440.52	980000.14	-17.66	-213.91	.39	-213.52
EH 5	37. 57.77	113. 1.84	5810.	979437.25	980000.83	-17.10	-214.99	.40	-214.59
EH 6	37. 59.09	113. 1.84	5958.	979436.84	980002.75	-5.51	-208.44	.45	-207.99
EH 6	37. 58.66	113. 1.84	5910.	979437.29	980002.12	-8.95	-210.24	.42	-209.82

STAT.	LATITUDE	LONGITUDE	ELEV.	OBSERVED GRAVITY	THEOR. GRAVITY	FREE-AIR	SIMPLE BOUGUER	T.C	T.C. BOUGUER
EH 7	37. 59.52	113. 1.84	6020.	979435.80	980003.37	-1.34	-206.38	.51	-205.87
EH 8	37. 55.36	113. .39	5581.	979450.34	979997.30	-22.03	-212.12	.51	-211.61
EH 9	37. 55.95	113. 3.45	5652.	979443.62	979998.16	-22.92	-215.43	.36	-215.07
EH 10	37. 56.13	113. 4.28	5688.	979442.97	979998.42	-20.45	-214.18	.35	-213.83
EH 11	37. 57.12	113. 5.24	5730.	979447.71	979999.87	-13.20	-208.36	.37	-207.99
EH 12	37. 57.01	113. 6.22	5707.	979452.40	979999.70	-10.51	-204.89	.38	-204.51
EH 13	37. 57.31	113. 7.91	5580.	979462.04	980000.14	-13.25	-203.30	.42	-202.88
EH 14	37. 57.32	113. 9.57	5295.	979484.37	980000.16	-17.74	-198.09	.58	-197.51
EH 15	37. 55.73	113. 9.86	5297.	979479.09	979997.84	-20.52	-200.94	.31	-200.63
EH 16	37. 55.00	113. 9.37	5313.	979475.52	979996.77	-21.53	-202.49	.33	-202.16
EH 17	37. 54.50	113. 8.27	5336.	979469.50	979996.05	-24.65	-206.39	.36	-206.03
EH 18	37. 53.49	113. 7.37	5358.	979463.02	979994.57	-27.59	-210.08	.35	-209.73
EH 18	37. 53.49	113. 7.37	5358.	979463.02	979994.57	-27.59	-210.08	.35	-209.73
EH 19	37. 53.69	113. 5.51	5427.	979454.54	979994.87	-29.87	-214.71	.33	-214.38
EH 20	37. 53.84	113. 4.37	5451.	979451.21	979995.09	-31.16	-216.82	.38	-216.44
EH 21	37. 53.95	113. 3.73	5482.	979448.89	979995.24	-30.72	-217.44	.39	-217.05
EH 22	37. 53.13	113. 8.65	5516.	979455.87	979994.05	-19.36	-207.23	.29	-206.94
EH 23	37. 52.84	113. 10.24	5470.	979461.57	979993.64	-17.57	-203.88	.26	-203.62
EH 24	37. 52.69	113. 11.46	5541.	979463.41	979993.43	-8.85	-197.58	.27	-197.31
EH 25	37. 53.11	113. 12.03	5499.	979468.10	979994.02	-8.69	-195.99	.26	-195.73
EH 26	37. 53.49	113. 12.54	5386.	979474.30	979994.57	-13.67	-197.12	.20	-196.92
EH 27	37. 54.02	113. 13.67	5257.	979473.75	979995.35	-27.14	-206.19	.17	-206.02
EH 27	37. 54.68	113. 14.00	5223.	979473.16	979996.31	-31.88	-209.78	.14	-209.64
EH 28	37. 55.53	113. 12.87	5289.	979480.01	979997.55	-20.07	-200.21	.15	-200.06
EH 29	37. 55.98	113. 13.98	5232.	979476.12	979998.20	-29.97	-208.17	.11	-208.06
EH 31	37. 56.38	113. 12.42	5333.	979480.02	979998.79	-17.16	-198.80	.17	-198.63
EH 32	37. 55.93	113. 11.14	5416.	979475.08	979998.13	-13.64	-198.11	.17	-197.94
EH 33	37. 58.72	113. 10.54	5245.	979495.09	980002.21	-13.78	-192.42	.58	-191.84
EH 35	37. 54.62	113. .00	5528.	979453.96	979996.22	-22.30	-210.58	.66	-209.92
EH 36	37. 53.16	113. 1.84	5425.	979453.03	979994.09	-30.79	-215.57	.62	-214.95
EH 37	37. 51.65	113. 1.85	5398.	979456.08	979991.91	-28.10	-211.96	.88	-211.08
EH 38	37. 50.97	113. 2.16	5408.	979454.76	979990.91	-27.49	-211.69	.91	-210.78

STAT.	LATITUDE	LONGITUDE	ELEV.	OBSERVED GRAVITY	THEOR. GRAVITY	FREE-AIR	SIMPLE BOUGUER	T.C	T.C. BOUGUER
EH 39	37. 51.01	113. 4.06	5395.	979449.76	979990.98	-33.77	-217.52	.55	-216.97
EH 40	37. 52.29	113. 4.90	5383.	979453.15	979992.84	-33.37	-216.71	.43	-216.23
EH 40	37. 51.88	113. 5.80	5385.	979454.05	979992.24	-31.69	-215.10	.41	-214.69
EH 41	37. 50.17	113. 2.97	5416.	979449.18	979989.75	-31.15	-215.62	.74	-214.88
EH 42	37. 50.79	113. .89	5701.	979440.74	979990.66	-13.68	-207.86	.88	-206.98
EH 42	37. 49.93	113. 2.16	5457.	979450.84	979989.40	-25.28	-211.15	.88	-210.27
EH 43	37. 49.60	113. .36	5584.	979448.45	979988.92	-15.25	-205.44	1.21	-204.23
EH 44	37. 49.37	113. 1.60	5494.	979450.37	979988.59	-21.45	-208.58	1.00	-207.58
EH 45	37. 49.45	113. 2.97	5430.	979447.76	979988.70	-30.21	-215.16	.82	-214.34
EH 46	37. 49.46	113. 4.64	5423.	979446.94	979988.72	-31.70	-216.41	.62	-215.79
EH 47	37. 49.46	113. 6.27	5428.	979450.30	979988.72	-27.86	-212.74	.50	-212.24
EH 48	37. 48.76	113. .49	5583.	979447.47	979987.70	-15.10	-205.26	1.35	-203.91
EH 48	37. 47.36	113. 1.20	5532.	979447.05	979985.66	-18.28	-206.70	1.76	-204.94
EH 49	37. 48.15	113. 6.30	5449.	979448.33	979986.80	-25.95	-211.54	.59	-210.95
EH 50	37. 47.91	113. 5.18	5452.	979444.99	979986.45	-28.65	-214.35	.71	-213.64
EH 51	37. 48.56	113. 2.98	5441.	979446.43	979987.41	-29.21	-214.53	.94	-213.59
EH 52	37. 47.70	113. 2.99	5451.	979445.70	979986.15	-27.73	-213.39	1.11	-212.28
EH 53	37. 46.76	113. 3.00	5470.	979444.47	979984.78	-25.81	-212.12	1.34	-210.78
EH 54	37. 45.89	113. 3.00	5490.	979443.73	979983.52	-23.41	-210.40	1.63	-208.77
EH 55	37. 45.87	113. 1.43	5601.	979440.29	979983.48	-16.37	-207.14	2.59	-204.55
EH 55	37. 46.18	113. .30	5755.	979429.00	979983.94	-13.63	-209.65	3.54	-206.11
EH 56	37. 45.89	113. 4.39	5497.	979440.18	979983.52	-26.29	-213.52	1.14	-212.38
EH 56	37. 45.89	113. 5.22	5496.	979440.26	979983.52	-26.31	-213.50	.95	-212.55
EH 57	37. 45.89	113. 6.32	5491.	979442.52	979983.52	-24.53	-211.55	.79	-210.76
EH 58	37. 46.53	113. 6.55	5480.	979444.67	979984.45	-24.33	-210.98	.70	-210.28
EH 59	37. 48.17	113. 7.87	5508.	979451.85	979986.84	-16.91	-204.51	.50	-204.01
EH 60	37. 49.40	113. 8.81	5585.	979452.80	979988.62	-10.51	-200.74	.38	-200.36
EH 61	37. 50.33	113. 8.51	5536.	979452.84	979989.98	-16.43	-204.99	.35	-204.64
EH 62	37. 50.00	113. 10.26	5601.	979450.95	979989.51	-11.73	-202.50	.32	-202.18
EH 63	37. 51.20	113. 10.20	5548.	979453.52	979991.25	-15.89	-204.85	.32	-204.53
EH 64	37. 52.02	113. 9.88	5508.	979456.23	979992.45	-18.15	-205.75	.27	-205.48
EH 65	37. 51.64	113. 8.75	5613.	979446.69	979991.89	-17.25	-208.43	.34	-208.09

STAT.	LATITUDE	LONGITUDE	ELEV.	OBSERVED GRAVITY	THEOR. GRAVITY	FREE-AIR	SIMPLE BOUGUER	T.C	T.C. BOUGUER
EH 66	37. 51.39	113. 6.99	5450.	979454.11	979991.53	-24.80	-210.43	.36	-210.07
EH 66	37. 51.21	113. 6.60	5410.	979455.07	979991.27	-27.34	-211.60	.39	-211.21
EH 67	37. 47.52	113. 7.65	5477.	979451.31	979985.89	-19.42	-205.97	.57	-205.40
EH 68	37. 45.90	113. 8.04	5496.	979449.02	979983.53	-17.56	-204.75	.64	-204.11
EH 69	37. 45.93	113. 9.30	5674.	979444.61	979983.57	-5.27	-198.53	.60	-197.93
EH 70	37. 46.75	113. 9.93	5813.	979440.16	979984.77	2.16	-195.83	.63	-195.20
EH 71	37. 47.33	113. 10.39	5865.	979440.19	979985.62	6.23	-193.53	.61	-192.92
EH 72	37. 47.33	113. 12.24	5696.	979450.96	979985.62	1.11	-192.90	.48	-192.42
EH 73	37. 46.62	113. 12.92	5588.	979458.86	979984.58	-.12	-190.45	.54	-189.91
EH 74	37. 48.48	113. 11.41	5714.	979446.93	979987.29	-2.91	-197.53	.37	-197.16
EH 75	37. 48.77	113. 12.93	5649.	979453.44	979987.71	-2.93	-195.33	.51	-194.82
EH 76	37. 48.15	113. 10.29	5770.	979447.89	979986.80	3.81	-192.72	.49	-192.23
EH 77	37. 52.08	113. 22.19	5171.	979469.77	979992.53	-36.38	-212.50	.07	-212.43
EH 78	37. 53.07	113. 21.84	5164.	979472.20	979993.96	-36.04	-211.93	.05	-211.88
EH 79	37. 53.03	113. 19.97	5181.	979468.12	979993.91	-38.47	-214.93	.06	-214.87
EH 80	37. 53.74	113. 19.05	5174.	979470.21	979994.94	-38.07	-214.30	.05	-214.25
EH 81	37. 55.52	113. 16.78	5162.	979475.98	979997.53	-36.03	-211.85	.05	-211.80
EH 82	37. 54.88	113. 15.42	5176.	979473.07	979996.60	-36.68	-212.97	.09	-212.88
EH 83	37. 52.73	113. 13.99	5286.	979470.77	979993.48	-25.52	-205.56	.21	-205.35
EH 84	37. 51.21	113. 14.01	5380.	979467.89	979991.27	-17.34	-200.58	.25	-200.33
EH 85	37. 49.79	113. 14.10	5460.	979467.05	979989.20	-8.59	-194.56	.34	-194.22
EH 86	37. 47.23	113. 14.82	5399.	979469.80	979985.47	-7.84	-191.73	.35	-191.38
EH 87	37. 45.87	113. 15.21	5360.	979472.36	979983.48	-6.97	-189.53	.43	-189.10
EH 88	37. 47.68	113. 16.98	5321.	979467.30	979986.12	-18.34	-199.57	.25	-199.32
EH 89	37. 48.66	113. 18.34	5279.	979470.73	979987.55	-20.29	-200.09	.20	-199.89
EH 90	37. 49.73	113. 19.43	5239.	979469.34	979989.11	-27.00	-205.44	.15	-205.29
EH 91	37. 50.38	113. 20.70	5212.	979467.88	979990.05	-31.94	-209.46	.12	-209.34
EH 92	37. 52.03	113. 19.18	5203.	979468.27	979992.47	-34.82	-212.03	.09	-211.94
EH 93	37. 52.35	113. 18.20	5209.	979470.17	979992.93	-32.81	-210.23	.09	-210.14
EH 94	37. 51.17	113. 17.24	5235.	979472.27	979991.21	-26.55	-204.85	.13	-204.72
EH 95	37. 51.19	113. 16.18	5235.	979472.38	979991.23	-26.46	-204.76	.17	-204.59
EH 96	37. 50.26	113. 16.35	5254.	979472.57	979989.88	-23.13	-202.08	.18	-201.90

STAT.	LATITUDE	LONGITUDE	ELEV.	OBSERVED GRAVITY	THEOR. GRAVITY	FREE-AIR	SIMPLE BOUGUER	T.C	T.C. BOUGUER
EH 98	37. 56.30	113. 18.40	5150.	979482.05	979998.67	-32.22	-207.63	.02	-207.61
EH 99	37. 56.90	113. 19.50	5141.	979485.12	979999.55	-30.88	-205.98	.01	-205.97
EH100	37. 57.85	113. 21.28	5122.	979489.16	980000.95	-30.01	-204.47	.01	-204.46
EH101	37. 58.73	113. 21.54	5111.	979488.16	980002.23	-33.33	-207.41	.02	-207.39
EH102	37. 59.02	113. 20.69	5117.	979489.34	980002.65	-32.01	-206.30	.01	-206.29
EH103	37. 59.35	113. 19.58	5117.	979490.88	980003.13	-30.95	-205.24	.03	-205.21
EH104	37. 58.78	113. 19.58	5124.	979489.97	980002.30	-30.37	-204.89	.02	-204.87
EH104	37. 57.63	113. 17.94	5147.	979488.66	980000.62	-27.85	-203.16	.01	-203.15
EH105	37. 57.77	113. 16.72	5158.	979489.72	980000.83	-25.96	-201.64	.03	-201.61
EH106	37. 57.70	113. 13.99	5186.	979484.73	980000.73	-28.21	-204.85	.09	-204.76
EH107	37. 58.56	113. 13.96	5179.	979485.98	980001.98	-28.86	-205.26	.09	-205.17
EH108	37. 59.54	113. 13.95	5175.	979489.03	980003.41	-27.62	-203.88	.10	-203.78
EH110	37. 50.71	113. 22.80	5177.	979468.41	979990.54	-35.18	-211.51	.10	-211.41
EH111	37. 49.40	113. 22.88	5203.	979468.32	979988.62	-30.92	-208.13	.18	-207.95
EH112	37. 49.89	113. 23.79	5174.	979468.53	979989.34	-34.15	-210.38	.15	-210.23
EH114	37. 47.61	113. 25.62	5349.	979464.37	979986.02	-18.53	-200.72	.46	-200.26
EH115	37. 47.70	113. 23.45	5402.	979463.41	979986.15	-14.63	-198.62	.41	-198.21
EH116	37. 47.64	113. 22.23	5423.	979460.83	979986.06	-15.15	-199.86	.43	-199.43
EH117	37. 47.24	113. 21.07	5457.	979459.25	979985.48	-12.95	-198.82	.35	-198.47
EH118	37. 46.60	113. 21.93	5570.	979455.16	979984.55	-5.48	-195.19	.48	-194.71
EH119	37. 46.86	113. 20.00	5427.	979458.43	979984.93	-16.04	-200.88	.32	-200.55
EH120	37. 46.28	113. 18.39	5404.	979461.91	979984.08	-13.87	-197.93	.30	-197.63
EH121	37. 47.54	113. 18.39	5327.	979467.03	979985.92	-17.84	-199.28	.25	-199.03
EH122	37. 52.77	113. 21.32	5151.	979480.48	979993.54	-28.56	-204.00	.05	-203.95
EH123	37. 57.26	113. 23.31	5110.	979487.91	980000.07	-31.52	-205.57	.01	-205.56
EH125	37. 59.88	113. 24.89	5086.	979485.47	980003.91	-40.06	-213.29	.08	-213.21
EH126	37. 58.91	113. 27.78	5106.	979486.12	980002.49	-36.11	-210.02	.15	-209.87
EH127	37. 58.13	113. 28.76	5144.	979485.49	980001.35	-32.02	-207.22	.11	-207.11
EH128	37. 57.61	113. 29.71	5149.	979487.08	980000.59	-29.21	-204.58	.15	-204.43
EH129	37. 56.79	113. 28.30	5106.	979485.88	979999.38	-33.24	-207.15	.07	-207.08
EH130	37. 55.71	113. 26.20	5101.	979490.05	979997.81	-27.97	-201.71	.03	-201.68
EH131	37. 55.78	113. 24.18	5115.	979489.82	979997.91	-26.99	-201.21	.03	-201.18

STAT.	LATITUDE	LONGITUDE	ELEV.	OBSERVED GRAVITY	THEOR. GRAVITY	FREE-AIR	SIMPLE BOUGUER	T.C	T.C. BOUGUER
EH132	37. 56.37	113. 23.68	5116.	979488.75	979998.77	-28.82	-203.07	.02	-203.05
EH133	37. 54.65	113. 22.80	5145.	979486.57	979996.27	-25.76	-201.00	.01	-200.99
EH134	37. 52.90	113. 22.80	5169.	979475.11	979993.73	-32.43	-208.49	.05	-208.44
EH135	37. 52.90	113. 23.94	5163.	979482.55	979993.73	-25.56	-201.41	.04	-201.37
EH136	37. 52.88	113. 25.04	5149.	979486.21	979993.70	-23.18	-198.55	.06	-198.49
EH137	37. 53.43	113. 25.43	5145.	979491.27	979994.48	-19.28	-194.52	.08	-194.44
EH138	37. 54.36	113. 25.65	5124.	979493.76	979995.84	-20.13	-194.65	.07	-194.58
EH139	37. 57.93	113. 26.44	5093.	979486.05	980001.06	-35.97	-209.44	.06	-209.38
EH140	37. 58.72	113. 26.18	5088.	979485.48	980002.21	-38.17	-211.47	.08	-211.39
EH141	37. 53.26	113. 26.63	5172.	979489.99	979994.24	-17.78	-193.94	.16	-193.78
EH142	37. 52.69	113. 28.30	5103.	979493.04	979993.43	-20.41	-194.22	.18	-194.04
EH143	37. 52.90	113. 29.37	5104.	979495.15	979993.73	-18.51	-192.35	.08	-192.27
EH144	37. 53.78	113. 29.37	5102.	979497.59	979995.00	-17.53	-191.30	.04	-191.25
EH147	37. 56.38	113. 28.30	5101.	979488.01	979998.79	-30.99	-204.73	.06	-204.67
EH148	37. 50.12	113. 23.06	5148.	979476.31	979989.68	-29.15	-204.49	.16	-204.33
EH149	37. 50.77	113. 26.11	5145.	979484.20	979990.62	-22.49	-197.73	.14	-197.59
EH151	37. 49.39	113. 28.63	5125.	979487.54	979988.61	-19.02	-193.58	.21	-193.37
EH152	37. 48.19	113. 28.94	5128.	979475.80	979986.87	-28.74	-203.40	.27	-203.13
EH153	37. 47.66	113. 29.08	5129.	979472.26	979986.09	-31.41	-206.10	.32	-205.78
EH154	37. 47.66	113. 27.46	5151.	979472.20	979986.09	-29.40	-204.84	.52	-204.32
EH155	37. 48.39	113. 26.86	5150.	979472.32	979987.16	-30.43	-205.84	.33	-205.51
EH156	37. 49.13	113. 26.58	5142.	979475.65	979988.24	-28.94	-204.08	.21	-203.87
EH157	37. 47.16	113. 27.45	5157.	979473.78	979985.36	-26.52	-202.17	.98	-201.19
EH158	37. 46.99	113. 25.56	5464.	979460.50	979985.12	-10.68	-196.78	.65	-196.13
EH159	37. 38.12	113. 16.32	5775.	979421.90	979972.22	-7.13	-203.83	1.64	-202.19
EH159	37. 38.11	113. 18.14	6269.	979393.86	979972.20	11.32	-202.20	1.32	-200.88
EH159	37. 37.94	113. 18.04	5974.	979413.41	979971.96	3.36	-200.11	1.58	-198.53
EH160	37. 37.55	113. 18.94	6115.	979402.21	979971.38	6.00	-202.28	1.40	-200.88
EH161	37. 36.46	113. 21.48	6416.	979386.98	979969.80	20.67	-197.86	1.62	-196.24
EH162	37. 36.63	113. 22.31	6394.	979390.37	979970.05	21.74	-196.04	1.48	-194.56
EH162	37. 37.11	113. 21.76	6515.	979383.24	979970.74	25.30	-196.60	1.50	-195.10
EH163	37. 36.68	113. 22.94	6387.	979391.67	979970.12	22.32	-195.22	1.37	-193.85

STAT.	LATITUDE	LONGITUDE	ELEV.	OBSERVED GRAVITY	THEOR. GRAVITY	FREE-AIR	SIMPLE BOUGUER	T.C	T.C. BOUGUER
EH165	37. 37.98	113. 21.06	6608.	979378.83	979972.01	28.37	-196.70	1.92	-194.78
EH167	37. 39.73	113. 22.21	6268.	979407.23	979974.55	22.24	-191.25	1.47	-189.78
EH168	37. 40.30	113. 21.43	5943.	979427.51	979975.38	11.12	-191.30	1.14	-190.16
EH168	37. 40.83	113. 21.40	5944.	979429.11	979976.16	12.04	-190.41	.93	-189.48
EH169	37. 40.63	113. 22.73	6213.	979412.52	979975.87	21.05	-190.56	1.06	-189.50
EH169	37. 40.71	113. 23.44	6348.	979404.48	979975.98	25.59	-190.62	1.10	-189.52
EH170	37. 40.94	113. 24.35	6365.	979403.24	979976.31	25.62	-191.17	1.29	-189.88
EH171	37. 40.66	113. 25.39	6262.	979407.31	979975.91	20.41	-192.87	1.46	-191.41
EH172	37. 40.17	113. 26.22	6099.	979415.16	979975.20	13.64	-194.09	1.47	-192.62
EH173	37. 39.45	113. 27.41	5872.	979422.82	979974.16	.99	-199.01	1.19	-197.82
EH173	37. 38.71	113. 28.95	5516.	979433.32	979973.08	-20.93	-208.80	1.23	-207.57
EH174	37. 37.75	113. 25.43	6030.	979419.66	979971.68	15.16	-190.22	.99	-189.23
EH174	37. 38.50	113. 26.42	5976.	979420.19	979972.77	9.52	-194.02	.94	-193.08
EH175	37. 37.75	113. 24.42	6195.	979406.48	979971.68	17.50	-193.50	1.76	-191.74
EH175	37. 36.33	113. 25.56	6123.	979406.69	979969.61	13.00	-195.55	1.06	-194.49
EH176	37. 36.06	113. 26.77	5870.	979420.03	979969.22	2.94	-196.99	1.70	-195.29
EH177	37. 40.28	113. 29.13	5722.	979428.70	979975.35	-8.44	-203.33	1.30	-202.03
EH177	37. 40.63	113. 30.50	5536.	979439.53	979975.87	-15.63	-204.19	.85	-203.34
EH177	37. 40.45	113. 33.00	5314.	979444.84	979975.59	-30.93	-211.92	.56	-211.36
EH177	37. 43.33	113. 32.00	5193.	979454.91	979979.80	-36.45	-213.32	.47	-212.85
EH177	37. 45.90	113. 31.00	5175.	979463.20	979983.53	-33.58	-209.84	.34	-209.50
EH178	37. 43.89	113. 29.96	5208.	979465.37	979980.61	-25.39	-202.77	1.54	-201.23
EH179	37. 43.21	113. 29.62	5441.	979454.12	979979.62	-13.73	-199.05	2.05	-197.00
EH180	37. 45.12	113. 29.96	5196.	979465.93	979982.40	-27.74	-204.72	.80	-203.92
EH181	37. 45.86	113. 29.52	5184.	979467.39	979983.47	-28.48	-205.05	.72	-204.33
EH182	37. 45.64	113. 16.57	5396.	979468.13	979983.15	-7.47	-191.26	.35	-190.91
EH183	37. 45.26	113. 15.28	5426.	979467.35	979982.59	-4.88	-189.69	.42	-189.27
EH184	37. 45.16	113. 14.47	5389.	979469.45	979982.45	-6.12	-189.67	.54	-189.13
EH185	37. 44.72	113. 13.55	5405.	979465.66	979981.80	-7.76	-191.85	.73	-191.12
EH186	37. 44.16	113. 12.13	5457.	979458.87	979980.99	-8.84	-194.71	.82	-193.89
EH187	37. 38.74	113. 14.58	5624.	979426.22	979973.12	-17.92	-209.47	.94	-208.53
EH188	37. 39.53	113. 12.94	5472.	979434.96	979974.28	-24.63	-211.01	.89	-210.12

STAT.	LATITUDE	LONGITUDE	ELEV.	OBSERVED GRAVITY	THEOR. GRAVITY	FREE-AIR	SIMPLE BOUGUER	T.C	T.C. BOUGUER
EH189	37. 40.66	113. 12.94	5503.	979437.36	979975.91	-20.94	-208.37	.99	-207.38
EH190	37. 40.44	113. 11.04	5471.	979437.73	979975.59	-23.26	-209.60	.87	-208.73
EH191	37. 41.11	113. 9.60	5493.	979440.20	979976.56	-19.70	-206.79	.92	-205.87
EH192	37. 42.13	113. 11.03	5482.	979443.41	979978.05	-19.00	-205.72	.75	-204.97
EH193	37. 41.51	113. 11.85	5471.	979441.11	979977.15	-21.44	-207.78	.90	-206.88
EH194	37. 42.88	113. 11.87	5535.	979449.10	979979.15	-9.43	-197.95	.74	-197.21
EH195	37. 42.87	113. 13.00	5742.	979437.23	979979.13	-1.82	-197.39	1.00	-196.39
EH196	37. 42.55	113. 13.81	5912.	979426.49	979978.66	3.91	-197.45	1.47	-195.98
EH197	37. 42.13	113. 15.13	5938.	979425.60	979978.05	6.08	-196.17	1.10	-195.07
EH198	37. 41.76	113. 16.63	5651.	979442.19	979977.52	-3.80	-196.27	.70	-195.57
EH199	37. 43.72	113. 16.04	5556.	979454.51	979980.37	-3.27	-192.51	.64	-191.87
EH199	37. 43.79	113. 15.15	5831.	979437.73	979980.47	5.73	-192.87	1.00	-191.87
EH200	37. 41.59	113. 17.57	5627.	979445.84	979977.26	-2.15	-193.81	.66	-193.15
EH201	37. 40.70	113. 18.01	5725.	979437.27	979975.96	-.21	-195.20	.90	-194.30
EH202	37. 41.39	113. 18.65	5689.	979443.96	979976.97	2.10	-191.67	.65	-191.02
EH203	37. 41.24	113. 19.43	5727.	979441.12	979976.75	3.05	-192.01	.69	-191.32
EH204	37. 42.41	113. 21.36	5887.	979436.56	979978.46	11.83	-188.68	.85	-187.83
EH205	37. 43.30	113. 21.06	5837.	979440.16	979979.76	9.43	-189.38	.68	-188.70
EH206	37. 45.03	113. 18.39	5472.	979461.84	979982.26	-5.72	-192.10	.36	-191.74
EH207	37. 43.98	113. 22.06	5859.	979434.72	979980.73	5.08	-194.48	.68	-193.80
EH208	37. 43.20	113. 23.32	6110.	979418.50	979979.61	13.60	-194.51	1.09	-193.42
EH209	37. 44.61	113. 24.65	6052.	979425.83	979981.65	13.43	-192.70	1.08	-191.62
EH210	37. 45.92	113. 13.37	5557.	979459.55	979983.55	-1.32	-190.59	.52	-190.07
EH211	37. 41.41	113. 3.09	5874.	979427.18	979977.00	2.69	-197.38	3.34	-194.04
EH212	37. 42.47	113. 3.70	5682.	979432.09	979978.54	-12.00	-205.53	2.49	-203.04
EH213	37. 43.38	113. 3.43	5704.	979431.04	979979.87	-12.32	-206.60	2.20	-204.40
EH214	37. 43.88	113. 3.26	5671.	979432.28	979980.60	-14.91	-208.06	2.15	-205.91
EH215	37. 44.56	113. 2.32	5648.	979437.36	979981.58	-12.97	-205.34	2.70	-202.64
EH216	37. 44.14	113. 4.09	5548.	979439.08	979980.96	-20.04	-209.00	1.66	-207.34
EH217	37. 45.04	113. 3.27	5524.	979441.84	979982.27	-20.85	-209.00	1.80	-207.20
EH218	37. 45.02	113. 5.50	5514.	979439.22	979982.24	-24.39	-212.20	1.03	-211.17
EH219	37. 44.14	113. 5.50	5540.	979436.99	979980.96	-22.89	-211.58	1.17	-210.41

STAT.	LATITUDE	LONGITUDE	ELEV.	OBSERVED GRAVITY	THEOR. GRAVITY	FREE-AIR	SIMPLE BOUGUER	T.C	T.C. BOUGUER
EH220	37. 41.75	113. 4.68	5671.	979433.20	979977.50	-10.89	-204.04	2.00	-202.04
EH220	37. 42.41	113. 4.68	5625.	979435.42	979978.46	-13.96	-205.55	1.84	-203.71
EH221	37. 40.62	113. 4.82	5767.	979425.84	979975.85	-7.58	-204.00	2.32	-201.68
EH222	37. 40.00	113. 3.96	5910.	979419.24	979974.94	.20	-201.09	3.19	-197.90
EH223	37. 41.13	113. 6.61	5561.	979436.76	979976.59	-16.77	-206.18	1.55	-204.63
EH224	37. 42.39	113. 6.34	5569.	979436.56	979978.43	-18.06	-207.74	1.28	-206.46
EH225	37. 43.26	113. 6.32	5557.	979436.17	979979.70	-20.84	-210.11	1.14	-208.97
EH226	37. 45.03	113. 6.58	5512.	979440.60	979982.26	-23.21	-210.95	.84	-210.11
EH227	37. 45.90	113. 7.41	5488.	979446.14	979983.53	-21.20	-208.12	.68	-207.44
EH228	37. 45.03	113. 7.96	5504.	979446.08	979982.26	-18.48	-205.95	.69	-205.26
EH229	37. 44.59	113. 7.95	5505.	979444.77	979981.62	-19.06	-206.56	.72	-205.84
EH230	37. 43.27	113. 7.96	5531.	979438.82	979979.71	-20.65	-209.04	.86	-208.18
EH231	37. 42.39	113. 7.46	5544.	979437.72	979978.43	-19.25	-208.08	1.05	-207.03
EH233	37. 42.40	113. 8.52	5518.	979439.77	979978.45	-19.67	-207.61	.89	-206.72
EH234	37. 43.27	113. 8.53	5515.	979441.85	979979.71	-19.13	-206.97	.79	-206.18
EH235	37. 43.29	113. 9.63	5495.	979446.41	979979.74	-16.47	-203.63	.70	-202.93
EH236	37. 42.40	113. 9.63	5499.	979442.59	979978.45	-18.62	-205.92	.77	-205.15
EH237	37. 43.71	113. 10.77	5478.	979455.07	979980.35	-10.03	-196.61	.66	-195.95
EH238	37. 44.16	113. 9.63	5498.	979449.31	979980.99	-14.54	-201.80	.65	-201.15
EH239	37. 39.34	113. 11.28	5469.	979436.38	979973.99	-23.20	-209.47	.96	-208.51
EH240	37. 39.78	113. 9.63	5488.	979438.34	979974.62	-20.09	-207.01	1.12	-205.89
EH241	37. 39.78	113. 8.53	5507.	979439.52	979974.62	-17.12	-204.69	1.39	-203.30
EH242	37. 39.80	113. 7.97	5540.	979438.00	979974.65	-15.57	-204.26	1.63	-202.63
EH243	37. 40.68	113. 7.00	5549.	979437.91	979975.93	-16.08	-205.08	1.64	-203.44
EH244	37. 39.85	113. 6.35	5760.	979425.65	979974.73	-7.30	-203.49	2.10	-201.39
EH245	37. 39.32	113. 4.62	5996.	979414.02	979973.96	4.04	-200.18	3.14	-197.04
EH246	37. 40.89	113. 3.70	5800.	979428.89	979976.23	-1.80	-199.35	2.89	-196.46
EH246	37. 40.71	113. 3.67	5832.	979426.61	979975.98	-.82	-199.46	2.96	-196.50
EH247	37. 38.40	113. 3.62	6872.	979364.37	979972.63	38.12	-195.94	5.59	-190.35
EH247	37. 38.80	113. 4.06	6400.	979390.81	979973.21	19.58	-198.40	4.89	-193.51
EH248	37. 39.28	113. 2.31	7963.	979289.71	979972.45	66.25	-204.97	8.63	-196.34
EH249	37. 37.31	113. 1.87	8992.	979222.52	979971.03	97.27	-209.00	9.90	-199.10

STAT.	LATITUDE	LONGITUDE	ELEV.	OBSERVED GRAVITY	THEOR. GRAVITY	FREE-AIR	SIMPLE BOUGUER	T.C	T.C. BOUGUER
EH250	37. 36.91	113. 1.08	9168.	979210.34	979970.45	102.23	-210.03	10.08	-199.95
EH250	37. 35.84	113. 2.06	9303.	979198.23	979968.90	104.38	-212.48	12.19	-200.29
EH251	37. 36.18	113. .82	9230.	979208.70	979969.40	107.47	-206.90	7.29	-199.61
EH252	37. 34.68	113. .82	9236.	979205.75	979967.22	107.27	-207.31	6.13	-201.18
EH253	37. 33.60	113. .81	9195.	979207.20	979965.66	106.42	-206.76	5.40	-201.36
EH254	37. 33.16	113. 1.48	9336.	979197.43	979965.02	110.55	-207.43	6.30	-201.13
EH255	37. 32.72	113. 2.91	9418.	979191.04	979964.37	112.52	-208.26	7.83	-200.43
EH256	37. 31.92	113. 3.06	9217.	979203.54	979963.21	107.28	-206.65	6.73	-199.92
EH257	37. 31.22	113. 3.12	9199.	979203.80	979962.20	106.87	-206.45	6.56	-199.89
EH258	37. 31.88	113. 4.36	9454.	979185.15	979963.16	111.24	-210.76	9.42	-201.34
EH259	37. 32.14	113. 5.94	8617.	979241.09	979963.54	88.06	-205.44	9.89	-195.55
EH261	37. 32.98	113. 6.99	7990.	979282.44	979964.76	69.22	-202.92	10.21	-192.71
EH262	37. 33.60	113. 7.00	7724.	979300.23	979965.66	61.08	-202.00	10.15	-191.85
EH263	37. 34.21	113. 8.10	6177.	979402.95	979966.53	17.43	-192.96	5.26	-187.70
EH263	37. 34.59	113. 9.64	5552.	979436.62	979967.09	-8.25	-197.35	3.36	-193.99
EH264	37. 36.18	113. 6.86	6011.	979409.21	979969.40	5.21	-199.52	3.47	-196.05
EH265	37. 37.24	113. 6.60	5855.	979418.92	979970.94	-1.30	-200.72	3.04	-197.68
EH266	37. 37.70	113. 6.70	5795.	979422.21	979971.61	-4.33	-201.71	2.73	-198.98
EH268	37. 35.25	113. 3.98	7264.	979330.81	979968.04	46.03	-201.38	8.01	-193.37
EH268	37. 35.61	113. 4.98	7024.	979352.39	979968.56	44.50	-194.74	7.79	-186.95
EH269	37. 34.80	113. 3.17	8002.	979284.33	979967.40	69.60	-202.95	9.66	-193.29
EH271	37. 37.68	113. 8.02	5647.	979429.95	979971.58	-10.48	-202.82	2.11	-200.71
EH274	37. 36.12	113. 10.74	5469.	979436.35	979969.30	-18.54	-204.81	1.71	-203.10
EH275	37. 36.11	113. 9.60	5514.	979437.70	979969.29	-12.95	-200.76	2.46	-198.30
EH276	37. 35.24	113. 10.28	5477.	979439.95	979968.02	-12.91	-199.46	2.30	-197.16
EH278	37. 34.37	113. 10.85	5490.	979437.70	979966.77	-12.69	-199.68	2.23	-197.45
EH279	37. 33.48	113. 11.24	5498.	979436.95	979965.49	-11.40	-198.66	2.35	-196.31
EH280	37. 32.82	113. 10.66	5542.	979437.02	979964.52	-6.24	-195.00	3.29	-191.71
EH281	37. 33.48	113. 10.25	5509.	979437.20	979965.49	-10.13	-197.77	3.46	-194.31
EH282	37. 34.09	113. 9.88	5541.	979436.16	979966.36	-9.03	-197.76	3.26	-194.50
EH283	37. 35.46	113. 9.65	5553.	979436.03	979968.34	-10.00	-199.14	2.64	-196.50
EH284	37. 37.02	113. 8.99	5568.	979433.79	979970.62	-13.11	-202.76	2.17	-200.59

STAT.	LATITUDE	LONGITUDE	ELEV.	OBSERVED GRAVITY	THEOR. GRAVITY	FREE-AIR	SIMPLE BOUGUER	T.C	T.C. BOUGUER
EH285	37. 38.40	113. 12.93	5458.	979432.88	979972.63	-26.38	-212.28	1.04	-211.24
EH285	37. 37.94	113. 12.93	5470.	979431.83	979971.96	-25.63	-211.94	1.08	-210.86
EH286	37. 36.11	113. 12.93	5486.	979432.83	979969.29	-20.46	-207.31	1.51	-205.80
EH286	37. 36.66	113. 14.92	5636.	979425.24	979970.09	-14.73	-206.69	1.88	-204.81
EH286	37. 36.12	113. 14.02	5603.	979426.48	979969.30	-15.81	-206.65	1.77	-204.88
EH287	37. 35.23	113. 12.38	5535.	979432.09	979968.01	-15.30	-203.82	1.61	-202.21
EH287	37. 35.24	113. 13.62	5803.	979412.47	979968.02	-9.73	-207.38	1.73	-205.65
EH288	37. 33.71	113. 12.41	5599.	979429.84	979965.82	-9.35	-200.05	1.88	-198.17
EH289	37. 34.36	113. 13.63	5813.	979417.73	979966.76	-2.27	-200.26	2.04	-198.22
EH289	37. 32.61	113. 14.62	6406.	979380.25	979964.21	18.59	-199.60	2.55	-197.05
EH289	37. 31.80	113. 14.42	6086.	979398.21	979963.04	7.62	-199.67	2.28	-197.39
EH289	37. 31.18	113. 14.46	5924.	979408.69	979962.13	3.77	-198.00	2.33	-195.67
EH290	37. 33.48	113. 12.68	5658.	979425.82	979965.49	-7.49	-200.20	1.84	-198.36
EH291	37. 32.44	113. 12.14	5472.	979438.55	979963.97	-10.72	-197.10	2.39	-194.71
EH292	37. 30.30	113. 13.45	5342.	979446.42	979960.85	-11.97	-193.92	2.42	-191.50
EH292	37. 31.12	113. 12.90	5369.	979444.91	979962.05	-12.13	-195.00	2.84	-192.16
EH293	37. 31.36	113. 11.51	5528.	979436.59	979962.40	-5.85	-194.13	3.18	-190.95
EH294	37. 31.95	113. 11.04	5537.	979435.68	979963.25	-6.77	-195.36	3.55	-191.81
EH295	37. 34.07	113. 25.31	6102.	979402.43	979966.33	10.06	-197.77	1.98	-195.79
EH296	37. 33.81	113. 26.29	6160.	979397.87	979965.97	11.32	-198.49	2.03	-196.46
EH297	37. 33.46	113. 27.67	6317.	979388.05	979965.46	16.77	-198.39	1.83	-196.56
EH297	37. 31.93	113. 28.47	6812.	979352.80	979963.23	30.31	-201.71	1.89	-199.82
EH297	37. 31.96	113. 26.95	7109.	979329.66	979963.27	35.07	-207.06	2.84	-204.22
EH298	37. 33.09	113. 28.76	6594.	979370.19	979964.91	25.50	-199.09	1.47	-197.62
EH298	37. 32.71	113. 29.88	6242.	979389.45	979964.37	12.20	-200.40	1.72	-198.68
EH298	37. 32.40	113. 32.00	6052.	979399.56	979963.91	4.91	-201.22	2.19	-199.03
EH298	37. 30.17	113. 29.39	6328.	979376.21	979960.66	10.77	-204.76	2.73	-202.03
EH299	37. 32.87	113. 24.36	6330.	979385.98	979964.59	16.79	-198.81	3.80	-195.01
EH300	37. 32.44	113. 23.28	6434.	979378.15	979963.97	19.36	-199.78	3.76	-196.02
EH301	37. 32.44	113. 22.75	6577.	979371.02	979963.97	25.68	-198.33	2.60	-195.73
EH302	37. 32.41	113. 22.21	6627.	979368.85	979963.92	28.26	-197.46	2.10	-195.36
EH303	37. 32.45	113. 20.76	6264.	979386.60	979963.98	11.81	-201.54	3.21	-198.33

STAT.	LATITUDE	LONGITUDE	ELEV.	OBSERVED GRAVITY	THEOR. GRAVITY	FREE-AIR	SIMPLE BOUGUER	T.C	T.C. BOUGUER
EH304	37. 31.52	113. 19.77	5851.	979406.65	979962.62	-5.64	-204.93	3.92	-201.01
EH305	37. 30.68	113. 19.31	5656.	979414.16	979961.41	-15.25	-207.89	4.46	-203.43
EH306	37. 30.26	113. 19.21	5629.	979414.23	979960.80	-17.11	-208.83	3.38	-205.45
EH306	37. 30.68	113. 18.24	5946.	979395.44	979961.41	-6.70	-209.22	2.65	-206.57
EH306	37. 31.99	113. 18.46	7168.	979323.88	979963.31	34.79	-209.35	8.34	-201.01
EH306	37. 32.70	113. 17.73	7741.	979289.43	979964.35	53.20	-210.46	9.57	-200.89
EH306	37. 33.84	113. 17.90	8211.	979259.91	979966.01	66.22	-213.45	10.30	-203.15
EH306	37. 34.35	113. 18.43	8015.	979279.09	979966.74	66.24	-206.75	7.14	-199.61
EH306	37. 34.67	113. 18.71	7888.	979284.36	979967.20	59.10	-209.57	6.04	-203.53
EH310	37. 31.28	113. 7.04	7863.	979291.20	979962.27	68.53	-199.28	5.79	-193.49
EH311	37. 30.15	113. 7.47	8090.	979273.55	979960.63	73.87	-201.68	7.88	-193.80
EH333	37. 30.34	113. 12.25	5383.	979444.26	979960.91	-10.34	-193.68	3.15	-190.53
EH460	37. 57.72	113. 4.56	5917.	979436.62	980000.75	-7.58	-209.11	.51	-208.60
EH464	37. 53.81	113. 10.69	5421.	979466.70	979995.05	-18.45	-203.09	.20	-202.89
EH465	37. 54.68	113. 12.89	5325.	979476.20	979996.31	-19.25	-200.62	.15	-200.47
EH470	37. 57.29	113. 14.00	5186.	979483.89	980000.11	-28.43	-205.07	.10	-204.97
EH471	37. 56.41	113. 14.00	5214.	979478.83	979998.83	-29.58	-207.17	.10	-207.07
EH472	37. 55.54	113. 14.00	5234.	979473.97	979997.56	-31.29	-209.56	.12	-209.44
EH473	37. 53.81	113. 14.54	5213.	979471.64	979995.05	-33.08	-210.63	.15	-210.48
EH474	37. 54.36	113. 14.33	5213.	979471.80	979995.84	-33.72	-211.27	.13	-211.14
EH475	37. 57.27	113. 20.67	5131.	979488.41	980000.09	-29.06	-203.82	.00	-203.82
EH476	37. 56.39	113. 20.68	5138.	979486.23	979998.80	-29.30	-204.30	.01	-204.29
EH477	37. 55.51	113. 20.69	5147.	979482.09	979997.52	-31.30	-206.61	.02	-206.59
EH479	37. 59.00	113. 22.81	5100.	979486.34	980002.62	-36.58	-210.29	.02	-210.27
EH480	37. 59.88	113. 24.50	5088.	979485.70	980003.91	-39.64	-212.94	.07	-212.87
EH481	37. 55.08	113. 25.43	5115.	979492.65	979996.89	-23.14	-197.36	.03	-197.33
EH483	37. 57.11	113. 26.84	5093.	979488.48	979999.85	-32.33	-205.80	.05	-205.75
EH487	37. 47.66	113. 28.35	5128.	979471.95	979986.09	-31.81	-206.47	.42	-206.05
EH490	37. 49.40	113. 27.23	5139.	979482.18	979988.62	-23.08	-198.11	.19	-197.92
EH491	37. 48.06	113. 25.64	5261.	979467.83	979986.67	-24.00	-203.19	.38	-202.81
EH492	37. 48.53	113. 25.00	5233.	979469.20	979987.36	-25.95	-204.19	.29	-203.90
EH494	37. 50.12	113. 21.90	5202.	979467.41	979989.68	-32.98	-210.16	.13	-210.03

STAT.	LATITUDE	LONGITUDE	ELEV.	OBSERVED GRAVITY	THEOR. GRAVITY	FREE-AIR	SIMPLE BOUGUER	T.C	T.C. BOUGUER
EH497	37. 48.52	113. 20.70	5313.	979464.34	979987.34	-23.27	-204.23	.21	-204.02
EH498	37. 49.40	113. 20.70	5245.	979467.34	979988.62	-27.95	-206.59	.17	-206.42
EH499	37. 51.62	113. 21.70	5183.	979468.20	979991.86	-36.15	-212.68	.08	-212.60
EH500	37. 52.02	113. 21.20	5183.	979468.26	979992.45	-36.69	-213.22	.08	-213.14
EH503	37. 48.46	113. 17.35	5299.	979469.40	979987.27	-19.45	-199.93	.22	-199.71
EH504	37. 46.78	113. 16.19	5342.	979469.77	979984.81	-12.59	-194.54	.31	-194.23
EH507	37. 45.03	113. 20.59	5620.	979450.27	979982.26	-3.37	-194.79	.45	-194.34
EH508	37. 46.41	113. 14.89	5342.	979474.52	979984.27	-7.29	-189.24	.45	-188.79
EH511	37. 45.92	113. 14.66	5356.	979473.12	979983.55	-6.65	-189.08	.49	-188.59
EH516	37. 50.27	113. 9.50	5665.	979445.22	979989.90	-11.84	-204.79	.42	-204.37
EH518	37. 49.46	113. 7.40	5484.	979451.05	979988.72	-21.85	-208.64	.43	-208.21
EH519	37. 49.80	113. 6.62	5430.	979451.38	979989.22	-27.10	-212.05	.46	-211.59
EH521	37. 47.11	113. 5.48	5469.	979443.37	979985.30	-27.52	-213.79	.76	-213.03
EH522	37. 49.46	113. 5.18	5424.	979447.77	979988.72	-30.78	-215.52	.57	-214.95
EH525	37. 48.60	113. 4.18	5437.	979444.90	979987.46	-31.17	-216.35	.76	-215.59
EH526	37. 47.70	113. 4.21	5453.	979443.56	979986.15	-29.68	-215.41	.87	-214.54
EH527	37. 47.34	113. 4.38	5458.	979443.14	979985.63	-29.12	-215.02	.90	-214.12
EH529	37. 45.89	113. 3.70	5494.	979441.59	979983.52	-25.16	-212.29	1.35	-210.94
EH530	37. 45.89	113. 2.44	5490.	979444.09	979983.52	-23.04	-210.03	1.94	-208.09
EH531	37. 45.89	113. 1.88	5526.	979443.34	979983.52	-20.40	-208.62	2.29	-206.33
EH533	37. 46.33	113. 2.43	5478.	979444.80	979984.16	-24.10	-210.68	1.73	-208.95
EH534	37. 46.38	113. 1.42	5548.	979444.20	979984.23	-18.18	-207.14	2.25	-204.89
EH537	37. 48.30	113. .77	5559.	979446.81	979987.02	-17.34	-206.68	1.50	-205.18
EH540	37. 43.42	113. 4.07	5601.	979435.87	979979.93	-17.24	-208.01	1.88	-206.13
EH541	37. 43.92	113. 4.95	5547.	979437.23	979980.66	-21.68	-210.61	1.38	-209.23
EH543	37. 41.88	113. 5.20	5634.	979433.95	979977.69	-13.82	-205.71	1.76	-203.95
EH544	37. 43.70	113. 6.59	5544.	979436.90	979980.34	-21.98	-210.81	1.02	-209.79
EH545	37. 41.76	113. 6.61	5565.	979436.59	979977.52	-17.49	-207.03	1.35	-205.68
EH548	37. 38.93	113. 5.22	5977.	979413.53	979973.40	2.33	-201.25	2.94	-198.31
EH549	37. 41.11	113. 7.72	5532.	979437.64	979976.56	-18.59	-207.01	1.24	-205.77
EH550	37. 41.11	113. 8.53	5518.	979438.93	979976.56	-18.62	-206.56	1.07	-205.49
EH551	37. 41.11	113. 9.09	5504.	979440.09	979976.56	-18.78	-206.25	.99	-205.26

STAT.	LATITUDE	LONGITUDE	ELEV.	OBSERVED GRAVITY	THEOR. GRAVITY	FREE-AIR	SIMPLE BOUGUER	T.C	T.C. BOUGUER
EH552	37. 41.56	113. 10.45	5486.	979440.66	979977.21	-20.55	-207.40	.80	-206.60
EH553	37. 41.11	113. 10.73	5477.	979439.32	979976.56	-22.08	-208.63	.83	-207.80
EH557	37. 38.04	113. 9.17	5551.	979433.43	979972.10	-16.55	-205.62	1.56	-204.06
EH558	37. 38.03	113. 10.73	5471.	979435.65	979972.09	-21.84	-208.18	1.23	-206.95
EH559	37. 38.05	113. 8.16	5622.	979431.77	979972.12	-11.54	-203.03	1.90	-201.13
EH560	37. 38.40	113. 8.00	5607.	979431.73	979972.63	-13.51	-204.48	1.94	-202.54
EH561	37. 40.64	113. 9.65	5493.	979439.47	979975.88	-19.75	-206.84	.98	-205.86
EH562	37. 42.36	113. 11.55	5471.	979447.27	979978.38	-16.51	-202.85	.83	-202.02
EH563	37. 43.45	113. 11.94	5525.	979451.48	979979.97	-8.82	-197.00	.65	-196.35
EH564	37. 43.90	113. 11.43	5463.	979456.85	979980.62	-9.93	-196.00	.71	-195.29
EH565	37. 44.15	113. 10.74	5517.	979454.62	979980.98	-7.43	-195.34	.63	-194.71
EH566	37. 44.16	113. 10.00	5489.	979452.80	979980.99	-11.91	-198.87	.66	-198.21
EH568	37. 44.14	113. 8.52	5509.	979444.61	979980.96	-18.18	-205.82	.72	-205.10
EH569	37. 43.71	113. 7.69	5526.	979439.67	979980.35	-20.91	-209.13	.83	-208.30
EH571	37. 44.95	113. 14.03	5391.	979468.23	979982.14	-6.84	-190.46	.64	-189.82
EH573	37. 38.42	113. 15.40	5689.	979423.84	979972.66	-13.72	-207.49	1.08	-206.41
EH575	37. 44.16	113. 18.37	5527.	979458.80	979980.99	-2.33	-190.58	.41	-190.17
EH576	37. 43.29	113. 18.37	5556.	979455.38	979979.74	-1.77	-191.01	.47	-190.54
EH578	37. 42.42	113. 18.37	5611.	979449.67	979978.48	-1.04	-192.15	.53	-191.62
EH579	37. 41.05	113. 20.36	5815.	979435.13	979976.48	5.61	-192.45	.76	-191.69
EH580	37. 40.66	113. 19.52	5778.	979436.66	979975.91	4.23	-192.57	.77	-191.80
EH581	37. 39.76	113. 20.62	5959.	979427.52	979974.60	13.42	-189.54	1.09	-188.45
EH584	37. 40.80	113. 21.84	6025.	979424.08	979976.11	14.68	-190.53	1.00	-189.53
EH586	37. 37.10	113. 15.13	5638.	979424.29	979970.73	-16.14	-208.17	1.69	-206.48
EH588	37. 33.48	113. 11.84	5546.	979435.07	979965.49	-8.77	-197.67	2.02	-195.65
EH589	37. 32.41	113. 15.45	6781.	979354.96	979963.92	28.86	-202.10	4.13	-197.97
EH592	37. 33.07	113. 16.57	7375.	979318.39	979964.88	47.20	-203.99	4.89	-199.10
EH593	37. 36.11	113. 12.39	5468.	979433.54	979969.29	-21.44	-207.68	1.48	-206.20
EH595	37. 37.16	113. 10.72	5466.	979434.02	979970.82	-22.68	-208.85	1.44	-207.41
EH596	37. 37.38	113. 9.48	5531.	979433.45	979971.14	-17.46	-205.85	1.69	-204.16
EH609	37. 34.55	113. 7.70	6330.	979392.59	979967.03	20.96	-194.64	4.30	-190.34
EH612	37. 33.48	113. 9.63	5637.	979432.08	979965.49	-3.21	-195.21	4.67	-190.54

STAT.	LATITUDE	LONGITUDE	ELEV.	OBSERVED GRAVITY	THEOR. GRAVITY	FREE-AIR	SIMPLE BOUGUER	T.C	T.C. BOUGUER
EH613	37. 32.30	113. 11.37	5499.	979437.66	979963.77	-8.87	-196.17	2.80	-193.37
EH770	37. 40.45	113. 7.72	5524.	979438.95	979975.59	-17.06	-205.21	1.46	-203.75
EH771	37. 41.52	113. 9.11	5506.	979440.39	979977.16	-18.89	-206.42	.92	-205.50
EH772	37. 44.53	113. 11.07	5703.	979444.55	979981.53	-.56	-194.80	.70	-194.10
EH773	37. 36.11	113. 11.84	5460.	979434.62	979969.29	-21.11	-207.08	1.50	-205.58
EH774	37. 35.24	113. 11.84	5493.	979435.52	979968.02	-15.84	-202.93	1.67	-201.26
EH780	37. 39.72	113. 14.30	5570.	979431.87	979974.54	-18.75	-208.46	.88	-207.58
EH775	37. 43.04	113. 5.50	5580.	979435.80	979979.37	-18.72	-208.77	1.37	-207.40
EH776	37. 44.59	113. 4.40	5530.	979439.39	979981.62	-22.08	-210.43	1.43	-209.00
EH777	37. 44.59	113. 3.27	5573.	979438.38	979981.62	-19.04	-208.86	1.95	-206.91
EH778	37. 49.46	113. 4.18	5422.	979446.26	979988.72	-32.47	-217.14	.67	-216.47
EH779	37. 46.59	113. 5.48	5479.	979442.34	979984.53	-26.85	-213.46	.82	-212.64
EH781	37. 39.12	113. 13.78	5528.	979431.16	979973.67	-22.56	-210.84	.89	-209.95
EH782	37. 47.07	113. 20.59	5442.	979461.17	979985.23	-12.20	-197.55	.34	-197.21
EH784	37. 45.91	113. 17.27	5402.	979466.92	979983.54	-8.51	-192.50	.32	-192.18
EH783	37. 47.64	113. 25.00	5383.	979463.20	979986.06	-16.55	-199.89	.42	-199.47
EH785	37. 41.10	113. 5.80	5625.	979432.53	979976.55	-14.94	-206.53	1.86	-204.67
EH786	37. 39.48	113. 5.70	5880.	979417.48	979974.20	-3.65	-203.92	2.43	-201.49
EH787	37. 44.75	113. 22.06	5805.	979438.34	979981.85	2.50	-195.22	.57	-194.65
EH788	37. 45.03	113. 20.00	5582.	979452.77	979982.26	-4.45	-194.57	.41	-194.16
EH789	37. 53.34	113. 23.70	5149.	979484.20	979994.36	-25.85	-201.22	.03	-201.19
EH790	37. 54.53	113. 24.77	5128.	979492.29	979996.09	-21.47	-196.13	.03	-196.10
EH791	37. 56.66	113. 27.35	5094.	979490.34	979999.20	-29.72	-203.22	.05	-203.17
EH792	37. 57.45	113. 28.29	5113.	979483.81	980000.36	-35.63	-209.78	.08	-209.70
EH793	37. 58.15	113. 29.40	5175.	979487.51	980001.38	-27.12	-203.38	.13	-203.25
EH794	37. 59.40	113. 24.00	5095.	979485.60	980003.20	-38.37	-211.91	.05	-211.86
EH795	37. 58.28	113. 22.37	5110.	979487.07	980001.57	-33.86	-207.91	.02	-207.89
EH796	37. 58.14	113. 21.72	5116.	979488.01	980001.37	-32.15	-206.40	.02	-206.38
EH797	37. 57.57	113. 20.71	5128.	979488.87	980000.54	-29.33	-203.99	.00	-203.99
EH798	37. 53.81	113. 21.10	5163.	979473.84	979995.05	-35.58	-211.43	.04	-211.39
EH799	37. 50.27	113. 20.10	5231.	979467.76	979989.90	-30.12	-208.29	.13	-208.16
EH800	37. 40.64	113. 3.25	5862.	979427.45	979975.88	2.94	-196.72	3.50	-193.22

STAT.	LATITUDE	LONGITUDE	ELEV.	OBSERVED GRAVITY	THEOR. GRAVITY	FREE-AIR	SIMPLE BOUGUER	T.C	T.C. BOUGUER
EH801	37. 40.43	113. 2.66	5902.	979422.96	979975.58	2.53	-198.49	5.64	-192.85
EH802	37. 40.42	113. 1.94	6038.	979413.77	979975.56	6.14	-199.51	6.96	-192.55
EH803	37. 40.36	113. 1.30	6101.	979406.12	979975.47	4.51	-203.29	7.50	-195.79
EH804	37. 40.10	113. .60	6213.	979397.41	979975.09	6.72	-204.89	8.18	-196.71
EH805	37. 49.04	113. 18.60	5253.	979471.54	979988.10	-22.47	-201.39	.19	-201.20
EH806	37. 47.30	113. 16.54	5330.	979468.55	979985.57	-15.68	-197.22	.28	-196.94
EH807	37. 46.39	113. 15.78	5335.	979472.12	979984.24	-10.32	-192.03	.38	-191.65
EH808	37. 53.78	113. 4.90	5465.	979450.82	979995.00	-30.15	-216.29	.36	-215.93
EH809	37. 53.83	113. 6.25	5373.	979460.48	979995.07	-29.21	-212.21	.36	-211.85
EH810	37. 53.96	113. 7.28	5353.	979465.34	979995.26	-26.42	-208.74	.37	-208.37
EH811	37. 52.95	113. 9.60	5492.	979458.45	979993.79	-18.77	-205.83	.23	-205.60
EH812	37. 53.73	113. 13.06	5321.	979475.24	979994.92	-19.19	-200.42	.17	-200.25
EH813	37. 56.10	113. 14.65	5205.	979475.23	979998.37	-33.57	-210.85	.09	-210.75
EH814	37. 54.70	113. 1.85	5546.	979448.31	979996.34	-26.38	-215.28	.45	-214.83
EH815	37. 59.98	113. 4.74	6157.	979435.98	980004.05	11.07	-198.64	.61	-198.03
EH816	37. 60.03	113. 6.04	6067.	979442.62	980004.12	9.15	-197.49	.57	-196.92
EH817	37. 55.95	113. .45	5640.	979446.91	979998.16	-20.76	-212.86	.47	-212.39
EH818	37. 37.14	113. 14.60	5589.	979426.40	979970.79	-18.70	-209.06	1.42	-207.64
LU 1	37. 40.33	113. 32.89	5293.	979445.02	979975.42	-32.55	-212.83	.60	-212.23
LU 2	37. 41.09	113. 35.21	5207.	979443.77	979976.54	-43.00	-220.35	.33	-220.02
LU 3	37. 41.78	113. 37.21	5183.	979452.15	979977.54	-37.89	-214.42	.22	-214.20
LU 4	37. 42.56	113. 39.33	5180.	979468.95	979978.67	-22.50	-198.93	.18	-198.75
LU 5	37. 43.31	113. 39.31	5172.	979472.79	979979.77	-20.51	-196.67	.16	-196.51
LU 6	37. 44.20	113. 39.31	5165.	979474.98	979981.05	-20.27	-196.19	.13	-196.06
LU 7	37. 44.65	113. 39.33	5161.	979475.75	979981.71	-20.53	-196.31	.13	-196.18
LU 8	37. 45.06	113. 39.31	5159.	979475.91	979982.30	-21.15	-196.87	.12	-196.75
LU 9	37. 45.50	113. 39.33	5155.	979474.84	979982.95	-23.23	-198.81	.11	-198.70
LU 10	37. 45.95	113. 39.32	5152.	979474.12	979983.60	-24.89	-200.36	.10	-200.26
LU 11	37. 46.37	113. 39.32	5150.	979473.52	979984.21	-26.29	-201.70	.10	-201.60
LU 12	37. 46.82	113. 39.31	5149.	979473.14	979984.87	-27.42	-202.79	.09	-202.70
LU 13	37. 47.25	113. 39.32	5146.	979472.41	979985.49	-29.06	-204.33	.09	-204.24
LU 14	37. 47.68	113. 39.32	5143.	979471.62	979986.12	-30.76	-205.93	.09	-205.84

STAT.	LATITUDE	LONGITUDE	ELEV.	OBSERVED GRAVITY	THEOR. GRAVITY	FREE-AIR	SIMPLE BOUGUER	T.C	T.C. BOUGUER
LU 15	37. 48.55	113. 39.33	5138.	979473.32	979987.39	-30.80	-205.80	.09	-205.71
LU 16	37. 50.30	113. 39.33	5131.	979479.80	979989.94	-27.52	-202.28	.10	-202.18
LU 17	37. 52.90	113. 39.35	5138.	979491.99	979993.73	-18.47	-193.47	.15	-193.32
LU 18	37. 49.88	113. 41.52	5142.	979478.13	979989.33	-27.54	-202.68	.12	-202.56
LU 19	37. 49.86	113. 42.61	5151.	979481.24	979989.30	-23.56	-199.00	.12	-198.88
LU 20	37. 48.56	113. 41.52	5147.	979469.01	979987.41	-34.28	-209.59	.11	-209.48
LU 21	37. 47.68	113. 41.51	5151.	979467.42	979986.12	-34.21	-209.65	.11	-209.54
LU 22	37. 47.25	113. 41.51	5153.	979467.87	979985.49	-32.93	-208.45	.11	-208.34
LU 23	37. 46.18	113. 41.51	5155.	979468.80	979983.94	-30.27	-205.85	.11	-205.74
LU 24	37. 46.38	113. 41.51	5156.	979470.01	979984.23	-29.25	-204.87	.11	-204.76
LU 25	37. 45.94	113. 41.51	5158.	979471.50	979983.59	-26.93	-202.61	.12	-202.49
LU 26	37. 45.28	113. 41.51	5163.	979473.52	979982.62	-23.48	-199.33	.13	-199.20
LU 27	37. 44.20	113. 41.51	5171.	979475.20	979981.05	-19.48	-195.61	.14	-195.47
LU 28	37. 43.36	113. 41.51	5176.	979475.59	979979.84	-17.40	-193.70	.16	-193.54
LU 30	37. 45.93	113. 44.83	5191.	979472.02	979983.57	-23.30	-200.11	.14	-199.97
LU 31	37. 46.81	113. 44.83	5188.	979468.47	979984.85	-28.41	-205.11	.13	-204.98
LU 32	37. 56.91	113. 44.83	5556.	979470.22	979999.56	-6.75	-195.98	.62	-195.36
LU 33	37. 57.08	113. 43.73	5512.	979475.52	979999.80	-5.84	-193.58	.54	-193.04
LU 34	37. 57.26	113. 42.63	5461.	979481.50	980000.07	-4.92	-190.92	.51	-190.41
LU 35	37. 57.26	113. 41.54	5430.	979484.72	980000.07	-4.61	-189.55	.46	-189.09
LU 36	37. 57.26	113. 40.45	5403.	979484.83	980000.07	-7.04	-191.07	.42	-190.65
LU 37	37. 58.99	113. 39.30	5692.	979468.69	980002.60	1.47	-192.40	.69	-191.71
LU 38	38. 1.17	113. 39.09	6045.	979447.92	980005.78	10.73	-195.17	.71	-194.46
LU039	38. 2.54	113. 38.13	5735.	979465.44	980007.77	-2.90	-198.24	.78	-197.46
LU 40	38. 3.27	113. 38.63	5821.	979458.11	980008.84	-3.22	-201.48	.73	-200.75
LU 41	38. 1.88	113. 36.49	5606.	979473.82	980006.82	-5.71	-196.65	.84	-195.81
LU 42	38. .68	113. 34.79	5514.	979479.41	980005.07	-7.02	-194.82	.45	-194.37
LU 43	38. .39	113. 32.65	5480.	979478.35	980004.64	-10.85	-197.50	.35	-197.15
LU 44	37. 59.85	113. 30.53	5350.	979488.49	980003.86	-12.15	-194.37	.32	-194.05
LU 45	38. .39	113. 28.60	5265.	979495.95	980004.64	-13.47	-192.80	.39	-192.41
LU 46	38. .36	113. 27.48	5088.	979494.38	980004.60	-31.65	-204.95	.35	-204.60
LU 47	38. 1.18	113. 27.31	5084.	979503.08	980005.80	-24.53	-197.69	.74	-196.95

STAT.	LATITUDE	LONGITUDE	ELEV.	OBSERVED GRAVITY	THEOR. GRAVITY	FREE-AIR	SIMPLE BOUGUER	T.C	T.C. BOUGUER
LU 48	38. .38	113. 26.51	5079.	979488.73	980004.63	-38.18	-211.17	.22	-210.95
LU049	38. .01	113. 25.08	5087.	979485.76	980004.09	-39.86	-213.12	.10	-213.02
LU 50	37. 58.71	113. 22.80	5104.	979486.41	980002.20	-35.72	-209.56	.02	-209.54
LU051	38. 1.63	113. 24.40	5077.	979486.28	980006.45	-42.64	-215.57	.14	-215.43
LU 52	38. 1.63	113. 22.81	5087.	979486.17	980006.45	-41.81	-215.07	.09	-214.98
LU 53	37. 58.92	113. 27.78	5106.	979486.41	980002.51	-35.83	-209.74	.16	-209.58
LU 54	37. 57.60	113. 29.72	5149.	979486.25	980000.59	-30.03	-205.40	.15	-205.25
LU 55	37. 57.27	113. 30.50	5159.	979488.41	980000.09	-26.43	-202.15	.18	-201.97
LU 56	37. 56.48	113. 32.19	5205.	979486.66	979998.94	-22.71	-200.00	.11	-199.89
LU 57	37. 55.48	113. 34.95	5200.	979488.04	979997.48	-20.33	-197.45	.12	-197.33
LU 58	37. 57.27	113. 34.95	5287.	979487.95	980000.09	-14.85	-194.93	.21	-194.72
LU 59	37. 54.65	113. 37.15	5163.	979492.67	979996.27	-17.97	-193.82	.15	-193.67
LU 60	37. 53.78	113. 40.44	5163.	979495.74	979995.00	-13.64	-189.49	.19	-189.30
LU 61	37. 53.28	113. 40.85	5152.	979496.42	979994.27	-13.25	-188.72	.19	-188.53
LU 62	37. 45.94	113. 42.63	5164.	979470.56	979983.59	-27.31	-203.19	.12	-203.07
LU 63	37. 46.82	113. 42.62	5166.	979465.95	979984.87	-33.01	-208.96	.11	-208.85
LU 64	37. 46.82	113. 43.71	5176.	979466.96	979984.87	-31.06	-207.35	.12	-207.23
LU 65	37. 47.68	113. 42.62	5160.	979464.77	979986.12	-36.02	-211.77	.11	-211.66
LU 66	37. 45.50	113. 42.63	5169.	979472.63	979982.95	-24.12	-200.18	.13	-200.05
LU 67	37. 44.41	113. 42.62	5169.	979477.41	979981.36	-17.76	-193.81	.15	-193.66
LU 68	37. 42.75	113. 42.62	5170.	979478.22	979978.95	-14.45	-190.54	.40	-190.14
LU 69	37. 43.32	113. 42.61	5192.	979477.32	979979.79	-14.11	-190.95	.22	-190.73
LU 70	37. 42.45	113. 42.61	5239.	979471.27	979978.52	-14.47	-192.91	.29	-192.62
LU 71	37. 41.55	113. 42.78	5220.	979468.13	979977.20	-18.08	-195.87	.56	-195.31
LU 72	37. 39.78	113. 42.95	5250.	979459.28	979974.62	-21.53	-200.34	.79	-199.55
LU 73	37. 41.55	113. 41.88	5199.	979467.97	979977.20	-20.22	-197.29	.25	-197.04
LU 74	37. 41.55	113. 41.00	5194.	979469.78	979977.20	-18.88	-195.79	.20	-195.59
LU 75	37. 41.54	113. 40.16	5193.	979468.80	979977.20	-19.94	-196.81	.20	-196.61
LU 76	37. 41.99	113. 39.33	5187.	979466.09	979977.85	-23.88	-200.55	.18	-200.37
LU 77	37. 42.45	113. 40.41	5184.	979472.39	979978.52	-18.53	-195.09	.17	-194.92
LU 78	37. 42.45	113. 41.51	5186.	979473.19	979978.52	-17.54	-194.18	.19	-193.99
LU 79	37. 42.96	113. 40.42	5179.	979473.95	979979.26	-18.18	-194.57	.16	-194.41

STAT.	LATITUDE	LONGITUDE	ELEV.	OBSERVED GRAVITY	THEOR. GRAVITY	FREE-AIR	SIMPLE BOUGUER	T.C	T.C. BOUGUER
LU 80	37. 42.08	113. 37.96	5178.	979457.76	979977.98	-33.18	-209.54	.19	-209.35
LU 81	37. 40.22	113. 39.62	5204.	979461.96	979975.26	-23.82	-201.06	.25	-200.81
LU 82	37. 40.23	113. 37.96	5195.	979452.12	979975.27	-34.51	-211.45	.27	-211.18
LU 83	37. 39.80	113. 37.97	5200.	979450.89	979974.65	-34.65	-211.76	.30	-211.46
LU 84	37. 40.65	113. 37.42	5190.	979449.82	979975.90	-37.92	-214.69	.26	-214.43
LU 85	37. 40.65	113. 36.31	5197.	979445.02	979975.90	-42.05	-219.06	.30	-218.76
LU 86	37. 40.40	113. 35.20	5209.	979443.63	979975.53	-41.95	-219.37	.39	-218.98
LU 87	37. 40.40	113. 34.50	5223.	979443.51	979975.53	-40.75	-218.64	.45	-218.19
LU 88	37. 39.72	113. 35.21	5205.	979445.37	979974.54	-39.60	-216.88	.48	-216.40
LU 89	37. 39.72	113. 34.50	5223.	979445.87	979974.54	-37.40	-215.30	.57	-214.73
LU 90	37. 39.72	113. 33.36	5286.	979445.86	979974.54	-31.49	-211.54	.85	-210.69
LU 91	37. 38.84	113. 33.66	5354.	979446.88	979973.27	-22.80	-205.16	1.78	-203.38
LU 92	37. 41.50	113. 32.81	5246.	979446.04	979977.13	-37.66	-216.34	.47	-215.87
LU 93	37. 42.15	113. 32.18	5224.	979450.40	979978.08	-36.32	-214.25	.53	-213.72
LU 94	37. 43.31	113. 31.63	5183.	979454.97	979979.77	-37.30	-213.83	.56	-213.27
LU 95	37. 44.18	113. 31.07	5169.	979459.02	979981.02	-35.81	-211.87	.60	-211.27
LU 96	37. 45.05	113. 31.63	5157.	979460.13	979982.29	-37.10	-212.74	.37	-212.37
LU 97	37. 46.81	113. 31.63	5137.	979468.73	979984.85	-32.94	-207.91	.21	-207.70
LU 98	37. 47.69	113. 31.06	5133.	979473.92	979986.13	-29.41	-204.24	.18	-204.06
LU 99	37. 47.64	113. 27.47	5151.	979472.73	979986.06	-28.83	-204.28	.53	-203.75
LU100	37. 47.68	113. 32.80	5130.	979471.88	979986.12	-31.72	-206.45	.13	-206.32
LU101	37. 47.68	113. 34.40	5133.	979475.55	979986.12	-27.78	-202.61	.11	-202.50
LU102	37. 47.68	113. 37.95	5141.	979473.95	979986.12	-28.63	-203.73	.09	-203.64
LU103	37. 47.67	113. 40.40	5144.	979470.69	979986.11	-31.58	-206.78	.11	-206.67
LU104	37. 48.55	113. 40.42	5139.	979471.30	979987.39	-32.73	-207.76	.12	-207.64
LU105	37. 51.11	113. 39.32	5131.	979484.20	979991.12	-24.31	-199.07	.10	-198.97
LU106	37. 52.05	113. 39.33	5134.	979489.39	979992.49	-20.21	-195.07	.12	-194.95
LU107	37. 45.94	113. 37.97	5153.	979474.36	979983.59	-24.54	-200.05	.11	-199.94
LU108	37. 45.07	113. 38.21	5158.	979474.05	979982.32	-23.11	-198.79	.12	-198.67
LU109	37. 45.05	113. 36.29	5155.	979466.98	979982.29	-30.43	-206.01	.14	-205.87
LU110	37. 40.53	113. 31.05	5437.	979445.49	979975.72	-18.83	-204.01	.79	-203.22
LU111	37. 39.45	113. 27.41	5872.	979423.35	979974.16	1.52	-198.48	1.19	-197.29

STAT.	LATITUDE	LONGITUDE	ELEV.	OBSERVED GRAVITY	THEOR. GRAVITY	FREE-AIR	SIMPLE BOUGUER	T.C	T.C. BOUGUER
WU432	37. 45.50	112. 50.74	7421.	979301.62	979982.95	16.69	-236.07	9.21	-226.86
WU546	37. 53.22	112. 46.84	5897.	979416.51	979994.18	-23.01	-223.86	2.42	-221.44
WU547	37. 48.85	112. 56.15	5947.	979412.98	979987.83	-15.48	-218.04	2.11	-215.93
WU548	37. 50.37	112. 55.25	5739.	979429.80	979990.04	-20.44	-215.91	1.70	-214.21
WU549	37. 51.89	112. 55.25	5696.	979434.69	979992.26	-21.81	-215.81	1.46	-214.35
WU550	37. 53.55	112. 56.38	5684.	979446.62	979994.66	-13.41	-207.01	1.85	-205.16
WU551	37. 54.69	112. 59.21	5547.	979459.00	979996.33	-15.58	-204.51	1.09	-203.42
WU552	37. 52.97	112. 52.54	5724.	979427.26	979993.81	-28.16	-223.12	1.21	-221.91
WU553	37. 52.97	112. 49.18	5794.	979417.76	979993.81	-31.08	-228.43	1.66	-226.77
WU554	37. 54.55	112. 49.18	5723.	979425.65	979996.12	-32.17	-227.10	1.42	-225.68
WU555	37. 56.97	112. 49.18	5700.	979435.00	979999.65	-28.51	-222.65	1.34	-221.31
WU556	37. 58.71	112. 49.18	5813.	979435.43	980002.20	-20.01	-218.00	1.25	-216.75
WU557	38. .48	112. 49.04	6118.	979430.41	980004.78	1.08	-207.30	1.27	-206.03
WU623	37. 34.54	113. 49.58	5485.	979454.57	979967.02	3.47	-183.34	1.24	-182.10
WU624	37. 35.12	113. 52.15	5591.	979446.39	979967.84	4.43	-186.00	.80	-185.20
WU625	37. 36.25	113. 54.93	5815.	979425.66	979969.49	3.12	-194.94	.79	-194.15
WU626	37. 36.75	113. 58.75	5973.	979409.66	979970.22	1.26	-202.18	.63	-201.55
WU628	37. 31.10	113. 50.94	5760.	979422.89	979962.02	2.66	-193.52	1.62	-191.90
WU630	37. 31.88	113. 35.58	6010.	979402.15	979963.16	4.29	-200.41	1.08	-199.33
WU631	37. 31.50	113. 33.61	6560.	979365.40	979962.59	19.84	-203.59	2.04	-201.55
WU632	37. 32.37	113. 30.93	6052.	979400.50	979963.87	5.89	-200.24	1.63	-198.61
WU633	37. 34.59	113. 31.65	5824.	979418.66	979967.09	-.64	-199.01	1.95	-197.06
WU634	37. 37.99	113. 32.04	5789.	979427.87	979972.02	.36	-196.81	1.25	-195.56
WU635	37. 40.47	113. 32.94	5314.	979445.16	979975.62	-30.64	-211.64	.56	-211.08
WU636	37. 43.33	113. 31.60	5193.	979454.91	979979.80	-36.45	-213.33	.55	-212.78
WU637	37. 45.87	113. 31.68	5175.	979463.87	979983.48	-32.86	-209.12	.28	-208.84
WU638	37. 47.65	113. 32.82	5151.	979472.14	979986.08	-29.44	-204.89	.12	-204.77
WU639	37. 46.75	113. 36.04	5149.	979473.30	979984.77	-27.15	-202.53	.11	-202.42
WU640	37. 44.21	113. 37.18	5153.	979467.68	979981.07	-28.71	-204.23	.14	-204.09
WU641	37. 52.00	113. 39.33	5136.	979489.42	979992.42	-19.92	-194.85	.11	-194.74
WU642	37. 49.85	113. 39.37	5143.	979478.34	979989.28	-27.19	-202.36	.09	-202.27
WU643	37. 47.65	113. 39.38	5148.	979472.23	979986.08	-29.63	-204.97	.09	-204.88

STAT.	LATITUDE	LONGITUDE	ELEV.	OBSERVED GRAVITY	THEOR. GRAVITY	FREE-AIR	SIMPLE BOUGUER	T.C	T.C. BOUGUER
WU644	37. 45.00	113. 39.35	5142.	979475.95	979982.22	-22.61	-197.75	.12	-197.63
WU645	37. 42.63	113. 39.38	5170.	979468.99	979978.78	-23.50	-199.59	.17	-199.42
WU646	37. 41.82	113. 37.27	5185.	979451.45	979977.59	-38.46	-215.06	.21	-214.85
WU647	37. 38.84	113. 38.03	5197.	979448.94	979973.27	-35.51	-212.52	.36	-212.15
WU648	37. 36.16	113. 38.08	5380.	979446.97	979969.37	-16.36	-199.60	.61	-198.99
WU649	37. 33.85	113. 46.41	5420.	979449.06	979966.02	-7.16	-191.76	1.83	-189.93
WU671	37. 51.49	113. 56.62	5946.	979433.78	979991.67	1.39	-201.13	1.11	-200.02
WU672	37. 54.82	113. 57.00	6292.	979406.91	979996.52	2.22	-212.09	1.97	-210.12
WU673	37. 58.18	113. 57.01	6603.	979382.32	980001.42	1.98	-222.91	.99	-221.92
WU674	37. 59.97	113. 56.97	6634.	979376.52	980004.03	-3.52	-229.47	.89	-228.58
WU675	37. 59.94	113. 53.77	6565.	979391.24	980003.99	4.75	-218.85	.85	-218.00
WU676	37. 59.95	113. 52.38	6702.	979402.49	980004.00	28.88	-199.39	1.25	-198.14
WU678	38. 1.10	113. 58.09	6742.	979375.09	980005.68	3.56	-226.07	.92	-225.15
WU679	38. 3.56	113. 58.09	6670.	979387.40	980009.27	5.51	-221.67	.84	-220.83
WU680	38. 6.25	113. 58.09	6570.	979391.59	980013.19	-3.64	-227.41	.79	-226.62
WU705	38. 7.47	113. 38.41	6113.	979439.68	980014.98	-.32	-208.52	.68	-207.84
WU706	38. 4.82	113. 38.28	5935.	979446.45	980011.10	-6.42	-208.57	1.21	-207.36
WU707	38. 2.24	113. 36.88	5694.	979470.12	980007.33	-1.64	-195.58	.76	-194.82
WU708	38. .71	113. 34.82	5519.	979479.51	980005.12	-6.50	-194.48	.44	-194.04
WU709	37. 58.06	113. 34.88	5345.	979484.77	980001.25	-13.74	-195.79	.23	-195.56
WU710	37. 59.89	113. 30.60	5288.	979488.62	980003.91	-17.92	-198.04	.58	-197.46
WU711	38. 2.80	113. 26.57	5121.	979501.41	980008.14	-25.06	-199.48	.80	-198.68
WU712	38. 1.56	113. 19.56	5116.	979490.48	980006.35	-34.66	-208.91	.02	-208.89
WU713	38. 1.58	113. 15.12	5156.	979499.04	980006.38	-22.38	-197.99	.09	-197.90
WU714	38. 3.70	113. 15.18	5129.	979505.52	980009.47	-21.52	-196.21	.18	-196.03
WU715	38. 5.96	113. 16.31	5092.	979507.09	980012.76	-26.72	-200.15	.12	-200.03
WU724	38. 6.82	113. 22.82	5355.	979496.71	980014.02	-13.62	-196.01	.38	-195.63
WU725	38. 5.30	113. 25.48	5406.	979498.63	980011.80	-4.68	-188.82	.51	-188.31
WU726	38. 7.31	113. 25.69	5539.	979489.16	980014.74	-4.59	-193.24	.85	-192.39
65B24	38. 7.41	113. 12.76	5107.	979507.05	980014.89	-27.48	-201.42	.30	-201.12
65B36	38. 4.22	112. 58.30	6561.	979413.62	980010.23	20.52	-202.95	.77	-202.18
65B37	38. 5.20	112. 58.98	6500.	979418.73	980011.66	18.46	-202.93	.96	-201.97

STAT.	LATITUDE	LONGITUDE	ELEV.	OBSERVED GRAVITY	THEOR. GRAVITY	FREE-AIR	SIMPLE BOUGUER	T.C	T.C. BOUGUER
65B38	38. 4.94	113. .40	6686.	979408.91	980011.28	26.51	-201.22	1.16	-200.06
65B39	38. 4.68	113. 2.36	6525.	979422.09	980010.90	24.93	-197.31	.90	-196.41
65B40	38. 5.80	113. 3.80	6107.	979447.16	980012.53	9.06	-198.94	.95	-197.99
65B41	38. 5.46	113. 4.95	6071.	979446.89	980012.04	5.89	-200.89	.72	-200.17
65B42	38. 6.12	113. 6.25	6023.	979448.59	980013.00	2.11	-203.03	.57	-202.45
75252	38. 7.01	113. 20.64	5106.	979499.99	980014.30	-34.04	-207.95	.23	-207.72
75253	38. 6.85	113. 21.70	5168.	979499.62	980014.06	-28.35	-204.37	.32	-2.04
75254	38. 6.84	113. 22.80	5287.	979497.09	980014.05	-19.67	-199.75	.43	-199.32
75255	38. 6.51	113. 23.58	5330.	979499.89	980013.57	-12.35	-193.89	.48	-193.41
75256	38. 6.16	113. 24.30	5358.	979498.18	980013.05	-10.91	-193.40	.45	-192.95
SG142	38. 6.91	113. 38.41	6037.	979441.54	980014.15	-4.78	-210.41	1.03	-209.38
SG143	38. 6.09	113. 38.65	5988.	979440.80	980012.95	-8.93	-212.88	.93	-211.95
SG144	38. 5.14	113. 38.43	5922.	979444.85	980011.57	-9.71	-211.41	1.09	-210.32
SG145	38. 3.76	113. 38.63	5821.	979458.05	980009.55	-3.99	-202.26	1.03	-201.23
SG146	38. 3.17	113. 38.07	5791.	979462.60	980008.70	-1.41	-198.65	.87	-197.78
SG147	38. 2.54	113. 37.22	5682.	979469.27	980007.77	-4.06	-197.59	.95	-196.64
SG148	38. 1.53	113. 36.00	5557.	979477.79	980006.30	-5.83	-195.10	.88	-194.22
SG149	38. .67	113. 34.75	5514.	979479.28	980005.05	-7.14	-194.95	.42	-194.53
SG150	38. .39	113. 32.66	5480.	979478.23	980004.64	-10.97	-197.61	.32	-197.29
SG151	38. 3.62	113. 58.13	6592.	979389.31	980009.35	.00	-226.66	.83	-225.83
SG152	38. 2.57	113. 58.13	6646.	979382.21	980007.81	-.49	-226.86	.88	-225.98
SG153	38. 1.65	113. 58.13	6650.	979377.87	980006.48	-3.13	-229.63	.94	-228.69
SG154	38. 1.08	113. 58.15	6678.	979374.52	980005.65	-3.00	-230.45	.95	-229.50
SG155	38. .30	113. 58.14	6709.	979371.75	980004.52	-1.72	-230.23	.99	-229.24
SG156	38. .03	113. 59.93	6911.	979363.30	980004.12	9.22	-226.17	1.49	-224.68
SG157	38. .78	113. 59.43	6827.	979367.83	980005.21	4.76	-227.76	1.30	-226.47
SG158	38. 5.13	113. 58.13	6529.	979390.54	980011.55	-6.90	-229.28	.81	-228.47
SG159	38. 6.59	113. 57.96	6484.	979392.02	980013.68	-11.78	-232.62	.84	-231.78
SG166	38. 5.99	113. 54.82	6566.	979397.12	980012.80	1.92	-221.72	.84	-220.88
SG167	38. 5.12	113. 51.69	6761.	979375.60	980011.54	.00	-202.90	1.10	-201.80
SG168	38. 5.12	113. 53.15	6639.	979397.94	980011.54	10.86	-215.26	.91	-214.35
SG253	38. 5.58	113. 56.30	6380.	979404.64	980012.21	-7.47	-224.77	.86	-223.91

STAT.	LATITUDE	LONGITUDE	ELEV.	OBSERVED GRAVITY	THEOR. GRAVITY	FREE-AIR	SIMPLE BOUGUER	T.C	T.C. BOUGUER
SG254	38. 5.11	113. 50.79	6891.	979399.29	980011.52	35.93	-198.78	1.26	-197.52
SG255	38. 5.11	113. 49.72	7040.	979392.16	980011.52	42.82	-196.96	1.88	-195.08
SG256	38. .34	113. 52.66	6561.	979402.59	980004.57	15.15	-208.32	1.01	-207.31
SG257	38. .77	113. 54.83	6509.	979387.52	980005.20	-5.46	-227.16	.73	-226.43
SG258	38. 2.13	113. 59.24	6788.	979372.82	980007.18	4.12	-227.08	1.11	-225.97
SG259	38. 2.51	113. 57.05	6551.	979389.11	980007.73	-2.44	-225.57	.78	-224.79
SG260	38. 1.65	113. 56.34	6546.	979386.58	980006.48	-4.20	-227.15	.76	-226.39
SG261	38. 2.51	113. 54.83	6464.	979396.16	980007.73	-3.57	-223.74	.70	-223.04
SG300	38. 7.15	113. 47.99	7546.	979364.70	980014.50	59.98	-197.04	2.74	-194.30
SG301	38. 6.51	113. 46.97	7035.	979392.04	980013.57	40.18	-199.43	2.00	-197.43
SG302	38. 6.92	113. 46.51	6924.	979397.46	980014.16	34.57	-201.26	1.72	-199.54
SG316	38. .09	113. 29.59	5306.	979505.13	980004.21	.00	-192.06	.41	-191.65
SG317	37. 59.92	113. 30.50	5354.	979488.43	980003.96	-11.94	-194.30	.30	-194.00
SG318	38. .06	113. 31.55	5381.	979484.09	980004.16	-13.94	-197.22	.33	-196.89
SG319	38. 1.17	113. 30.54	5552.	979483.56	980005.78	.00	-195.93	.44	-195.49
SG320	38. 1.98	113. 30.97	5702.	979470.63	980006.96	.00	-194.10	.63	-193.47
SG321	38. 1.78	113. 32.36	5592.	979479.71	980006.67	-.99	-191.45	.60	-190.85
SG322	38. 2.72	113. 33.49	5710.	979472.31	980008.03	1.36	-193.12	.62	-192.50
SG323	38. 3.81	113. 33.33	5884.	979456.19	980009.63	.00	-196.02	.63	-195.39
SG324	38. 4.61	113. 33.28	6017.	979456.10	980010.80	11.26	-193.68	.67	-193.01
SG325	38. 5.12	113. 32.94	6103.	979450.68	980011.54	13.19	-194.68	.73	-193.95
SG326	38. .68	113. 33.80	5524.	979479.16	980005.07	-6.33	-194.48	.39	-194.09
SG327	38. 1.25	113. 35.37	5525.	979480.34	980005.90	-5.88	-194.06	.67	-193.39
SG328	38. 1.94	113. 35.60	5683.	979470.26	980006.91	-2.11	-195.68	.57	-195.11
SG329	38. 2.50	113. 35.68	5821.	979460.04	980007.71	-.16	-198.43	.88	-197.55
SG330	38. 2.99	113. 35.69	5912.	979451.96	980008.42	-.39	-201.75	.81	-200.94
SG331	38. 1.88	113. 36.49	5606.	979473.72	980006.82	-5.81	-196.75	.96	-195.79
SG332	38. 2.12	113. 40.18	5976.	979453.48	980007.16	8.42	-195.13	.74	-194.39
SG333	38. 1.60	113. 39.34	6019.	979449.97	980006.41	9.70	-195.31	.70	-194.60
SG334	38. 1.15	113. 39.09	6044.	979447.95	980005.76	10.68	-195.18	.72	-194.47
SG350	38. 7.21	113. 35.63	6254.	979429.41	980014.59	3.08	-209.93	.87	-209.06
SG351	38. 6.38	113. 35.53	6200.	979431.10	980013.37	.90	-210.27	1.11	-209.16

STAT.	LATITUDE	LONGITUDE	ELEV.	OBSERVED GRAVITY	THEOR. GRAVITY	FREE-AIR	SIMPLE BOUGUER	T.C	T.C. BOUGUER
SG352	38. 5.72	113. 34.79	6100.	979445.09	980012.41	6.45	-201.32	1.03	-200.29
SG353	38. 7.19	113. 34.34	6376.	979430.78	980014.55	15.95	-201.21	.97	-200.24
SG649	38. .36	113. 27.47	5088.	979526.03	980004.60	.00	-205.02	.35	-204.67
SG650	38. .40	113. 28.60	5265.	979495.97	980004.66	-13.47	-192.80	.42	-192.38
SG651	38. .37	113. 27.99	5127.	979496.51	980004.62	-25.87	-200.50	.41	-200.09
SG652	38. 1.20	113. 27.30	5084.	979503.08	980005.83	-24.56	-197.72	.70	-197.02
SG653	38. 2.04	113. 26.93	5100.	979504.91	980007.05	-22.45	-196.16	.85	-195.31
SG654	38. 2.93	113. 26.57	5148.	979501.23	980008.34	-22.89	-198.32	.73	-197.59
SG655	38. 3.47	113. 26.34	5177.	979522.19	980009.13	.00	-198.61	.68	-197.93
SG656	38. 4.33	113. 25.99	5257.	979515.92	980010.39	.00	-195.55	.65	-194.90
SG657	38. 4.51	113. 26.48	5387.	979496.06	980010.66	-7.90	-191.38	.95	-190.43
SG658	38. 4.91	113. 26.98	5571.	979486.61	980011.23	-.62	-190.37	.96	-189.41
SG659	38. 3.57	113. 26.88	5299.	979497.05	980009.28	-13.81	-194.29	.84	-193.45
SG660	38. 3.82	113. 27.45	5482.	979494.02	980009.65	.00	-189.81	1.08	-188.73
SG661	38. 4.45	113. 28.62	6120.	979449.42	980010.56	14.50	-193.95	3.00	-190.95
SG662	38. 5.54	113. 25.38	5380.	979495.13	980012.15	-10.98	-194.22	.59	-193.63
SG663	38. 6.09	113. 25.17	5431.	979489.44	980012.95	-12.68	-197.66	.51	-197.15
SG664	38. 7.39	113. 25.82	5504.	979497.16	980014.87	.00	-197.47	.95	-196.52
SG754	38. 5.77	113. 58.13	6531.	979389.34	980012.48	-8.84	-231.29	.80	-230.50
SG755	38. 4.25	113. 58.15	6555.	979389.81	980010.27	-3.90	-227.16	.84	-226.32
SG756	38. 4.25	113. 59.23	6701.	979380.22	980010.27	.24	-227.99	.97	-227.02
SG757	38. 4.25	113. 58.68	6638.	979384.66	980010.27	-1.25	-227.35	.88	-226.47
SG758	38. 4.25	113. 57.59	6526.	979392.18	980010.27	-4.27	-226.55	.77	-225.78
SG759	38. 5.73	113. 54.25	6572.	979398.82	980012.43	4.55	-219.30	.88	-218.42
SG760	38. 4.25	113. 51.75	6715.	979399.37	980010.27	20.71	-208.00	.96	-207.04
SG761	38. 3.46	113. 51.63	6666.	979399.16	980009.12	17.04	-210.00	.92	-209.08
SG762	38. 2.66	113. 52.05	6606.	979398.81	980007.94	12.24	-212.77	.84	-211.93
SG763	38. 2.08	113. 52.65	6508.	979398.98	980007.11	4.02	-217.65	.79	-216.86
RG022	37. 36.79	113. 36.24	5450.	979442.86	979970.28	-14.80	-200.31	1.02	-199.29
RG079	37. 31.89	113. 45.36	5703.	979419.49	979963.17	-7.26	-201.36	1.08	-200.28
RG080	37. 30.28	113. 46.81	6322.	979361.68	979960.82	-4.50	-198.88	1.60	-197.28
RG085	37. 33.57	113. 56.78	6231.	979395.09	979965.62	15.56	-196.49	.92	-195.57

STAT.	LATITUDE	LONGITUDE	ELEV.	OBSERVED GRAVITY	THEOR. GRAVITY	FREE-AIR	SIMPLE BOUGUER	T.C	T.C. BOUGUER
RG086	37. 32.85	113. 56.53	6215.	979392.83	979964.56	12.85	-196.50	1.04	-195.46
RG087	37. 31.50	113. 57.06	6398.	979386.41	979962.59	25.61	-192.14	1.88	-190.26
RG092	37. 31.76	113. 35.23	6058.	979396.03	979962.98	2.87	-203.40	1.11	-202.29
RG405	37. 30.23	113. 51.83	5803.	979420.80	979960.75	5.88	-191.77	1.29	-190.48
RG467	37. 30.09	113. 57.80	6488.	979385.70	979960.55	35.42	-185.56	2.12	-183.44
RG468	37. 30.24	113. 58.23	6454.	979386.51	979960.77	32.81	-187.02	1.87	-185.15
RG574	37. 32.20	113. 39.39	6023.	979408.21	979963.62	11.11	-193.91	1.31	-192.60
RG578	37. 36.30	113. 59.24	5938.	979410.33	979969.57	-.72	-202.84	.70	-202.14
RG596	37. 32.55	113. 42.15	5662.	979427.16	979964.13	-4.41	-197.20	.80	-196.40
RG597	37. 32.05	113. 41.67	5816.	979417.39	979963.40	1.04	-197.01	.91	-196.10
RG598	37. 30.76	113. 39.22	7229.	979324.13	979961.52	42.57	-203.56	9.68	-193.97
RG601	37. 34.99	113. 59.75	6127.	979393.02	979967.67	1.66	-206.92	.78	-206.14
RG612	37. 31.73	113. 42.88	5545.	979432.17	979962.93	-9.20	-198.04	1.80	-196.24
RG623	37. 32.75	113. 44.58	5757.	979413.91	979964.42	-9.01	-204.99	.82	-204.17
RG655	37. 32.75	113. 50.74	5694.	979440.15	979964.42	11.30	-182.49	1.42	-181.07
RG660	37. 31.13	113. 48.35	6910.	979340.30	979962.06	28.19	-207.05	3.37	-203.68
RG662	37. 31.31	113. 45.94	5923.	979407.10	979962.32	1.90	-199.73	1.20	-198.53
RG673	37. 34.52	113. 36.86	5670.	979429.73	979966.98	-3.94	-197.06	1.03	-196.03
RG674	37. 35.43	113. 36.31	5735.	979430.38	979968.30	1.52	-193.81	1.23	-192.58
RG675	37. 30.71	113. 33.41	6522.	979365.43	979961.45	17.44	-204.70	1.75	-202.95
RG678	37. 32.34	113. 33.39	6621.	979363.03	979963.83	21.97	-203.54	2.48	-201.06

APPENDIX B

LOGS OF DRILL HOLES AND SUMMARY OF DRILLING RESULTS

The latitudes, longitudes, and collar elevations of all drill holes were determined approximately from U.S.G.S. 7 1/2-minute topographic quadrangle maps.

Geothermal test well DeArman #1*

(Lat 37° 50.33' N, Long 113° 41.18' W)

(Collar elevation -- 5,138 ft (1,566 m))

Geothermal test well DeArman #1 is about 4 mi (6.4 km) south of Beryl in the Escalante Desert. The well penetrated a total depth of 12,295 ft (3,748 m).

From 470 to 1,625 ft (143 to 495 m), the well penetrated a layer of claystone. The claystone is mixed with sand siltstone and welded tuff near the base, at a depth of between 1,340 and 1,625 ft (408 and 495 m). The well penetrated volcanics (welded tuff) from 1,625 to 4,610 ft (495 to 1,405 m).

In this sequence of volcanics, 75 percent quartz monzonite was found between 1,700 and 2,270 ft (518 and 692 m). From 4,610 to 5,320 ft (1,405 to 1,622 m), the well passed through a sedimentary section of limestone and dolostone. In this section, volcanics were found associated with limestone and dolostone between 4,920 and 4,990 ft (1,500 and 1,521 m). From 5,320 to 6,180 ft (1,622 to 1,884 m), the well penetreated a mixture of mostly volcanics, and limestone and dolostone. In the section of this mixture between 5,570 and 5,660 ft (1,698 and 1,726 m), 70 percent quartz monzonite with 30 percent welded tuff was found. From 6,180 to 7,720 ft (1,884 to 2,353 m), the well again penetrated dolostone, limestone, and shaly limestone. In this section between 7,110 and 7,180 ft (2,168 and 2,189 m), a few percent

*Well log furnished by Dr. Val A. Finlayson, Utah Power and Light Company. Well designated "DH1" on Figures 3 and 4.

of altered volcanics were found in limestone and shaly limestone, which shows 10 ft (3 m) of minor slickenside zone at a depth of 7,140 ft (2,177 m).

Between 7,720 and 8,465 ft (2,354 and 2,581 m), there was lost circulation and no sample was returned. From 8,465 to the bottom of the well, at 12,295 ft (2,581 to 3,748 m), the well passed through a series of limestone, dolostone and in some places, shaly limestone. In this section, occasional slickensides were found between 9,480 and 9,490 ft (2,890 and 2,893 m) in limy shale, limestone, and dolostone.

Geothermal test well State #1*

(Lat 37° 50.14' N, Long 113° 37.90' W)

(Collar elevation -- 5,128 ft (1,563 m))

Geothermal test well State #1 is about 5 km east of the DeArman #1 well. The well penetrated a total depth of 4,986 ft (1,520 m).

The well penetrated soft clay valley fill from 470 to 770 ft (143 to 235 m). A moderately soft conglomerate was then penetrated between 770 and 830 ft (235 and 253 m). The well pased through siltstone between 830 and 920 ft (253 and 280 m), and claystone between 920 and 1,090 ft (280 and 332 m). Then the well penetrated a thick layer of shale from 1,090 to 1,890 ft (280 to 576 m).

The well penetrated a thin layer of volcanics comprising 60 percent welded tuff and 40 percent quartz monzonite porphyry between 1,890 and 1,905 ft (576 and 581 m). Then the well passed through moderately hard quartz monzonite from 1,905 to 4,560 ft (581 to 1,390 m). An open fracture zone was penetrated between 4,560 and 4,579 ft (1,390 and 1,396 m). From 4,579 to 4,622 ft (1,396 to 1,409 m), the well penetrated altered quartz monzonite porphyry in a fracture zone. The bottom hole temperature of 177° F was observed at a depth of 4,579 ft (1,396 m). No sample was returned from 4,622 to 4,986 ft (1,409 to 1,520 m).

* Well log furnished by Dr. Val A. Finlayson, Utah Power and Light Company. Well designated "DH2" in Figures 3 and 4.

Geothermal test well Jones #1*

(Lat 37° 51.85' N, Long 113° 19.95' W)

(Collar elevation 5,199 ft (1,585 m))

Geothermal test well Jones #1 is near Avon in the Escalante Desert. The well penetrated a total depth of 5,855 ft (1,785 m) without reaching bedrock.

The well penetrated principally a thick layer of silty claystone from 620 to 4,500 ft (189 to 1,372 m). In this thick layer of silty claystone, thin layers of minor volcanics including mostly welded tuff with individual thicknesses of less than 100 ft (30.5 m) were occasionally found. From 4,500 to 5,500 ft (1,372 to 1,677 m), the well penetrated mostly volcanics of crystal welded tuff, some of which are altered. Some claystones were occasionally found in the tuff and the percentage of claystone increased to 80 percent in some places. From 5,500 ft (1,677 m) to the bottom of the hole, that is, 5,855 ft (1,785 m), the well passed through a mixture of 80 percent silty claystone and 20 percent welded tuff.

* Abbreviated well log data only, furnished by Dr. Norman Harthill, Geothermal Kinetics, Inc. Well designated "DH3" on Figures 3 and 4.

Little Salt Lake well #1

(Lat 37° 51.55' N, Long 112° 58.65° W)

(Collar elevation -- 6,115 ft (1,864 m))

The well is in the Red Hills area, about 6 km south of Parowan Gap. The well was abandoned after drilling a total depth of 4,400 ft (1,341 m). The well bottomed in quartz monzonite.

The well penetrated a series of Tertiary sedimentary rocks, including siltstone, shale, coal (black), and sandstone, from the surface to a depth of 2,925 ft (892 m). Then the well passed through a sequence of shale and siltstone of Jurassic age from 2,925 ft (829 m) until it reached the top of quartz monzonite at a depth of 3,490 ft (1,064 m). The well penetrated monzonite from 3,490 ft (1,064 m) to 4,400 ft (1,341 m).

*Drill log furnished by Utah Oil, Gas and Mining division. Well designated "DH4" on Figures 3 and 4.

Shurtz Creek well* #1

(Lat 37° 36.18' N, Long 113° 05.36' W)

(Collar elevation -- 6,497 ft (1,981 m))

The well is about 8 km south of Cedar City in the Hurricane Cliffs area. The well was abandoned after drilling a total depth of 5,996 ft (1,828 m). The condensed log of the drill hole is shown in the following table.

Table 3. Log of Shurtz Creek well #1.

Depth to the top (feet) (meters)	Formation	Age
0 (0)	Virgin Limestone	Triassic
100 (30)	Moenkopi	Triassic
540 (165)	Timpoweap	Triassic
746 (227)	Kaibab	Permian
905 (276)	Toroweap	Permian
2,477 (755)	Coconino	Permian
3,418 (1,042)	Pakoon	Permian
4,664 (1,422)	Callville	Pennsylvanian
5,070 (1,546)	Redwall	Mississippian (?)
5,784 (1,763)	Devonian	Devonian

*Drill log furnished by Utah Oil, Gas and Mining division. Well designated "DH5" on Figures 3 and 4.

Fee well* #1-B

(Lat 37° 52.80' N, Long 113° 29.00' W)

(Collar elevation - 5,105 ft (1,556 m))

The well is in the Escalante Desert near Table Butte and was drilled to a total depth of 6,762 ft (2,062 m).

Complete information is not available for this well. However, the well reached the top of the Wasatch Formation at a depth of 2,900 ft (884 m). Then no sample was returned below 3,120 ft (951 m) because of lost circulation, until it reached the bottom of the hole.

*Utah Oil, Gas and Mining division. Well designated "DH6" on Figures 3 and 4.

APPENDIX C

DRY AND WET DENSITIES OF ROCK SAMPLES COLLECTED IN THE STUDY AREA

In order to determine the dry and wet densities of rock samples, the dry mass determination was made for each sample. Rock samples were then placed in a vacuum for at least 6 hours and then saturated with water. Each sample (saturated with water) was weighted in air and water, and the volume measurement was made by taking the contrast of these two weights. Finally, the dry and wet density of each sample was calculated from the dry mass, wet mass, and volume.

Table 4. Location and density of rock samples.

Sample	area*	Latitude N.		Longitude W.		Dry	Wet
		Deg	Min	Deg	Min	Density g/cc	Density g/cc
Basalt	1	38	06.01	113	0.70	2.67	2.71
Breccia	2	37	39.19	113	31.73	2.02	2.15
Dacite	3	37	58.98	113	39.30	2.51	2.56
Dacite	3	37	59.01	113	39.30	2.31	2.39
Rhyolite	4	37	42.72	113	25.93	2.29	2.40
Rhyolite	2	37	37.45	113	49.30	2.19	2.34
Rhyolite	5	37	54.51	112	38.18	2.48	2.53
Rhyolite	2	37	36.45	113	55.28	2.48	2.51
Tuff	2	37	37.63	113	50.25	2.20	2.32
Tuff	2	37	36.52	113	56.77	1.63	1.89
Tuff	2	37	36.65	113	56.78	1.81	2.05
Tuff	3	37	57.14	113	56.97	2.14	2.28
Tuff	3	37	58.30	113	53.50	2.53	2.57
Tuff	6	37	37.94	113	18.04	2.27	2.38
Tuff	2	37	33.48	113	32.78	1.57	1.97
Limestone	6	37	42.72	113	25.93	2.63	2.65
Limestone	6	37	37.75	113	24.42	2.65	2.67
Limestone	6	37	41.87	113	44.01	2.47	2.51
Limestone	6	37	42.70	113	25.93	2.66	2.67

*Areas are designated as follows: (1) Black Mountains; (2) Enterprise; (3) Needle Range; (4) Newcastle; (5) Hurricane Cliffs; (6) Iron Springs.

APPENDIX D

ERROR ANALYSIS IN THE MODELING OF THE GRAVITY PROFILES

The total error in the observed gravity values accumulated from several sources (previously described) was determined to have a maximum value of about 0.7 mgal. When modeling the gravity data, the parameters of the model were constrained so that the best possible fit of the model to the observed data occurred when the difference between each observed and computed values fell within the estimated error of 0.7 mgal, and the sum of the squares of all the differences was a minimum. A model was generally considered acceptable when it fulfilled the above criteria and also fitted the mapped surface geology and subsurface geology (if known).

Moreover, the profiles were modeled so that the errors between the computed and observed gravity values at the (relatively broad) gravity peaks and troughs were always within 0.15 mgal; and, using this constraint, the best vertical dimension of the model was obtained, although the accuracy of the data is determined within the limits of the capable techniques used in data processing. To determine the accuracy of the locations of the near-surface faults which bound the structural highs and lows, it was found that a normal fault dipping at an angle greater than 45° does not give a pronounced change in the gravity gradient but rather causes a slight horizontal change in the whole set of gravity values. Therefore, even for a

steeply dipping fault, the location and angle of dip of the fault are apparently impossible to resolve exactly, unless the trace of the fault is exposed at the surface. However, the accuracy of the locations of the steeply dipping faults is estimated to be generally within about 0.5 km, where there is no geological constraint. A steep fault in the model may represent a series of closely spaced step faults. For a series of gently dipping faults, the location of each fault on a profile is not certain because of this lack of resolution of the gravity data. In the three-layer modeling, the thickness of the top layer (where drill data were not available) and the configuration of the subsurface fault systems, composed of double layers, were adjusted in the modeling to be as geologically reasonable as possible.

In order to determine the variations in depth to basement beneath the large grabens, with regard to the changes of the observed gravity values within the error limit along the profile, some observed gravity values in the gravity trough over each graben were varied by ± 0.7 mgal, and the corresponding change in depth was studied. The thickness of the top layer was kept constant while studying the variation. The possible maximum and minimum depths of each graben, which correspond with the error extremes, are given in Table 5.

In gravity profile modeling, the error in the model may be introduced by three main sources of error. The first source is the error in the observed gravity value of an individual station. The second source is the error in the observed gravity value of the

Table 5. Variation (range) of calculated depth to basement beneath several grabens for change in gravity anomaly of ±0.7 mgal.

Graben	Profile	Depth modeled (in km)	Calculated range of depth (in km)	Minimum observed gravity value on the profile (in mgal)#
Newcastle	A-A'	3.05	3.13-2.98	-220.02
Lund	C-C'*	1.80	1.92-1.67	-213.02
Avon	C''-C'''	2.00	2.19-1.80	-214.87
South Beryl	B-B'	2.21	2.49-1.96	-211.56
East Modena	B-B'*	1.35	1.48-1.23	-202.39
Cedar Valley	D-D'	2.50	2.70-2.36	-217.05
Parowan Valley	D-D'*	2.57	2.72-2.41	-218.96

*The profile does not extend across the deepest part of the graben.

#Complete Bouguer gravity anomaly value (see Fig. 4).

station at which the entire set of calculated values along the profile is matched with the observed values. (The station or point along the profile where the matching is chosen, is designated the "match station" or "match point", respectively) The match station (or match point) should be at a sufficient distance from the steep gravity gradient; and, moreover, the detailed subsurface geology beneath the match station should be known. Otherwise, the depths to the basement of all subsurface features along the profile are not certain. If the match point is at or near one end of the profile, the profile should be temporarily extended beyond the end point for a reasonable distance to avoid the edge effect of the model. This procedure is important when the match station is located over a basement ridge at the end point. Therefore, selecting a match point is important in profile modeling. The third source is the error in the assumed density of each polygon of the model.

REFERENCES

Anderson, L. W., and Miller, D. G., 1979, Quaternary map of Utah: published by Fugro, Inc., Consulting Engineers and Geologists, Long Beach, California.

Anderson, R. E., and Bucknam, R. C., 1979, Two areas of probable Holocene deformation in southwestern Utah: Tectonophysics, v. 52, p. 417-430.

Anderson, P. N., and Axtel, L. H., 1972, Geothermal resources in California: Geothermal overviews of the western United States: published by Geothermal Resources Council, Davis, California.

Armstrong, R. L., 1968, Sevier orogenic belt in Nevada and Utah: Geol. Soc. America Bull., v. 79, p. 429-458.

Blank, H. R., Jr., 1959, Geology of the Bull Valley district: Washington County, Utah: Ph.D. Thesis, University of Michigan.

Blank, H. R., Jr., and Mackin, J. H., 1967, Geologic interpretation of an aeromagnetic survey of the Iron Springs district, Utah: U.S. Geol. Survey Prof. Paper 516-B, p. B1-B14.

Biehler, S., and Combs, J., 1972, Correlations of gravity and geothermal anomalies in the Imperial Valley, Southern California (abs.): Geol. Soc. America Abstracts with Programs, v. 4, no. 3, p. 128.

Carrier, D. L., 1979, Gravity and heat flow studies at Twin Peaks: an area of late Tertiary silicic volcanism in Millard County, Utah: M. S. Thesis, University of Utah, 120 p.

Carter, J. A., and Cook, K. L., 1978, Regional gravity and aeromagnetic surveys of the Mineral Mountains and vicinity, Millard and Beaver Counties, Utah: M. S. Thesis, University of Utah, 178 p.

Clement, M. D., 1980, Escalante Desert: Heat flow and geothermal assessment of the Oligocene/Miocene volcanic belt in southwestern Utah: M. S. Thesis, University of Utah.

Cook, E. F., 1957, Geology of the Pine Valley Mountains, Utah: Utah Geol. and Mineral. Survey Bull., 58, 111 p.

_____, 1960a, Geologic atlas of Utah, Washington, County: Utah

Geol. and Mineral. Survey Bull. 70, 119 p.

Cook, K. L., 1950, Magnetic surveys in the Iron Springs district, Iron County, Utah: U. S. Bureau of Mines Rept. Inv. 4586, 78 p.

Cook, K. L., Nilsen, T. H., and Lambert, J. F., 1971, Gravity base station network in Utah -- 1967: Utah Geol. and Mineral. Survey Bull. 92, 57 p.

Cook, K. L., and Hardman, E., 1967, Regional gravity survey of the Hurricane fault area and Iron Springs district, Utah: Geol. Soc. America Bull., v. 78, p. 1063-1076.

Crosby, G. W., 1973, Regional structure in southwestern Utah: Utah Geological Association Publication 3, p. 27-32.

Dobbin, C. E., 1939, Geologic structure of the St. George district, Washington County, Utah: Am. Assoc. Petroleum Geologists Bull., v. 23, p. 121-144.

Easton, G. P., Christiansen, R. L., Iyer, H. M., Pitt, A. M., Mabey, D. R., Blank, H. R., Zietz, I., and Gettings, M. E., 1975, Magma beneath Yellowstone National Park: Science, v. 188, p. 787-796.

Ekren, E. B., Bucknam, R. C., Carr, W. J., Dixon, G. L., and Quinlivan, W. D., 1976, East-trending structural lineaments in central Nevada: U. S. Geological Survey Prof. Paper 986, 16 p.

Erickson, M. P., and Dasch, E. J., 1968, Volcanic stratigraphy, magnetic data and alteration geologic map and sections of the Jarloose mining district southeast of Minersville, Beaver County, Utah: Utah Geol. and Mineral. Survey map no. 26.

Gabbert, S. C., 1980, Gravity survey of parts of Millard, Beaver, and Iron Counties, Utah: M. S. Thesis, University of Utah, 107 p.

Gardner, L. S., 1941, The Hurricane fault in southewestern Utah and northwestern Arizona: Am. Jour. Sci., v. 239, p. 241-260.

Granger, A. E., 1963, The Iron province of southwestern Utah, p. 146-150 in Guidebook to the geology of southwestern Utah: Intermountain Assoc. Petroleum Geologists, 12th Ann. Field Conf., 226 p.

Gregory, H. E., and Williams, N. C., 1947, Zion National Monument, Utah: Geol. Soc. America Bull., v. 58, p. 211-244.

Hansen, G. H., and Scoville, H. C., 1955, Drilling records for oil and gas in Utah: Utah Geol. and Mineralog. Survey Bull. 50, 110 p.

Hardman, E., 1964, Regional gravity survey of central Iron

and Washington Counties, Utah: M. S. Thesis, University of Utah, 107 p.

Hintze, L.F., 1963, Geologic map of southwestern Utah: Utah Geol. and Mineral. Survey.

Huntington, Ellseworth, and Goldthwait, J. W., 1903, The Hurricane fault in Southwestern Utah: Jour. Geology, v. 11, p. 46-63.

Isherwood, W. F., 1975, Gravity and magnetic studies of the Geysers Clear Lake geothermal region, California: Department of the Interior, Geol. Survey, Open-file report 73-368, 1975.

Jacob, K. H., 1972, Global tectonic implications of anomalous seismic P travel times from the nuclear explosion Longshot: Jour. Geophys. Research, v. 77, p. 2556.

Kane, M. F., Mabey, D. R., and Brace, R., 1976, A gravity and magnetic investigation of the Long Valley Caldera, Mono County, California: Jour. Geophy. Research, v. 81, no. 5, p. 754-762.

Leith, C. K., and Harder, E. C., 1908, The iron ores of the Iron Springs district, southern Utah: U.S. Geol. Survey Bull. 338, 102 p.

Mabey, D. R., 1960, Regional gravity survey of part of the Basin and Range province: U.S. Geol. Survey Prof. Paper 400-B, p. 283-285.

Mackin, J. H., 1947, Some structural features of the intrusions of the Iron Springs district, Utah: Utah Geol. Soc., Guidebook to the geology of Utah, no. 2, 62 p.

_____, 1954, Geology and iron ore deposits of the Granite Mountain area, Iron County, Utah: U.S. Geol. Survey Mineral Inv. Field Studies Map MF-14.

_____, 1960, Structural significance of Tertiary volcanic rocks in southwestern Utah: Am. Jour. Sci., v. 258, p. 81-131.

Miller, G. M., 1963, Outline of structural-stratigraphic units of the Wah Wah Mountains, southwestern Utah: in Guidebook to the geology of southwestern Utah: Intermountain Assoc. Petroleum Geologists, 12th Ann. Field Conf., p. 96-102.

Montgomery, J. R., 1973, A regional gravity survey of western Utah; PhD thesis, Univeristy of Utah.

Pakiser, L. C., 1963, Structure of the crust and upper mantle in the western United States: Jour. Geophys. Research, v. 68, p. 5747-5756.

_____, 1964, Gravity, volcanism, and crustal structure in the southern Cascade Range, California: Geol. Soc. America Bull., v. 75, p. 611-620.

Rowley, P. D., Steven, T. A., Anderson, J. J., Cunningham, C. G., 1979, Cenozoic stratigraphic and structural framework of southwestern Utah: U.S. Geol. Survey Prof. Paper 1149, 22 p.

Schmoker, J. W., 1972, Analysis of gravity and aeromagnetic data, San Francisco Mountains and vicinity, southwestern Utah: Utah Geol. and Mineralog. Survey Bulletin 98, 24 p.

Serpa, L. F., 1980, Detailed gravity and aeromagnetic surveys in the Black Rock Desert area, Utah: M.S. thesis, University of Utah, 211 p.

Smith, R. B., and Sbar, M. L., 1974, Contemporary tectonics and seismicity of the western United States with emphasis on the intermountain seismic belt: Geol. Soc. America Bull., v. 85, p. 1205-1218.

Smith, R. B., Braile, L., and Keller, G. R., 1975, Upper crustal low-velocity layers: Possible effect of high temperatures over a mantle upwarp at the Basin Range - Colorado Plateau transition: Earth and Planetary Sci. Letters., v. 28, p. 197-204.

Snow, J. H., 1978, A study of structural and tectonic patterns as interpreted from gravity and aeromagnetic data: unpublished M.S. thesis, University of Utah, 206 p.

Speiker, E. M., 1949, The transition between the Colorado Plateaus and the Great Basin in central Utah: Utah Geol. Soc., Guidebook to the geology of Utah, no. 4, p. 1-82.

Stewart, J. H., Moore, W. J., and Zietz, I., 1977, East-west patterns of Cenozoic igneous rocks, aeromagnetic anomalies, and mineral deposits, Nevada and Utah: Geol. Soc. America Bull., v. 88, p. 67-77.

Stewart, J. H., 1978, Basin-Range structure in western North America: A review, in Smith, R. B., and Eaton, G. P., eds., Cenozoic tectonics and regional geophysics of the western Cordillera: Geol. Soc. America Mem. 152, p. 1-31.

Stokes, W. L., and Heylmun, E. B., 1963, Tectonic history of southwestern Utah: in Guidebook to the geology of southwestern Utah: Intermountain Assoc. Petroleum Geologists, 12th Ann. Field Conf., p. 19-25.

Thomas, H. E., and Taylor, G. H., 1946, Geology and ground-water reservoirs of Cedar City and Parowan Valleys, Iron County, Utah:

U.S. Geol. Survey Water Supply Paper 993.

Threet, R. L., 1963a, Structure of the Colorado Plateau margin near Cedar City, Utah: in Guidebook to the geology of southwestern Utah: Intermountain Assoc. Petroleum Geologists, 12th Ann. Field Conf., p. 104-117.

_____, 1963b, Geology of the Parowan Gap area, Iron County, Utah: in Guidebook to the geology of southwestern Utah: Intermountain Assoc. Petroleum Geologists, 12th Ann. Field Conf., p. 136-145.

White, W. N., 1932, A method of estimating ground-water supplies based on discharge by plants and evaporation from soil -- results of investigations in Escalante Valley, Utah: U.S. Geol. Survey Water-Supply Paper 659-A, p. 1-105.

Yokoyama, I., 1958, Gravity survey on Kuttyaro Caldera Lake: Jour. Physics of the Earth, v. 6, p. 75-79.

Zietz, I., Shuey, R. T., and Kirby, J. R., Jr., 1976, Aeromagnetic map of Utah: U.S. Geol. Survey Map GP-907.

VITA

Name	Win Pe
Birthdate	23 February 1949
Birthplace	Kyaukse, Burma
High School	No. (2) State High School Kyaukse, Burma
University 1965-1969	Arts and Science University Mandalay, Burma
Degree 1969	B.Sc., in Physics Arts and Science University Mandalay, Burma
Professional Position 1970-1976	Assistant Geophysicist Department of Geological Survey and Mineral Exploration Rangoon,Burma
1977	Assistant Geophysicist Department of Applied Geology Arts and Science University Rangoon, Burma
Graduate Study 1977-1980	University of Utah Salt Lake City, Utah
Research Assistant Summers 1978 and 1979	Department of Geology and Geophysics University of Utah Salt Lake City, Utah
Professional Organization	Society of Exploration Geophysicists
Honors	
1977-1979	United Nations Fellowship
1979-1980	Fulbright Scholarship